Design of a turbine blade root connection with bushings

Joan Ann Mathew



Delft University of Technology

TUDelft

This page intentionally left blank.

Design of a turbine blade root connection with bushings

by

Joan Ann Mathew

in partial fulfillment of the requirements for the degree of
Master of Science
in Aerospace Engineering

Student Number:	5004292
Project Duration:	August, 2020 - July, 2021
Thesis Committee:	Dr. Rene Alderliesten
	Peter Joosse
	Dr. John-Alan Pascoe
	Dr. Julie J.E. Teuwen

Cover Image: General view of the Walney Extension offshore wind farm operated by Orsted off the coast of Blackpool, Britain September 5, 2018. REUTERS/Phil Noble/File Photo/File Photo

TU Delft

The work in this thesis was supported by Suzlon Energy Limited - Netherlands. Their cooperation is gratefully acknowledged.





Copyright ©Joan Ann Mathew
All rights reserved.
An electronic version of this dissertation is available at
http://repository.tudelft.nl/.

DELFT UNIVERSITY OF TECHNOLOGY
FACULTY OF AEROSPACE ENGINEERING
DEPARTMENT OF AEROSPACE STRUCTURES AND MATERIALS

GRADUATION COMMITTEE

Dated: 12 July 2021

Chair holder:

Dr.ir. Rene C. Alderliesten

Committee Members

Dr. John-Alan Pascoe

Dr. Julie J.E. Teuwen

Peter Joosse

This page intentionally left blank.

Abstract

With a growing demand for longer blades in the wind turbine industry for higher rated power per turbine, a structurally sound blade-root connection is of commercial importance. Bushing connections have been a commercially favoured design in the past few years, replacing the commonly used T-bolt connection as the joining method of choice. The new design replaces the barrel nut in the T-bolt with an axial bushing that the bolt connects to, and can be assembled with the laminate during the lay-up stage of the blade skin. It has been theorised that it can result in a reliable connection due to the elimination of laminate stress concentrations, improved fatigue performance, and enable longer blades. However, demonstrable literature outlining the performance of a blade-root connection with bushings is lacking in the current body of knowledge. While several patents for bushing designs exist, they don't provide verifiable results on their efficacy due to trademark laws.

The objective of this project is to design and conduct a numerical study of a blade-root connection with bushings with an aim to replace the T-bolt connection, along with providing evidence of the effect of various parameters on the structural performance of the blade root. The design is to be based on a Suzlon Energy-make blade with a pitch circle diameter of 3m and a blade length of 63m. The project has been planned in three phases: (1) Design of the root; (2) Validation of the design; (3) Comparative analysis. Modelling and FE analysis has been carried out in the ANSYS environment (running on the APDL solver). The inputs have been sourced from the study of existing literature, and load data provided by Suzlon Energy on the aerodynamic loads on the blade. Parameters of the bolted connection have been determined according to industry standards provided by VDI and Germanischer Lloyd. Design validation was conducted based on structural constraints; the key design constraint relevant to the blade-root as a sub-component of the wind turbine is the accumulated fatigue damage. For the final phase of the study, various parameters associated with the assembled root were identified and tested in iterations and their effect on the structural performance, weight, and cost of the assembly were studied.

The results confirm the hypothesis of reduction of stress concentrations within the laminate; this eliminates several failure modes associated with composite laminates at the blade root. As is, the bushing connection can be considered a viable alternative to the T-bolt joint. Within the connection, higher absolute stresses and stress gradients were developed in the bolt joining the blade to the hub. Hence, this was the area of focus for fatigue damage evaluations. Conservative estimates of the accumulated damage show values well within the acceptable range. The connection has been designed keeping several concurrent variables in mind. Given the commercial applicability of the design, a rigid optimised design is not feasible due to unpredictable parameters like certification costs, total assembly times, and procurement costs. Therefore, an effort has been made to understand the effect of varying component parameters. The design lends itself to flexibility of dimensioning and material choice within the sub-components; parameters can be optimised according to cost, manufacturability, and performance requirements. While the base design configuration for the bushing connection is heavier than the T-bolt design, improved fatigue performance can be seen as a favourable trade-off.

This page intentionally left blank.

Acknowledgements

Although this thesis marks the culmination of my time at TU Delft as a student of the Aerospace Department, the lessons I have learned over the past few months have been ingrained in me. Working through a pandemic brought its own set of challenges as life was reduced to talking to people through a screen and the months that seemed to merge into one. Persevering was a learning curve and it would have been impossible without the support, virtual and otherwise, of the key people in my life.

To begin with, I would like to thank my supervisor, Dr. René Alderliesten, for his unwavering support throughout the past months. It is fitting that the first class I attended at TU Delft was his Fatigue of Structures and Materials lecture, as his reasoning methods shaped my perspective towards approaching structural problems. I am grateful for his guidance, starting from arranging the thesis study with Suzlon, to helping with my defense.

Additionally, I would like to thank my supervisor and mentor at Suzlon, Mr. Peter Joosse, for providing me with constant support; his kind words helped me sustain my work throughout the duration of my thesis, and he proved to be reliable support for all my queries. Through this, I would also like to wish him a fulfilling retirement. Furthermore, I am immensely grateful for the assistance provided by Mr. Carlos Ochoa and Mr. Valter Bellotto at Suzlon; their help and insights proved to be invaluable during the course of this work and I am thankful to them for taking out their time to guide me.

I would also like to thank my parents and my brother for their support through all the highs and lows in the 26 and some odd years of my life. I owe the opportunity of studying at TU Delft to them and their numerous sacrifices.

I also want to take this opportunity to recognize the incredible support system that Arshdeep Brar, Karthik Narayanappa, and Ranjan Gaur have been in the past two years. You have been there for me through thick and thin, and I couldn't have asked for better friends. I am also indebted to the older friendships that have seen the test of time. And last but not anywhere near the least, I would like to show my gratitude to Rajit Devgan for being the greatest support I could imagine through all the crises I faced. People like you are rare and ought to be appreciated.

Joan Ann Mathew
Delft University of Technology
July, 2021

This page intentionally left blank.

Contents

Abstract iii

Acknowledgements v

Nomenclature ix

List of Figures xiii

List of Tables xvii

1 Introduction 1
- 1.1 Background . . . 1
- 1.2 Wind turbine Blade and Blade Root . . . 2
- 1.3 Research Objectives and Questions . . . 2
- 1.4 Structure of the report . . . 3

2 Literature Study and Theoretical Foundations 5
- 2.1 Blade Root Connections . . . 5
  - 2.1.1 Early Designs . . . 5
  - 2.1.2 T-bolt to Bushing Connection . . . 6
  - 2.1.3 Evaluation for the design of the bushing . . . 6
- 2.2 Bolted Joint . . . 6
  - 2.2.1 Standards and pre-requisites . . . 7
  - 2.2.2 Principles of Single Bolted Joints . . . 7
  - 2.2.3 Evaluation for the design of bolted joints . . . 9
- 2.3 Bonded Joints . . . 10
- 2.4 External Operating Loads . . . 11
  - 2.4.1 Load types . . . 11
  - 2.4.2 Load Cases . . . 12
  - 2.4.3 Design Loads: Procedures by Suzlon . . . 12
  - 2.4.4 Evaluation for design loads . . . 14
- 2.5 Procedures for Fatigue Analysis . . . 14
  - 2.5.1 Theory: Fatigue . . . 14
  - 2.5.2 Fatigue considerations for the design . . . 15
  - 2.5.3 Evaluation for fatigue analysis . . . 19

3 Design Study 21
- 3.1 Outline . . . 21
- 3.2 Finite Element Model of the Design . . . 21
  - 3.2.1 Sub-domain selection . . . 22
  - 3.2.2 Design constraints . . . 22
  - 3.2.3 Hub-side Assembly . . . 23
  - 3.2.4 Blade-side Assembly . . . 24
- 3.3 Meshing and Element Types . . . 27
  - 3.3.1 Choice of element type . . . 27
  - 3.3.2 Mesh Generation . . . 28
- 3.4 Coordinate System . . . 29
- 3.5 Contacts . . . 30
  - 3.5.1 No Separation Contact . . . 30
  - 3.5.2 Frictional Contact . . . 30
  - 3.5.3 Bonded Contact . . . 30

3.6 Boundary Conditions and Loads . . . 31
3.6.1 Boundary Conditions . . . 31
3.6.2 Definition of Loads . . . 32

4 Model Analysis and Validation **39**
4.1 Preliminary design verification . . . 39
4.2 Bolt Stress Profile . . . 41
4.3 Fatigue Analysis . . . 45

5 Comparative Analysis **51**
5.1 Parameter: Number of bolts . . . 52
5.1.1 Effect of modifying the number of bolts for a constant external moment . . . 52
5.1.2 Effect of number of bolts on external bending moment capacity . . . 54
5.2 Parameter: Material of insert . . . 55
5.3 Parameter: Bolt Length . . . 56
5.4 Parameter: Size of bushing . . . 57
5.5 Parameter: Wedge geometry . . . 58

6 Results **59**
6.1 Comparison with the T-bolt connection . . . 59
6.1.1 Stresses and stress ratios . . . 59
6.1.2 Weight, cost and manufacturing . . . 61
6.2 Performance of the bushing connection . . . 61
6.2.1 Fatigue performance . . . 61
6.2.2 Comparative analysis: Discussion of results . . . 62

7 Conclusions and Recommendations **65**
7.1 Conclusions . . . 65
7.2 Recommendations for Future work . . . 66

References **69**

A Material Data **71**

B FE Model - Iterations **73**

C Model Dimensions **75**

D MATLAB Code: Validation of bolt stress **77**

E Bolt Stress Profile **79**
E.1 Bolt stress profile - Minimum Pretension . . . 79
E.2 Bolt stress profile - Maximum Pretension . . . 80
E.3 Normal force and pretension: Varying bolt number . . . 81

Nomenclature

Abbreviations

Abbreviation	Definition
BCD	Bolt Circle Diameter
CFRP	Carbon Fibre Reinforced Polymer
GFRP	Glass Fibre Reinforced Polymer
GL	Germanischer Lloyd
IEC	International Electrotechnical Commission
SBJ	Single-Bolted Joint
SE	Suzlon Energy
SRF	Stress Reserve Factor
VARTM	Vacuum Assisted Resin Transfer Molding
VDI	Verein Deutscher Ingenieure (Association of German Engineers)
WTG	Wind Turbine Generator

Symbols

Symbol	Definition	Unit
a	eccentricity of the loading axis from the bolt axis	
A_D	sealing area	
A_{shank}	Area of bolt shank	
CoE	Cost of Energy	
CoT	Cost of Turbine	
CoI	Cost of Transport and installation	
CoM	Cost of Maintenance and operation	
C_p	Power coefficient or wind turbine efficiency	
d_2	Pitch diameter of the bolt thread	
$\mathcal{D}$	Total accumulated damage	
D_{shank}	Diameter of shank	
$\Delta\mathcal{D}_t$	Average damage rate over lifetime T	
ΔF_{Vth}	change in the preload as a result of a temperature different from room temperature; additional thermal load	
E	Young's Modulus	
F_A	Axial working load	N
F_{Amax}	Maximum axial working load	N
F_{ext}	applied external force	
F_{KA}	Minimum clamp load at the opening limit	N
F_{Kerf}	Clamp load required for sealing functions, friction grip and prevention of one-sided opening at the interface	N
F_{KP}	Minimum clamp load for ensuring a sealing function	N
F_{KQ}	Minimum clamp load for transmitting a transverse load and/or a torque by friction grip	N
F_{Mmin}	Minimum assembly preload or pretension	N
F_{Mmax}	Maximum assembly preload or pretension	N
F_{PA}	Proportion of external load that relieves the bolted joint	N
$F^b_{PT,EL}$	axial load at bolt with both external force and pretension	

Symbol	Definition	Unit
F_{PT}^{b}	axial load at bolt with only pretension	
F_Q	Transverse load normal to the bolt axis	N
F_{SA}	Total bolt load	
F_Z	loss of preload as a result of embedding during operation	
I_{BT}	moment of inertia of the clamped interface	
k_S	Fatigue reduction factor	
M_B	Bending moment at root	
M_{Bmax}	Maximum effective working moment	
M_m	Mean bending moment	
M_{max}	Maximum bending moment	
M_{min}	Minimum bending moment	
M_{Bmax}	Maximum effective working moment	
M_R	Bending moment range	
n_i	number of cycles in load history at stress i	
N_i	number of cycles to failure at stress i	
N	Number of cycles	
N_b	Number of bolts in the blade root	
p_U	Probability density function at inflow velocity U	
P	Pitch of thread	
P_n	Effective axial load	
P_{WT}	Power output of turbine	kW
PP	Total turbine yield over lifetime	
r	radius of rotor	m
R_{BCD}	radius associated with the Bolt Circle Diameter	m
s_{sym}	distance from the bolt axis to imaginary symmetrical axis of the clamped part	
S_a	Stress Amplitude	
S_m	Mean stress	
S_{range}	Stress Range	
T	Service life	
u	distance of the opening edge from the bolt axis	
U_{in}	Cut-in velocity	
U_{out}	Cut-out velocity	
V	wind speed	m/s
α_A	Tightening factor	
γ_M	Partial safety factor for fatigue	
μ_G	Coefficient of friction of thread	
ρ_{air}	Density of air at the site	$[kg/m^3]$
σ	stress	
σ_a	stress amplitude	
σ_{ext}	applied external stress	
σ_m	mean stress	
σ_{max}	maximum stress	
σ_{min}	minimum stress	
$\sigma_{PT,EL}^{b}$	stress at bolt with both external force and pretension	
σ_{PT}^{b}	stress at bolt with only pretension	
$\sigma_{pretension}$	stress at pretension	
σ_R	stress range	
σ_{HH}	Total effective stress (Huber's equation)	
$\sigma_{HH-oper}$	Total effective stress during operation (Huber's equation)	
$\sigma_{oper-no-preload}$	Maximum stress developed in shank during operation under zero preload	
σ_t	Maximum tensile stress in bolt shank due to pretension	

Symbol	Definition	Unit
σ_{yield}	Yield stress of bolt material	
τ	Torsional shear in shank due to friction in thread	
ϕ_{load}	load ratio	
$\phi_{load,at\mathcal{D}=1}$	Load ratio when damage $\mathcal{D} = 1$	
ϕ_{stress}	stress ratio	

This page intentionally left blank.

List of Figures

1.1 Wind energy generation by region . . . 1
1.2 T-bolt connection (left) and an insert connection (right) . . . 3

2.1 Various connection methods used for the blade-root joint: (a) Sucker-rod design [7] (b) T-bolt connection [9] (c) Insert connection [9] (d) Bushing design patent [10] . . . 5
2.2 An illustration of tension being developed in the bolt, and compression in the clamped parts, when torque is applied to the bolt through the nut . . . 7
2.3 Tubular lap joint (Source: Author) . . . 10
2.4 Stress distribution in a lap joint under shear [25] . . . 10
2.5 Coordinate system for the blade [15] [27] . . . 12
2.6 Flapwise and Edgewise loads that result in corresponding bending moments [28](*local coordinate system in the reference image differs from the standard used in this report*) . . . 13
2.7 Load envelope for all 10 segments [27] *(Coordinate system from FLEX5 software is used here, where M_z is the edgewise bending moment) (Exact values redacted for confidentiality purposes)* 13
2.8 Types of fatigue loading . . . 15
2.9 Fatigue test result: Unnotched steel specimen (SAE 4130) (from Grover et al (1951) taken from [19]) . . . 16
2.10 Accumulated damage from various estimation methods [31] . . . 17
2.11 Stress-strain hysteresis loops used for counting discrete cycles [33] . . . 17

3.1 Outline of methodology . . . 21
3.2 Phases of model reduction using symmetry (Global model shown on extreme right, final reduced model shown on extreme left) . . . 22
3.3 Hub (left) and the slew ring bearing (right) (not representative of the model) [38] [39] . . . 23
3.4 Geometric Model: Bearing Assembly, Hub, and Spacer . . . 24
3.5 Design - Exploded View . . . 24
3.6 Design - Blade Side . . . 25
3.7 Initial design (top) and improved design (bottom) . . . 26
3.8 Sectional view (top) and external view of the improved bushing (bottom) . . . 26
3.9 Bushing Design patented by Kuipers [10] . . . 27
3.10 Shell model of the full blade (top) [43], where the length is much greater than the thickness of the blade, and the solid model used in the thesis (bottom), where all dimensions are significant and the model includes stress concentrations. . . . 28
3.11 Evolution of the bolt through mesh structuring and refinement:(a) shows the bolt comprised of tetragonal elements, (b) shows the mesh redefined using hexagonal structured elements, and (c) shows the mesh refinement . . . 28
3.12 Mesh generated on the entire assembly (a) Right View (b) Left View (c) Mesh refinement at areas of stress concentration (i.e., on the bolt and the bushing) . . . 29
3.13 (a) Global coordinate system for the model (b) Local coordinate system for the laminate and the insert in case of UD material assignment . . . 29
3.14 'No Separation' contact regions between the races and the ball bearings (marked in the yellow frame) . . . 30
3.15 Frictional contacts are present between the bearing and the blade-side assemblies, between the hub section and the bearing assembly, and between each respective nut to the surfaces of the races (see labels A, B, C, D, and E) . . . 31
3.16 Bonded contact between threaded members, highlighted by the blue frames. . . . 31
3.17 Bonded contact between adhesively-bonded members: Bushing, insert, wedge, and the laminate. 31
3.18 Frictional support (on the faces shaded in blue) to replicate the effect of applying symmetry reduction (a) Right View (b) Left View . . . 32

3.19 Fixed boundary condition applied on three faces of the hub component (marked with red lines) . 32
3.20 Stresses induced at the blade root circumference due to the applied moment 33
3.21 Surface on which load has been applied 33
3.22 Tabular data of the applied normal force derived from Equation 3.1 (right) and the graph plotting the application of load with respect to the analysis step 34
3.23 Application of preload through electric torque wrench on a wind turbine blade root (left) and hydraulic tensioning, where the bolt thread or shank is stretched so that the nut needs zero torque (right) 34
3.24 The highlighted surfaces on the right shows the clamped area A_D. 35
3.25 Coefficients a and u with respect to the joint geometry 35
3.26 Pretension applied on the bolt shank for the main bolt and the hub bolt. 37

4.1 Deformations in the Y-axis at true scale (above) and 30x enlarged scale (below), at maximum compressive load 39
4.2 Deformations in the Y-axis at true scale (above) and 30x enlarged scale (below) at maximum tensile load 40
4.3 Strains in the laminate and wedge 40
4.4 Strains in the laminate and wedge 41
4.5 Maximum value of displacement in the Z-direction is 0.09mm, or 90μ m 41
4.6 Stresses are extracted from the nodes named A (BladeOutside), B (HubOutside), C (HubInside), and D (BladeInside). 42
4.7 Stress developed in the bolt when pretension ($F_{vmin} = 318.57kN$) has been applied and there is not external load. (a) shows the sectioned view, and (b) shows the un-sectioned view of the bolt. Tensile stresses were developed in the bolt shank due to pretension, and compressive stresses at the ends where the bonded connection simulates the threaded joint. Stress concentrations can be seen at the area where the diameter decreases (*All values in MPa*). 42
4.8 Stress developed in the bolt when pretension ($F_{Mmax} = 446kN$) has been applied and there is not external load.(a) shows the sectioned view, and (b) shows the un-sectioned view of the bolt. The increase in stress due to pretension can be seen in the legend (*All values in MPa*). 42
4.9 Stress developed in the bolt at F_{vmin} and at maximum compressive load corresponding to a bending moment of $-16000kNm$.(a) shows the bolt at 1x scale, and (b) shows the bolt at 50x scale. The compressive load relieves some of the stress in the preloaded bolt, which is evident from the decrease in stress compared to Figure 4.7(*All values in MPa*). 43
4.10 Stress developed in the bolt at F_{Mmin} and at maximum tensile load corresponding to a bending moment of $16000kNm$.(a) shows the bolt at 1x scale, and (b) shows the bolt at 50x scale. The external tensile load increases the effective stress in the bolt shank (*All values in MPa*). 43
4.11 (a) shows the normalised stress profile that was the result of FE analysis on the connection (at minimum pretension) (b) shows the results from the design prototype available with Suzlon [21] with respect to the external moment (*Exact values have been redacted due to confidentiality clauses*) 43
4.12 Displacement in the direction of tensile force at (a) 12000kNm (b) 14000kNm (c) 16000kNm (63x scale, $F_{vmin} = 318.57kN$) 44
4.13 (a) shows the normalised stress profile that was the result of FE analysis on the connection (at maximum pretension) (b) shows the results from the design prototype available with Suzlon [21] with respect to the external moment (*Exact values have been redacted due to confidentiality clauses*) 44
4.14 Stress Ratios and SRF 45
4.15 Steps used to evaluate fatigue damage 46
4.16 S-N Curve for bolt according to GL and Eurocode standards 47
4.17 Load history for a load ratio of $\phi_{load} = 0.117$ 48
4.18 Value of damage $\mathcal{D}$ with respect to load ratio ϕ_{load}, for the base blade root configuration of 96 bolts 49
4.19 Effect of load history on the numerical value of damage 49
4.20 Trend of SRF with respect to Load Ratio (96-bolt configuration) 50

5.1 Contributions of the blade-root components to the total weight and cost 51
5.2 Rear view of the connection. Angular section per bolt increases as the bolts decrease. 52
5.3 Change in Load ratio in the bolt with respect to number of bolts 53
5.4 Trend of damage values with respect to number of bolts 53

5.5 Trend of weight and cost of the full blade root with respect to number of bolts 54
5.6 Increased external moment developed at blade root 55
5.7 Effect of increased load on stress and load ratio 55
5.8 Performance of glass fibres 56
5.9 Performance of carbon fibres 56
5.10 57
5.11 Base configuration (top), and configuration with reduced diameter (bottom) 57
5.12 Effect of bushing size on load ratio, weight, and cost 57
5.13 (a) Geometry of wedge in base configuration; (b) Modified geometry featuring a ring wedge, seen for the full root 58
5.14 Effect of increasing wedge volume on load ratio, weight, and cost 58

6.1 Stress concentrations developed at the root laminate around the barrel nut hole 59
6.2 Failure mode of T-bolt 59

B.1 Iterations of the blade root, given in sequential order 73

C.1 Dimensions 75

This page intentionally left blank.

List of Tables

2.1 Values for maximum bending moment [27] [29] 14
2.2 Partial Safety Factors [15] 14

6.1 Stress ratios: Bushing connection and T-bolt connection 60
6.2 Weight comparison between the two connection types (Bolt weights have not been added) 61

A.1 Material Data: Base configuration 71
A.2 Material Data: Comparative Analysis 71
A.3 Material data used for generating SN Curve (Bolt steel) 71

E.1 Values of bolt stress, load ratios and stress ratios - Blade Side, for F_{Mmin} 79
E.2 Values of bolt stress, load ratios and stress ratios - Hub Side, for F_{Mmin} 79
E.3 Values of bolt stress, load ratios and stress ratios - Blade Side, for F_{Mmax} 80
E.4 Values of bolt stress, load ratios and stress ratios - Hub Side, for F_{Mmax} 80
E.5 Normal force developed per unit bolt connection for the given external moment, and calculated pretension for a uniform clamping force 81

This page intentionally left blank.

1 Introduction

1.1. Background

Climate change is, and has been for several decades, a growing concern globally. Most regions of the world will be directly affected by rising sea levels and unprecedented weather events, and other regions will face indefinite economic and social repercussions, or in some cases, both. There has hence been a sustained effort in decreasing the global dependency on fossil fuels for energy generation; wind energy accounts for 13% of the total electricity generated from renewable sources, following significant contributions by hydro-power and nuclear energy [1].

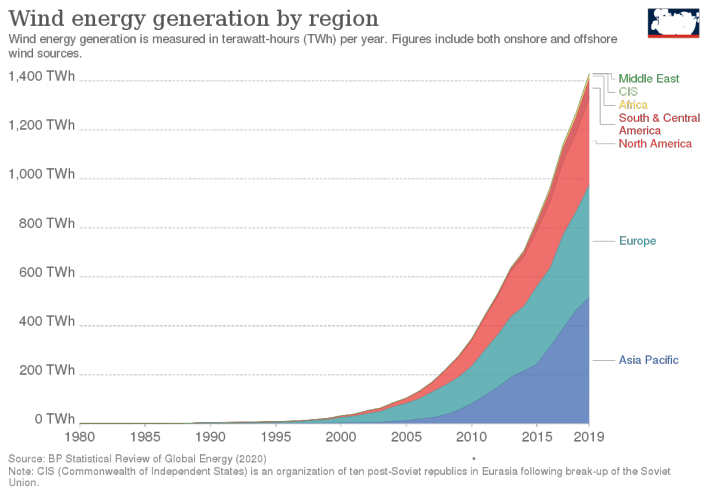

Figure 1.1: "Wind energy generation by region" [2]

Wind power has shown an exponential increase globally, rising from an installed capacity of 6.1 GW in 1996 to 651 GW as of 2019. Europe accounts for a significant share of the global energy output from wind, and when ranked for installed wind power capacity per capita, 11 European countries feature in the top 12 in the world [3]. There are efforts being carried out to triple capacity levels of 2015 by 2023, and naturally, large-scale on-shore and offshore wind projects are being drafted. As with other sustainable and clean sources of energy, wind power must prove to be cost-effective and efficient in order to justify the high initial investment required for manufacturing and installation, impact to wildlife, its significant use of land, and switching costs from conventional sources of energy. This is sometimes quantified as the Cost of Energy (CoE):

$$CoE = \frac{CoT + CoI + CoM}{PP} \tag{1.1}$$

where CoT is the cost of the turbine (materials and manufacturing), CoI is the cost of installation and transportation, CoM is lifetime cost of operation and maintenance, and PP is the total yield produced over the turbine's lifetime [4]. Future trends for wind turbines aim at decreasing the value of CoE, which can be summarised in the following points:

- Increase the annual yield.
- Decrease the costs associated with the production, installation, and operation of wind turbines.

A popular method used by most wind turbine manufacturers to reach the above goals is to increase the length of turbine blades. A simple reason for this lies in the following formula for the power output of a wind turbine [5]:

$$P_{WT} = \frac{1}{2} \cdot \rho_{air} \cdot C_p \cdot \pi r^2 \cdot V^3 \tag{1.2}$$

where P_{WT} is the power output of the wind turbine in kW, r is the radius of the rotor or the length of the blade, V is the wind speed, and ρ_{air} is the density of air at the site. Annual yield PP in the previous equation is directly proportional to P_{WT}. It can be seen that the power output is proportional to the square of the length of the wind turbine blade, and for this reason, the average blade length has increased over the years. This trend has been bolstered by the introduction of light materials and optimised designs. This has been quantified by Jensen and Branner [4] who note that while the weight of wind turbine blades should increase by an exponent of three with a linear increase in blade length, weights have only increased by a power of 2.3.

1.2. Wind turbine Blade and Blade Root

Structurally, wind turbine research is also focusing keenly on improving the reliability and life of the wind turbine, as the costs associated with manufacturing and installation need to reach and cross the break-even point for a wind farm. This leads to an expectation that the life of wind turbines should be in the region of at least 25 years. Blades are structurally the most load-bearing components in the wind turbine, and they are to be designed such that they sustain at least 10^9 fatigue cycles over the course of 25 years. This factor is much greater than, for example, bridges, which are expected to sustain 10^7 to 10^8 fatigue cycles over 50 to 70 years [4]. End-of-life uses of decommissioned wind turbine blades are few and most are scrapped, and additionally, repair costs are expensive in terms of capital, time, and manpower. Hence, a major design constraint is to improve the life of the blades.

Within the structure of the wind turbine blade, the blade root connection, or the joint that connects the blade to the hub, is of special concern. Aerodynamic and gravitational loads on the blade increase from the tip to the root, making it a highly stressed region in the structure. The root region is also critical due to the large gradient in stiffness; loads are transferred from the blade made of laminates or laminate-wood sandwich panels to the steel hub through steel bolts. Additionally, the bolted connections induce stress concentrations in the composite material of the blade. Hence, it is imperative that the connection be designed keeping in mind the following factors:

- It should satisfy structural and fatigue requirements.
- Material and manufacturing methods should be economically feasible.
- On-site assembly should be achievable given the current methods.
- Repair and maintenance requirements should be minimum.

1.3. Research Objectives and Questions

Almost all blade root connections feature threaded members secured co-axial to the blade axis. The most common type of blade-root design used by commercial wind turbine manufacturers for modern composite blades has been the T-bolt or the cross bolt connection. It was first designed with an objective to reduce blade weights and manufacturing costs. It consists of an axial bolt connected to a cylindrical barrel nut fixed perpendicular to the blade axis (See Figure 1.2). However, manufacturers have gradually replaced the T-bolt connection with variations of insert designs due to several shortcomings. The introduction of a lateral hole through drilling leads to severe stress concentrations at the blade root region, an already crucial area structurally. The laminate bears crushing stress and hence has to be thicker, costing the manufacturer in terms on money and weight.

Suzlon Energy Ltd currently uses the T-bolt connection in their blades. While the connection has shown adequate results over the years, present research trends focus on designing longer blades. The requirement for a blade root connection that is both reliable and feasible for longer blades has been the motivation behind this thesis. The problem statement provided by them is as follows:

"Develop a blade root connection with bushings."

Using a T-bolt connection means designing a thicker laminate due to the severe stress concentrations; for a longer blade, this translates to a proportional increase in weight of the blade and the cost incurred for the material.

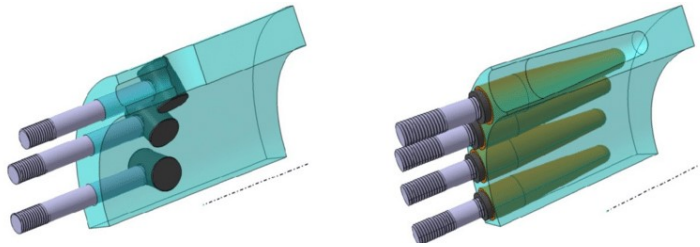

Figure 1.2: T-bolt connection (left) and an insert connection (right) [6]

Replacing the current connection with a bushing or an insert connection offers several advantages: the mode of load transfer is achieved through significantly less severe shear forces instead of bearing stress on the laminate. A lighter design is possible, leading to savings in weight and cost and allowing for longer blades. Due to fewer geometrical constraints, a higher number of bolts can be introduced for a given BCD (Bolt Circle Diameter). A higher number of bolts leads to quantifiably less load per bolt, improving fatigue life of the root, and allows for longer blades for the same root design.

The aim of this thesis is to provide a preliminary basis for the design of a bushing connection for a 63m Suzlon-make blade using FEA software (Ansys Inc as used by Suzlon Energy). The design constraint against which the design will be validated for will be the fatigue damage developed in the bolt, due to it bearing the most stress in a given bolted tubular lap joint. The objective is to also provide a comparative study on the effect of different geometrical and material configurations on the performance of the blade-root connection. While experimental coupon testing is beyond the scope of this study, the results of this thesis are expected to provide a foundation for feasible design of experiments. Given that it is a project with commercial implications, the weight of the joint, and cost of materials and manufacturing will also be of importance.

The objective of this master thesis can be summed up as follows:

"To conduct a study on a blade root connection incorporating bushings by: (i) ensuring the designs meet fatigue damage requirements set by industry standards (ii) comparing the effect of different material configurations (iii) comparing the effect of different geometrical configurations (iv) analyzing the implications on weight and cost of the joint."

Given the above research objective, the following research questions have been formulated:

1. What design requirements do the existing blade-root connections fulfill, and what are their drawbacks? Specifically, what are the limitations of the T-bolt design that can be overcome using a bushing design?
2. How can a design be realised such that the critical component in fatigue in the connection is the bolt instead of the laminate?
3. Given that the root design fulfills the criteria for fatigue damage, what key parameters within the design can be analysed for feasibility studies?

1.4. Structure of the report

Keeping in mind the research questions, the thesis report has been structured as follows:

1. Literature Study and Theoretical Foundations: The objective of this section is to give a brief introduction to blade-root joint designs, and the design principles followed by turbine manufacturers. The chapter also lays down the theoretical foundations of the connection type, the operating load conditions, and fatigue analysis principles followed for wind turbines. Standards followed by the wind turbine industry are also introduced.
2. Design Study: This chapter explains the design process followed by the in creating the FE model; design principles explained in the Literature Study are used throughout this section.
3. Model Analysis and Validation: This section follows the methods used to validate the model for applicability.
4. Comparative analysis: Given the commercial relevance of the blade-root connection, this section focuses on the influence of various parameters with respect to economic value to the industry.
5. Results: This chapter summarizes the observations of the design study, drawing up a comparison between the existing T-bolt design and the Bushing connection. It also discusses the implications of the comparative analysis.

This page intentionally left blank.

2

Literature Study and Theoretical Foundations

This chapter will touch upon the relevant designs that have been used by the industry, the theoretical foundations for the design, and analysis procedures based on previous research. Observations made of previous connections have been considered for the present design.

2.1. Blade Root Connections

2.1.1. Early Designs

The first wind turbines that were used commercially for power generation had blades made of wood-epoxy composites, and blade lengths were relatively shorter than those being produced now. Initial designs for blade root connections incorporated an embedded metal insert, usually a steel rod, that was adhesively bonded on one end to a drilled hole in the wood ply and epoxy laminate, and pretensioned on the other end, noted by Eckland and Frerotte [7]. As blade lengths grew, other designs were put into use, like the metal flange connection, which constituted up to a third of the total blade weight, as observed by Hau [8]. Insert connections were more popular during this era due to their light weight. Another popular design that was used was the sucker-rod connection, inspired from machines used in the oil industry [7]. The blade root region sees the interaction of several components, leading to a high degree of stiffness gradient; to counter this, use of materials like chopped carbon fiber have been demonstrated to improve fatigue performance.

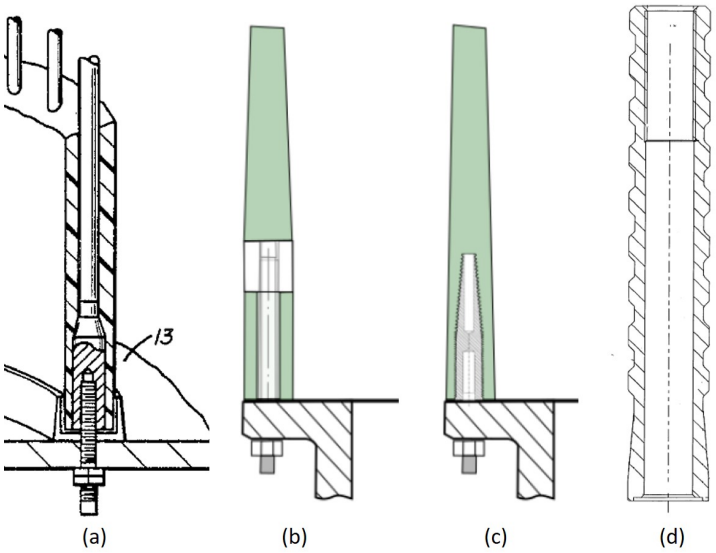

Figure 2.1: Various connection methods used for the blade-root joint: (a) Sucker-rod design [7] (b) T-bolt connection [9] (c) Insert connection [9] (d) Bushing design patent [10]

2.1.2. T-bolt to Bushing Connection

The T-bolt connection, also called the IKEA joint, has been used by wind turbine manufacturers exclusively in the last few decades owing to its reliable assembly methods, fault-tolerant manufacturing processes, and the potential to incorporate automated assembly. However, Nijssen [9] notes that local damage to the laminate caused by drilling lateral holes at the root results in mediocre fatigue performance and a thicker root. A study on the blade root connection comparisons by Jackson et al. [11] evaluated that for a blade root with a BCD of 2.66m, the weight of the root attachment can be decreased to 60% of the previous weight if a bushing connection with a double-threaded stud is used in place of a T-bolt connection, along with a 30% reduction in total cost. The elimination of a lateral hole (for the barrel nut) reduces the area of stress concentration in the blade root region, which means more bolts can be accommodated per BCD. Increasing the number of bolts leads to quantifiable improvement in fatigue performance as lower stress is developed per bolt.

A number of patents developed by wind turbine manufacturers exists for variations of bushing designs. Aerovide GMBH [12] developed a tapered bushing connection to streamline load transfer fromm the insert to the laminate. However, a drawback of this design is the difficulty in manufacturability while maintaining compliance to dimensional quality, increasing costs associated with assembly. Modern bushing designs are based on patents published by Vestas Wind Systems in 2006 [13]. The design consists of an insert than can be assembled through VARTM within the blade laminate, and is pretensioned using a stud bolt connected to its internal threads. Kuipers [10] patented another bushing design aimed at increasing the bonded area between the insert and the laminate; this was achieved through equivalently spaced ribs that increase the adhesion area. The design also claims to induce a lower shear stress in the laminate with the use of a tapered section on end of the bushing. The test results of this particular design were verified by Nijssen [9] through certified pull-out and fatigue tests.

2.1.3. Evaluation for the design of the bushing

Experiments and designs present in literature suggest that the basic geometrical design of the bushing/insert should aim at:

- Increasing the bonded area between the bushing and the laminate.
- Decreasing the severity of shear stress that is transferred from the bushing to the laminate.
- Optimising the manufacturability and ease of assembly of the design, along with reliability over multiple assembled parts.

The aforementioned points are common justifications to designs present in the literature for a bushing-incorporated root. However, blade root performance is often proprietary data, and it is hence difficult to obtain verifiable and quantifiable results about the efficiency of a particular bushing design. There are several published papers on both the analytical and experimental testing of T-bolt designs for fatigue performance, but there is a considerable gap in literature for a bushing connection that has been evaluated for fatigue performance and has also been optimised at a basic level for cost and weight.

This thesis study aims to close this gap by providing a comprehensive comparison of the effect of geometrical and material parameters on the performance of a bushing connection. The final stage of wind turbine design, and often a very crucial one, is the full-scale (in the order of several million cycles) blade testing, before which sub-components like the root undergo coupon testing. Experimental analysis is a cost-intensive exercise, and designs are required to be reliable to a satisfactory degree before coupons can be manufactured. The results of this study can be expected to provide a reference for future designs, and to serve as a base for experimental coupon testing.

2.2. Bolted Joint

The bushing connection has two interfaces for load transfer: the pretensioned bolted connection between double-ended stud and the internal threads of the bushing, and the adhesively bonded joint between the bushing and root laminate. The scope of this thesis is limited to the former for the following reasons:

- The stress developed due to the sum of the pretension and the external loads are concentrated on the bolted joint, making it a crucial area for fatigue.
- Numerical analysis of bonded joints is a challenging endeavour due to the non-linear behavior of adhesives, especially in the case of joining of dissimilar materials, and according to industrial standards for wind turbines, require extensive experimental testing before they can be certified.

While bonded joints will not be considered for numerical analysis, industry standards will be discussed and engineering judgement will be used to establish the interface.

2.2.1. Standards and pre-requisites

Suzlon Energy Limited refers to the standards set by Verein Deutscher Ingenieure (Association of German Engineers, or VDI) [14] for highly stressed bolted joints while designing the blade-root connection. A pre-requisite design criteria provided for this thesis is that a double-ended stud bolt is to be used with the bushing. The stud is required to have a reduced shank, and given that it is a highly stressed component, the grade of the bolt is taken to be 10.9. The length of the bolt is variable that will be quantified according to the results of the FE analysis and fatigue performance. The S/N curve for the bolt is referenced from standards set by Germanischer Lloyd (GL) [15].

2.2.2. Principles of Single Bolted Joints

Calculation of Pretension in Bolts

Pretension can be defined as "the tensile load developed in bolts during assembly when they are tightened using external torque or hydraulic tightening methods". It has been observed by multiple researchers independently (Fisher et al (1952) [16], Kate et al (2013) [17], Shahani et al (2015) [18] etc) that applied preload or pretension to bolted joints improves the fatigue performance of the joint. The theoretical backing for this phenomenon has been explained by Schijve [19] cites Elber [20] on plasticity induced crack closure, wherein a positive tensile stress near the yield limit of a ductile material aids in crack growth retardation, and hence increases fatigue life. The presence of a pretension or a preload on a bolt ensures that the external applied load is borne by the interface of the fastened bodies as well. Hence, the applied pretension of the bolt has a direct correlation to the fatigue damage sustained by the blade root.

Computational limits on the version of FEA solver used make the use of a symmetrical model necessary. Hence, the bolted joint will be analysed according to the principles provided for a Single Bolted Joint (SBJ) [14] [15]. For the purposes of this design study, the deviations of the symmetric model from a full model have been deemed acceptable [21].

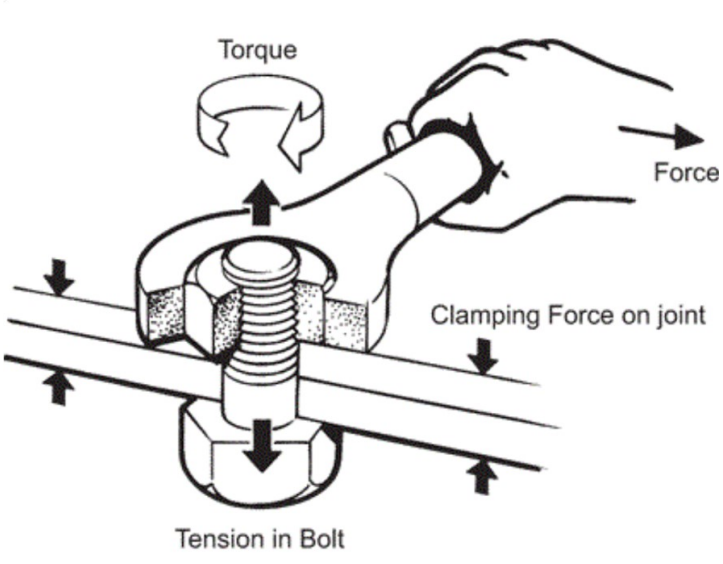

Figure 2.2: An illustration of tension being developed in the bolt, and compression in the clamped parts, when torque is applied to the bolt through the nut [22]

The steps that will be followed for calculating the bolt pretension are as follows:

1. Determine external forces: These are an input to the design of the joint to calculate the minimum preload levels. The loads to be known are: F_A - axial working load, F_Q - transverse load, M_b - bending moment, M_T - torque on the joint.
2. Determine nominal diameter d : This has been provided as an input by Suzlon. The standard bolts to be used are to be in the range of M36 to M39.
3. Determine tightening factor α_A: The tightening factor is the ratio between the maximum assembly preload and the minimum assembly preload. This factor is incorporated in the design phase because during as-

sembly, there is considerable scatter in the applied preload on the bolt. The value of α_A depends on the tightening and setting methods used.

4. Determine minimum clamp load F_{Kerf}: A minimum value of the clamp load is to be determined according to the following requirements:

   - There should be enough frictional grip (F_{KQ}) to transmit transverse loads, if any.
   - The clamp load should provide a sealing function (F_{KP})
   - The clamp load should prevent opening of the joint under an axial load (F_{KA})

   Hence, the following relationship is obtained:

   $$F_{Kerf} \geq max(F_{KQ}, F_{KP} + F_{KA}) \tag{2.1}$$

   In case of a bolted connection at the blade root, transverse loads are negligible compared to axial loads. Additionally, no sealing is required as there is no internal pressure from fluids or a cause to seal them from leaks. Hence, only F_{KA} is required to calculate the minimum clamp load, which is caluclated as follows:

   $$F_{Kerf} = F_{KA} = F_{A_{max}} \cdot \frac{A_D \cdot (a \cdot u - s_{sym} \cdot u)}{I_{BT} + s_{sym} \cdot u \cdot A_D} + M_{B_{max}} \cdot \frac{A_D \cdot u}{I_{BT} + s_{sym} \cdot u \cdot A_D} \tag{2.2}$$

   where $F_{A_{max}}$ is the maximum axial load, A_D is the sealing area, a is the eccentricity of the loading axis from the bolt axis, s_{sym} is the distance from the bolt axis to imaginary symmetrical axis of the clamped part, u is the distance of the opening edge from the bolt axis, and I_{BT} is the moment of inertia of the clamped interface. For a singular bolt under analysis, effective working moment $M_{B_{max}}$ is zero, and hence the second term of the equation will not be considered for calculation.

5. Determine load ratio ϕ: The load ratio is ratio between the total load on the bolt (preload and external) to the external load applied to the assembly.

   $$\phi_{load} = \frac{F_{SA}}{F_A} \tag{2.3}$$

   $$F_{PA} = (1 - \phi_{load})F_A$$

   where F_A is the external axial load, F_{SA} is the total bolt load (preload + external), and F_{PA} is the proportion for external load that relieves the bolted joint. For the bolted joint under analysis, the external load is not directly applied on the joint, but is borne by the laminate. Hence, the value of the load factor will be calculated from the results of the FE analysis. Estimation of the value of ϕ for the joint enables optimisation of the design and subsequently the calculation of fatigue damage.

6. Determining change in preload due to embedding and change in temperature: Temperature changes and the setting of clamped parts may act in decreasing the preload value. A factor within engineering limits has to be determined to account for relaxation due to the elasticity of the material and the temperature changes in the environment. The loss of preload due to setting of clamped parts is termed as F_Z and the loss due to differences in thermal coefficients of expansion is termed as ΔF_{Vth} in literature [14].

7. Determine minimum assembly preload: The above pre-requisite inputs and determined factors are used to calculate F_{Mmin} (defined as the "minimum assembly preload which can occur at F_{Mmax} as a result of lack of precision on the tightening technique and maximum friction" [14]), which can be summed up as follows:

   $$F_{Mmin} = F_{Kerf} + (1 - \phi^*_{en})F_A + F_Z + \Delta F_{Vth} \tag{2.4}$$

   where ϕ^*_{en} is the load factor in case of eccentric loading, F_Z is the loss of preload due to embedding during operation, and ΔF_{Vth} is the change in preload due to temperature gradient.

8. Determine maximum assembly preload: The above steps are consolidated to find F_{Mmax} (defined as "maximum assembly preload for which a bolt must be designed, so that, in spite of lack of precision in the tightening technique and the expected embedding during operation, the required clamp load in the joint is produced and maintained" [14]).

   $$F_{Mmax} = \alpha_A \cdot F_{Mmin} \tag{2.5}$$

A minimum and a maximum value of bolt pretension is considered necessary due to presence of scatter in the applied pretension during assembly. Application of torque on adjacent bolts affects the value of pretension. Additionally, post-assembly and during operation, the blade root sees the embedding of surfaces and relaxation of joints due to creep, leading to preload 'loss'. Finally, as the wind turbine is exposed to environmental conditions, a significant temperature gradient is expected. Differences in thermal expansion coefficients will affect the value of preload. Hence, a minimum value of pretension is necessary to ensure clamping, and a maximum value is necessary to analyse response to extreme loads and fatigue performance.

Calculation of stress in bolts
The following calculations are based on analytical methods provided in the standards set by VDI [14] and manuals provided by Suzlon Energy [23]. To validate the design(s), these initial conditions should be met.

1. Ultimate strength of bolt shank during assembly:
   Maximum tensile stress in bolt shank due to pretension:

$$\sigma_t = \frac{F_{Mmax}}{A_{shank}} \tag{2.6}$$

   Torsional shear in shank due to friction in the thread:

$$\tau = F_{Mmax} \frac{1.155 \cdot \mu_G \cdot \frac{d_2}{2} + \frac{P}{2\pi}}{\frac{\pi}{16} \cdot D_{shank}^3} \tag{2.7}$$

   where: d_2 is the pitch diameter of the bolt thread, P is the pitch of the thread, μ_G is the coefficient of friction for the thread, and D_{shank} is the diameter of the shank.
   The total stress, according to the relation based on distortion strain energy provided by Huber in 1904 [24], is calculated as follows:

$$\sigma_{HH} = \sqrt{\sigma_t^2 + 3\tau^2} \tag{2.8}$$

   According to the guidelines set by Germanischer Lloyd [15], a partial safety factor $\gamma_M = 1.1$ is to be followed for all load cases. The admissible stress is the ratio between the yield stress of the bolt σ_{yield} and σ_{HH}, and it is to be greater than γ_M so that the bolt stress stays within permissible limits during assembly.
2. Ultimate strength of shank during operation:
   According to the observations in Suzlon [23], the torsional stress due to preload in the shank during operation reduces to 50% of its value, i.e., $\tau_{0.5}$. The combined stress (when there is only preload) is hence:

$$\sigma_{HH-oper} = \sqrt{\sigma_t^2 + 3\tau_{0.5}^2} \tag{2.9}$$

   The maximum stress $\sigma_{oper-no-preload}$ developed in the shank during operation due to external applied load when there is no preload at the maximum bending moment M_{max} is found from the following analytical calculation:

$$\sigma_{oper-no-preload} = \frac{M_{max}}{R_{BCD} \cdot A_{shank} \cdot N_b} \tag{2.10}$$

   where R_{BCD} is the radius of the blade root at the BCD, A_{shank} is the area of the shank, and N_b is the total number of bolts in the BCD. Multiplying $\sigma_{oper-no-preload}$ with the bolt stress ratio ϕ found from the FE analysis results in the actual stress developed in the shank σ_{oper}. The total stress during operation is the sum of σ_{oper} and $\sigma_{HH-oper}$. The design will be validated if the stress reserve factor (the factor defining the extent by which the bolt material strength can be reduced) is greater than 1; it is calculated as follows:

$$SRF = \frac{\sigma_{yield} - \sigma_{HH-oper}}{\sigma_{oper}} \tag{2.11}$$

2.2.3. Evaluation for the design of bolted joints

Structural design and application of a bolted joint determine the joint's parameters like the applied pretension and its size. Wind turbine component design can only be certified on the basis of design standards set by organisations like IEC, GL, and VDI. FE analysis will be used in conjunction with the above steps to verify the strength and durability of the bolted joint. The design constraint for a bolted joint in a wind turbine root is fatigue damage, and this will be used to finalize the design parameters. As mentioned, scatter in the applied pretension on the bolt is to be expected, and hence the results of the study will have a tolerance value that has to be experimentally verified.

2.3. Bonded Joints

The design considerations for bonded joints incorporated in the design will be based on experimental observations made in literature, as a theoretical basis for these joints is beyond the scope of this thesis. The initial prototype of the blade root connection consists of bond between the bushing, made of steel, and the composite laminate or an bushing. The joint can be approximated as a "tubular lap joint", where the adhesive layer is subject to shear loading (as the part is subject to axial and bending loads), as can be seen in Figure 2.3 .

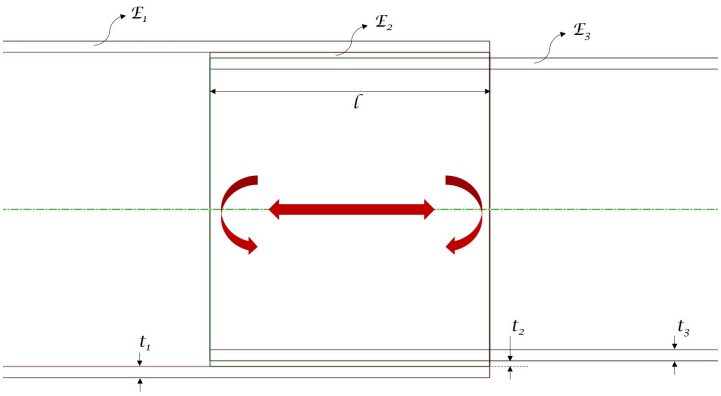

Figure 2.3: Tubular lap joint (Source: Author)

Shear tests on a lap joint produce a 'bathtub curve' for the stress in the adhesive layer when the data is plotted against the length of the bond, or the overlap. The shape of the curve suggests a stress concentration towards the edges of the lap joint; this has been explained in literature [25] by the differences in stiffness between the adhesive and the adherent, and because of the change in geometry and topology. The shape can be seen in Figure 2.4.

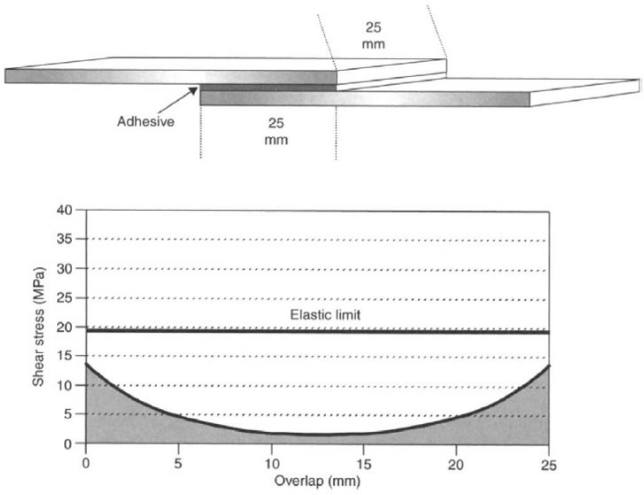

Figure 2.4: Stress distribution in a lap joint under shear [25]

According to Moulds [25], the strength of a bonded lap joint depends on: the Young's modulus of each adherend (E_1 and E_3), the thickness of each adherend (t_1 and t_3), the Young's modulus of the adhesive (E_2), and the thickness of the adhesive layer (t_2). He made the following observations for a general lap joint under shear from experimental results:

- While increasing the bond length or the overlap length did not decrease the maximum shear stress significantly, the stress around the centre of the joint reduced, which might improve creep performance.
- increasing (t_1 and/or t_3) resulted in a decrease in maximum stress values.
- Increasing the adhesive or the bond line thickness (t_2) also results in a decrease in the maximum shear stress, and flattens the bathtub curve.

- In case of significant differences in the stiffnesses of the two adherents (i.e., between E_1 and E_3), the resultant bathtub curve will be asymmetrical. Larger differences in the moduli result in a correspondingly higher stress concentration towards one end.

There is extensive literature present on the performance of a basic bonded lap joint, and considerably less research on tubular lap joints where the shafts are subject to axial and/or bending loads. Almost all studies present on the topic use experimental tests in conjunction with analytical and/or FE results to verify observations. As Sutherland [26] observes, performance of the joint varies according to geometry, adhesive material properties, operating conditions like temperature and humidity, and load application modes. As an experimental study is beyond the scope of this thesis, industrial standards and norms will be followed for the design of the bonded joint.

2.4. External Operating Loads

Wind turbine component design is influenced to a significant degree by the external loads acting on the blades. The following sections will discuss the external loads that are considered in the design phase and their sources [8]:

2.4.1. Load types

1. Steady state aerodynamic loads:
   These are caused by uniform and stable air flow over a significant period of time. Initial design iterations start with the assumption of a uniform and constant wind flow. Owing to the airfoil shape of the blade, the wind loads vary from root to tip. The cantilevered structure of the blade connected to the hub leads to bending moments being the primary load case. Aerodynamic loads from steady wind will have two components: a tangential component, which results in moments in the *chordwise direction* and contributes to blade torque, and the normal or the thrust component, which results in moments in the *flapwise direction* and contributes to blade thrust. Their net resultant produces the overall rotor load and moments. Thrust and torque are approximately directly proportional to the square of wind speed, but for turbines with pitch control, the control system of the rotor will limit power capture to the rated power.
2. Gravitational and Inertial Loads:
   (a) Gravitational loads are developed due to the dead weight of the blades, are sustained by the blade in a cyclic manner. The loads generated can be divided into alternating tensile and pressure forces when the blade is vertical, and alternating bending moments around the chordwise and the flapwise axis when the blades are at an angle with respect to the vertical axis. The intensity of loads increase from the tip to the blade root. Assuming a service life of 20 to 30 years, the cyclic bending moments have a spectrum of 10^7 to 10^8 cycles. As steel reaches its fatigue limit at around 10^6 cycles, gravitational load is one of the key factors in determining the fatigue performance of the wind turbine. This influence is directly proportional to the length and weight of the blade.
   (b) Centrifugal and Gyroscopic Loads: These are inertial loads brought about by the rotation of the blades. Compared to gravitational loads, these are significantly low. The effect of these loads can be controlled by introducing a cone angle in the rotor, and by controlling the yaw rates.
3. Wind turbulence and Gust loads:
   To determine fatigue strength and life of the wind turbine, short-term variations in wind speed, namely turbulence and gusts, need to be accounted for. Turbulent winds may induce both longitudinal and lateral components of forces in the blades, leading to non-nominal load distributions. Gust on the other hand is used to define a sharp increase or decrease (negative gust) in wind speed concentrated in a small amount of time. In order to define the effect of these winds, stochastic or statistical models are used. For initial calculations, deterministic approaches can be used. Extreme wind speeds are only taken into account if the geographical location of the turbine warrants it.
4. Other Sources:
   (a) Vertical wind shear: Due to the variation in wind speed with altitude, asymmetrical loads are borne by the rotor as it rotates.
   (b) Crosswinds: Winds that approach the rotor plane at an angle different than its normal.
   (c) Tower interference: The presence of the tower retards the wind flow to the rotor and leads to either the tower dam effect (up-wind) or the tower shadow effect (down-wind).

   These load cases lead to deviation from the nominal uniform load distribution.

2.4.2. Load Cases

The loads from various sources listed above act in various combinations. To dimension the blade root components, probabilistic classification of load cases are defined as follows:

Power Production: This refers to the nominal operating conditions of the wind turbine. The characteristic wind speeds are: Cut-in wind speed (minimum wind speed for power generation), cut-out wind speed (maximum wind speed beyond which blades stand the risk of being damaged), rated wind speed (at which maximum power production is reached).

(a) Normal Operation: This includes the nominal working conditions of power generation, start-up and shut-down of rotor, and parked rotor state. The latter two occur frequently enough in the lifetime for their influence on fatigue life to be considered.
(b) Technical faults: Due to events like emergency stop, control system faults, and rotor overspeed, severe flapwise bending loads may be sustained by the rotor; these loads have to considered in the load history of the blade-root.

For material selection and structural design, analysis has to be carried out for structural failure (eg: fracture) , structural stability (eg: buckling), and stiffness of components (i.e. critical deflection). In summary, load cases are to be considered for the following cases:

- Normal wind conditions with normal machine states.
- Normal wind conditions with defective machine states.
- Extreme wind conditions with normal machine states.

2.4.3. Design Loads: Procedures by Suzlon

The design parameter provided by Suzlon is that that blade root should be designed for a SE-make blade of 63m, and with a BCD of 3000mm. The following section discusses the general standards used by the industry in determining and defining loads:

Coordinate System

The coordinate system as standardised by GL for wind turbines [15] and adapted by SE Blades for their use is shown in Figure 2.5. The same will be used for the FE analysis of this thesis. The system is aligned with the local chord when the twist is at 0°.

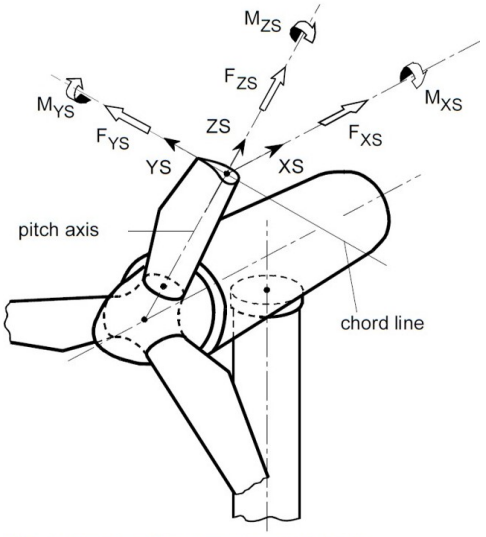

Figure 2.5: Coordinate system for the blade [15] [27]

Flapwise and Edgewise Bending Moments

The loads acting on a wind turbine blade are analysed in terms of bending moments acting about two primary axes, namely the flapwise and the edgewise bending moments. These moments are illustrated in Figure 2.6. With respect to Figure 2.5, the flapwise bending moment is M_{YS}, and the edgewise bending moment is M_{XS}.

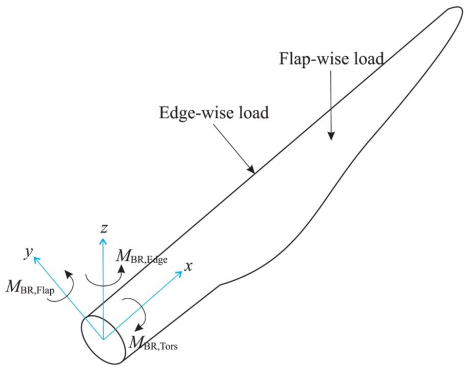

Figure 2.6: Flapwise and Edgewise loads that result in corresponding bending moments [28](*local coordinate system in the reference image differs from the standard used in this report*)

Calculated Bending Moments

Suzlon uses proprietary software (FOCUS and FLEX5) (*Note: FOCUS is commercial product licensed to LM Wind Power, and FLEX5 is an modifiable priced code developed and maintained by DTU*) for the calculation of extreme loads and resultant bending moments; these softwares are customized for wind turbine structural analyses. The blade is divided into ten segments along its length (positive Z axis), and the root section is divided into 5° segments, resulting in 72 equal sectors. The resultant component of the flapwise and edgewise moments is found and the vector with the maximum value is stored for each sector. This process is performed for each of the ten segments along the blade length, and a load envelope is obtained [27].

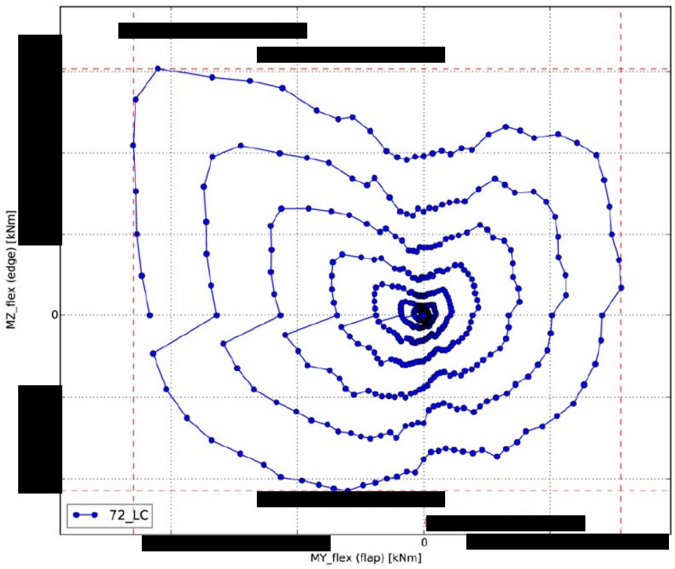

Figure 2.7: Load envelope for all 10 segments [27] *(Coordinate system from FLEX5 software is used here, where M_z is the edgewise bending moment) (Exact values redacted for confidentiality purposes)*

In Figure 2.7, the outermost load envelope corresponds to the bending moments at the blade root; it can be seen that the moments decrease from the root to the tip. These loads have been calculated by the Structural Design department of SE Blades from load sets provided for the S128 blade. For a conservative approach to the design, the values found for both SE Blade 1 (Length: 63m) and SE Blade 2 (Length: 65m) blades will be considered. These values are given in Table 2.1.

Blade	Resultant Root Bending Moment
SE Blade 1 (63m Blade)	12692.7 kNm
SE Blade 2 (65m Blade)	12997 kNm

Table 2.1: Values for maximum bending moment [27] [29]

Partial Safety Factors
The loads shown in the plot in Figure 2.7 and listed in Table 2.1 are design loads that incorporate relevant safety factors according to the standards set by Germanischer Lloyd [15]. The key safety factors related to wind turbines are listed in Table 2.2.

Load Source	Unfavourable Loads			Favourable Loads
	Design Situation			All cases
	Normal and Extreme	Abnormal	Transport and Erection	
Aerodynamic	1.35	1.1	1.5	0.9
Operational	1.35	1.1	1.5	0.9
Gravitational	1.35	1.1	1.25	0.9
Inertial	1.25	1.1	1.3	0.9

Table 2.2: Partial Safety Factors [15]

2.4.4. Evaluation for design loads

Turbine blades are subject to a number of different loads in various combinations. Considering all of them over millions of cycles for a 20-year lifetime is a complex procedure, so an intelligent estimate of critical load cases has to be made for a pragmatic analysis.

While considering a particular set of numerical data, deviations from several sources have to be considered, for example:

- Irregularities in material being used.
- Scatter in assembly loads such as pretension
- Dimensional and quality variations in composite infusion process
- Wind inflow characteristics in the area of installation.

Due to the above variations, industry standards (VDI, GL) deem it necessary for safety factors to be used for all load cases when considering analysis. As can be seen from the load envelope in Figure 2.7, the flapwise bending moment M_Y has a maximal value, and can be assumed to be symmetric about zero bending moment. Further, the factors affecting loads have to be considered in the final selection of loads to be applied on the model. It has hence been determined that a range of both negative and positive bending moments will be applied as external loads.

2.5. Procedures for Fatigue Analysis

Wind turbines are "fatigue-critical machines" [26], that is, fatigue failure is the leading cause of failure of components after early-life failures. A significant amount of loads acting on the wind turbine are both cyclic and random in nature and consequently affect the fatigue strength and total life of the structure. Wind turbines are semi-permanent structures involving heavy installation costs and minimal maintenance; hence it is expected that the design and structure of the turbine should withstand external and assembly loads for a period of at least 20 to 25 years.

2.5.1. Theory: Fatigue

Constant Amplitude Loading: All load cycles are identical with a constant S_m (Mean stress) and a constant S_a (Stress Amplitude) throughout the load history; this is often represented as a sinusoidal curve.
Block Loading: A few portions of load cycles are identical with a constant S_m and a constant S_a in the load history.

Variable Amplitude Loading: S_m and S_a are undefined and stochastic models have to be created to characterize the load history.

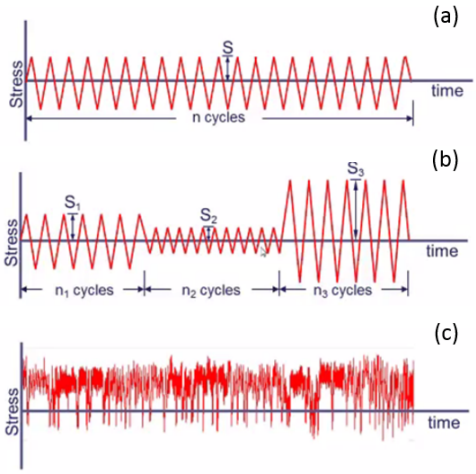

Figure 2.8: Types of fatigue loading: (a) Constant Amplitude Loading (b) Block Loading (c) Variable Amplitude Loading [30]

S-N Curve:
The S-N curve is the graphical representation of the relation between the stress amplitude S_a or the stress range S_{range} ($S_{range} = 2 \cdot S_a$) and the life (in number of cycles) for a structure under fatigue loading. This relation was first discovered by Wöhler (hence also called the Wöhler curve), and formulated by Basquin into the following equation [19]:

$$S_a^m \cdot N = K \tag{2.12}$$

where K is a constant, and m is the slope of the linear portion of the graph (on a log-log scale) and depends on the material.

2.5.2. Fatigue considerations for the design

Load history for wind turbine blades can be characterised as a variable amplitude loading when all load sources are considered. Gravitational loads are sinusoidal due to the rotation of the blades, but aerodynamic loads are stochastic and an approximate model is to be considered for the load history. The sum of these loads gives a variable amplitude model. For the scope of this study, it was found that the bolted joint was a critical member of the blade-root connection, and hence, only fatigue of ductile metals will be considered.

Fatigue life for constant amplitude cycles is calculated using the S-N curve; for a given stress range or amplitude, the corresponding number of cycles on the curve give an estimate for the life of the component under analysis. For variable amplitude loading however, the initial step before fatigue life is estimated is to define the load spectra. A load spectrum of a structure aims to summarise the stresses with respect to time that it bears during its lifetime. For a wind turbine, the characteristic wind speeds will define the type of the spectrum; loads will be plotted on the Y-axis against the frequency or time on the X-axis. For example, during start-up and shut-down conditions, the blades are subjected to higher flapwise bending moments than normal, and the number of times these operations are performed will be reflected in the frequency of these loads [8].

In case of normal operation state (when the inflow wind velocity ranges from cut-in velocity U_{ci} to cut-out velocity U_{co}), and 'buffeting' operation state (parked wind turbine being subjected to wind inflow), load spectra will be defined by the probability density function derived from the annual wind speed distribution. For the start-up and shut-down operations, the spectra is defined by the number of expected events and are deterministic. Extreme loads are not considered for fatigue analysis. For damage analysis the spectra has to be tabulated into discrete data, which can be done in three ways [26]:

1. Range Spectrum: This spectrum is a one-dimensional function which provides information about the ranges and the corresponding number of cycles.
2. Range and Mean Spectrum: This spectrum is a two-dimensional array of bins which classify cycles according to both the range and the mean and their corresponding number of cycles.

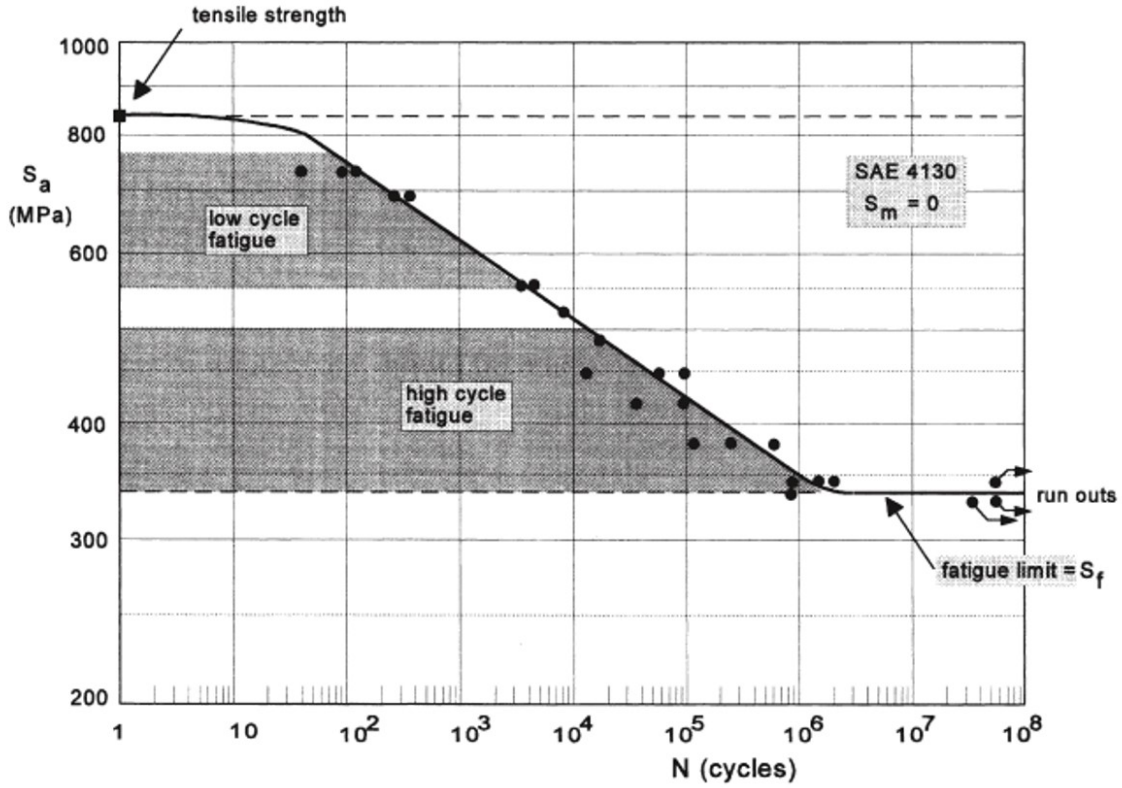

Figure 2.9: Fatigue test result: Unnotched steel specimen (SAE 4130) (from Grover et al (1951) taken from [19])

3. Markov Matrix: Data is stored in 'from-to' matrices, with cycle sequence information provided by a probability function describing which peak follows valley in the spectrum.

Range and mean spectrum provide an almost complete picture of the load history but doesn't describe the sequence of cycles. Sequence information can be obtained from Markov matrices, but as Palmgren-Miner linear damage accumulation is assumed, sequence of cycles is not necessary [26]. Suzlon uses the second characterisation of both range and mean spectrum with cycles to describe load history data.

Cycle Counting

To compute discrete cycles from the observed data, cycle counting techniques or algorithms are used. Of the existing algorithms, *Rainflow Counting algorithm* is the one typically used in the wind turbine industry. Berglind [31] compares estimation methods used widely for calculating fatigue damage in wind turbines: Rainflow Counting, Hysteresis Method (based on physical interpretation), and Markov Chain Method (takes sequence effects into account). His conclusions can be summarised into the plot in Figure 2.10. The overall damage calculated is the maximum in case of Rainflow Counting (RFC in Figure 2.10). The choice of using this algorithm is validated in the fact that it results in a conservative estimate, and that the design that is based on this estimate can be assumed to withstand fatigue loads observed on the field.

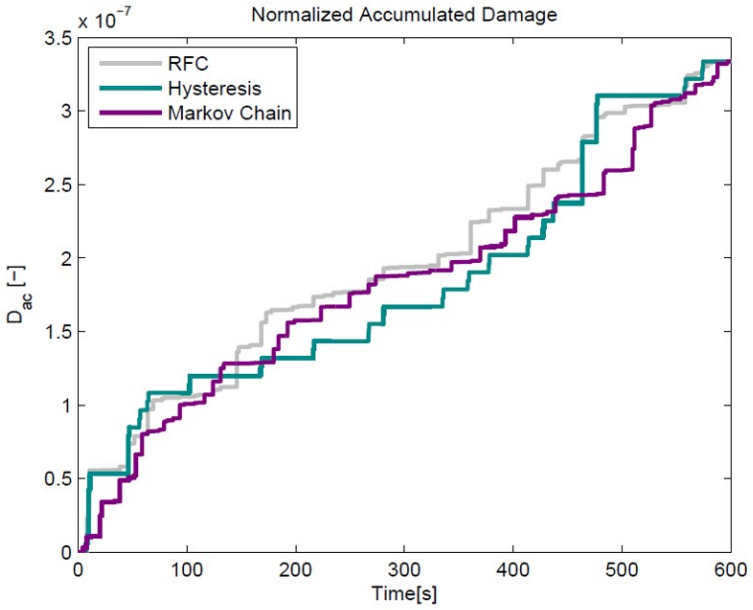

Figure 2.10: Accumulated damage from various estimation methods [31]

Rainflow Counting

Rainflow counting was first introduced by Matsuishi and Endo in 1968 [32], and it counts cycles on the basis of closed stress-strain hysteresis loops. As shown in Figure 2.11, the stress path A to D encompasses the cycle BC; it can also be seen that the hysteresis loop of cycle BC is completely within cycle AD. The algorithm of rainflow counting is based on counting closed hysteresis loops for the load history. The name was given on the basis of counting the cycles by visualising rain flowing over pagoda roofs when the cycle is rotated 90° clockwise. In case of the cycle given in Figure 2.11, the discrete cycles that are counted by the algorithm are B to C, E to D, F to G, and A to D.

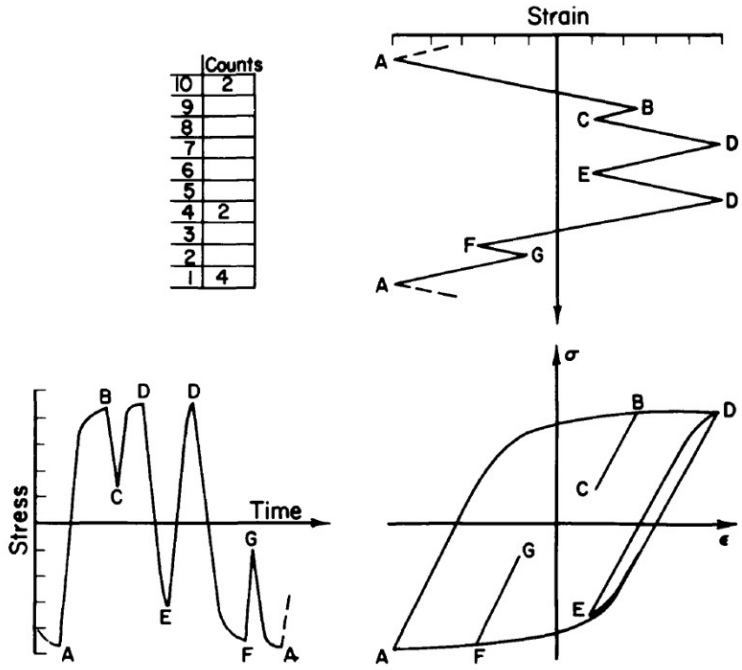

Figure 2.11: Stress-strain hysteresis loops used for counting discrete cycles [33]

1. Three-point Counting Technique: This method has been described by Downing and Socie [33] in detail. Referring to the cycles in Figure 2.11, if for cycle B-C-D, the stress states are namely σ_B, σ_C, and σ_D, and ranges are defined as $X = |\sigma_D - \sigma_C|$ and $Y = |\sigma_C - \sigma_B|$, then:

   - If $X \geq Y$, a cycle or hysteresis loop is defined and hence counted.
   - If $X < Y$, then no cycle is counted

   This method is applicable to both periodic and non-periodic load histories, and includes the contribution of residual cycles.
2. Four-point Counting Technique: This method has been described by Amzallag et al. in 1994 [34]. Again referring to Figure 2.11, if for a cycle A-B-C-D, the stresses are σ_A, σ_B, σ_C, and σ_D, and the consecutive ranges are $X = |\sigma_D - \sigma_C|$, $Y = |\sigma_C - \sigma_B|$, and $Y = |\sigma_B - \sigma_C|$, then:

   - If $X \geq Y$ AND $Z \geq Y$, then the cycle is counted.
   - In all other cases, no cycles are counted.

   Contrary to the three-point technique, this method excludes the contribution of residual cycles (unpaired reversed cycles), but can be easily applied to non-periodic load histories.

Once the cycles are counted using the Rainflow algorithm, 'bins' are specified to tabulate the data. Bins are defined as the values of mean stress and stress range for the corresponding cycles are counted. Each bin will be associated with a maximum stress S_{max} and minimum stress S_{min}, 'n' cycles counted within the loop, and this will have a corresponding value of S_{range} and S_{mean}. Since there will be a number of different stress cycles within each bin, a conservative approach is taken such that the bin size is kept small and the maximum stress range within each bin is considered.

Damage Rule Formulation

Once cycles are counted, the total damage to the component has to be calculated. In accordance with IEC standards, the *Palmgren-Miner linear damage accumulation rule*, or the *Miner's rule*, is widely used for the fatigue analysis of wind turbines. The generalized equation of this rule is given below:

$$\Sigma \frac{n_i}{N_i} = \mathcal{D} \tag{2.13}$$

Here, n_i is the number of cycles at stress level i sustained by the structure, N_i is the number of cycles to failure at that particular stress level, and $\mathcal{D}$ is the total damage caused by all the cycle taken into account. When $\mathcal{D} \geq 1$, the cycles lead to failure (i.e. fatigue resistance is consumed). [26]
The theoretical understanding of this rule has several assumptions, namely:

- Each set of cycles at a particular stress levels are independent of each other.
- If a particular stress cycle is below the fatigue limit, then N_i is infinite, i.e. the structure will never fail at that particular stress. This leads to the ratio of n_i/N_i at that stress being equal to zero, or in other words, not contributing to the total damage.

Schijve [19] notes that these assumptions are not completely valid in a variable amplitude stress cycle. It has been experimentally seen that cycles with stress below the fatigue limit does lead to crack growth and hence contributes to damage. Another shortcoming of this rule is that it does not taken into account the order of stress cycles. Plasticity induced crack growth retardation is an effect of low level stress cycles appearing after high level stress cycles, hence undermining the linear rule.

It has been experimentally found that the value of $\mathcal{D}$ range from 0.79 to 1.53 for a variety of applications[35]. Due to the different materials used and variable loading cycles, differences in damage calculation up to a factor of 2 is common for fatigue analysis of wind turbines. The conservative results obtained from applying the Miner's rule and the inherent safety factor make it suitable for fatigue analysis of wind turbine components.

The theoretical formulation that relates the life of the structure to the rate of damage accumulation in wind turbines is given as follows:

$$\frac{1}{T} = \Delta \mathcal{D}_t = \int_{U_{in}}^{U_{out}} p_U(u) \int \int_0 \frac{n_t(\sigma_m, \sigma_a, U)}{N(\sigma_m, \sigma_a)} d\sigma_m d\sigma_a du \tag{2.14}$$

Here, T is the structural service life of the turbine, and $\Delta\mathcal{D}_t$ is the average damage rate over the lifetime T. Fatigue damage is a function of the mean stress σ_m and the stress amplitude σ_a (or stress range: $\sigma_R = 2 \cdot \sigma_a$). The formulation evaluates life between cut-in velocity U_{in} (wind-speed at which power production starts) and U_{out} (wind-speed at which maximum power is produced and the turbine is shut down to prevent rotor damage). Cycle counts (numerical data of the load history in terms of number of cycles of varying load defined by a maximum and a minimum) in wind turbine load history are a function of the average inflow velocity u, given the assumption that almost all loads sustained by the blades are dependent of aerodynamic loads. Hence, damage is also a function of the probability density function p_U for inflow velocity U.

2.5.3. Evaluation for fatigue analysis

The standards documented by GL concurs with the above methodology for designing a component, in this case, a bolted joint, for fatigue performance. As the procedure considers several assumptions (linear damage accumulation, curve-fitting of S-N curve etc.), the procedure is termed as a *simplified fatigue analysis*. To accommodate for the assumptions and limitations on the field like monitoring and maintenance, safety factors that have been recommended for the analysis will be applied. The recommendations are given as follows:

1. **Partial safety factor**: $\gamma_M = 1.15$ for components with "Periodic monitoring and maintenance with poor accessibility", where the "component failure results in wind turbine failure" but not complete failure or endangerment as "a single bolt failure in a multiple bolt connection can be detected before complete failure of the connection" [15].
2. **S-N curve for bolted joints**: A reduction of the S-N curve by a factor k_S is to be applied when the bolts are larger than M30. k_S is calculated as:

$$k_S = \left(\frac{30}{d}\right)^{0.25} \tag{2.15}$$

where d: nominal diameter of the bolt in mm

Damage in the bolted connection at the root can be critical as the area is not easily accessible during regular maintenance procedures. The motivation for using the above procedure in the design for fatigue performance is the reasoning that the use of partial safety factors and the Rainflow Counting Algorithm results in a conservative design which is well suited for real-life application.

This page intentionally left blank.

3

Design Study

3.1. Outline

To perform the design study, the following iterative process has been outlined. This chapter explains the design process and the parameters involved in building a base model of the busing connection. The next stage is data validation, wherein the FEA results have been validated against existing data, standards, and performance requirements. The final stage is the analysis of results; several parameters that are key to the cost, weight and performance of the design have been varied to understand their effect on this particular design.

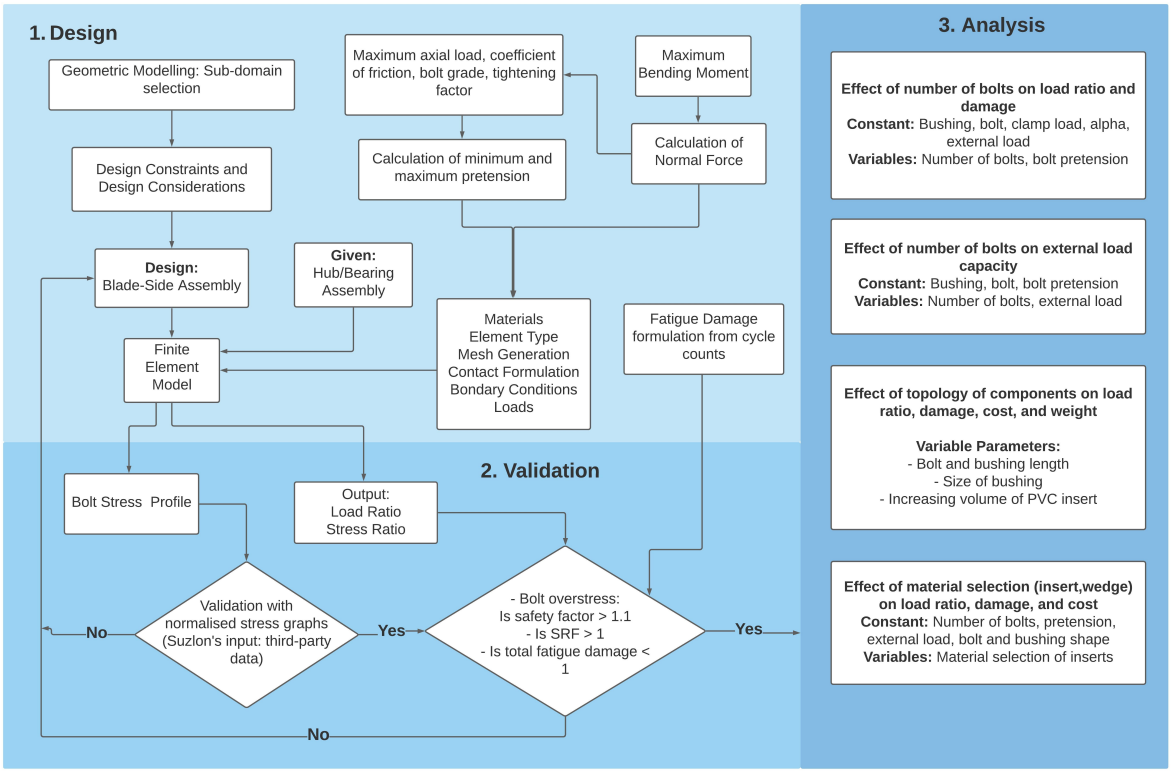

Figure 3.1: Outline of methodology

3.2. Finite Element Model of the Design

To build a geometric model for the FE analysis, design constraints and suggested factors were taken as an input. The general parameters that are required for an FEA study are symmetrical considerations, dimensional limits, component materials, boundary conditions, and applied loads. The selection process of these parameters have

been discussed in the following sections. Close approximations of the real-life assembly are adopted for the FE analysis. As a prototype model, effort has been taken to build a model as close to the actual components as possible. In order to conserve on computational time, an estimate of the actual conditions have been assumed.

3.2.1. Sub-domain selection

Design guidelines state that bolts have to be placed uniformly around the blade root circumference. While analyzing the full blade root will give near-accurate results, the general principle of FEA is that the modeling and computational time increases with the size of the model and the number of elements in the model. Moreover, Ansys Workbench on the Student License places a limit on the sum of elements and nodes at 32k. The diameter of the blade at the root is of the order of 3m, and the bolt measured 36mm at the thread in the initial designs. Therefore, the number of elements will be much more than 32k if the full root is modeled.

The turbine blade root has cyclic symmetry; a single bolt-bushing connection is a 'repetitive sub-domain'[36] that can be considered representative of the the entire root. Application of symmetric models reduces the meshing time, allows refinement of the mesh in the areas of concern, and reduces the computational time required to run each iteration of the model. Therefore, symmetric boundary conditions were used to reduce the size of the model. The general practice for FE analysis is to reduce models to the smallest repetitive size possible. In the first step, cyclic symmetry was used to reduce the model to one bolt and bushing assembly. The model was further simplified using axial symmetry that resulted in the design that can be seen in Figure 3.2. A trade-off was made between accuracy and computational limits. To offset deviations from the actual behaviour, standards note that partial safety factors must be applied for specified cases, such as for fatigue analysis and bolted joints. Ketele [37] provided results on a detailed analysis of a turbine blade-root, albeit with a T-bolt connection, and observed that the differences in the stress results between a global model and sub-model is within 5%, but only given the condition that the width of the sub-model chosen is at least 4 times that of the depth of the root. However, Ketele's study focuses on the stresses developed in the blade laminate, where the effects of stress concentrations are critical. It was observed during the design stages that in a bushing connection however, the normal stress quantity (in the direction of the applied load) developed within the steel bolt was several times the stress quantity developed within the laminate. It was hence considered sufficient to limit the scope of analysis to the smallest sub-model possible.

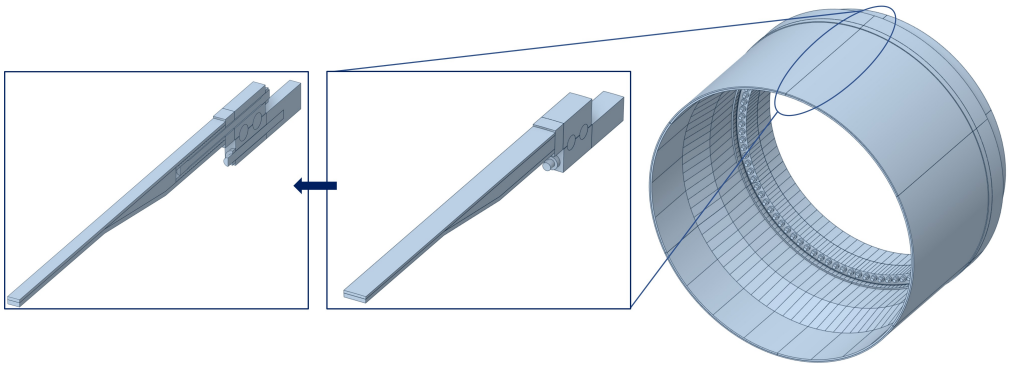

Figure 3.2: Phases of model reduction using symmetry (Global model shown on extreme right, final reduced model shown on extreme left)

3.2.2. Design constraints

The blade root is a sub-structure of the wind turbine, and as an interface between the blade and the hub, has several design constraints. The scope of the study is limited to the Suzlon-made 63m blade, to be used for the SE - S128 Wind Turbine Generator. The geometrical constraints that were provided for the design study was the Bolt Circle Diameter (BCD), the hub and bearing assembly, and the thickness of the laminate.

The bolt circle diameter is the diameter of the imaginary circle that passes through the axis of the bolt, with its geometrical centre in the blade root. The hub and bearing assembly (hub-side assembly) had to be incorporated in the design to study the actual response of the bolted root connection. The axis of the hub that acts as a fixed support, the axis of the bolt, and the axis of the application of load lie on different planes of the connection, which introduces significant bending response in the bolt, along with axial loads. This the dimensions and stiffness of the hub-side assembly a key part of the design. The wind turbine blade skin is built up of several layers of composite laminate. As the connection had to be compatible with the available commercial blade, the thickness of the blade skin, or effectively the laminate, was a constant with respect to the design.

For clarity, the design has been divided into two sub-sections: the hub-side assembly, and the blade-side assembly. The hub-side assembly consists of fixed members with pre-defined materials and dimensions that are based on technical drawings provided by Suzlon.[21]. The blade-side assembly consists of the bolted connection that joins the blade to the fixed (for the scope of this design) hub using a bushing.

3.2.3. Hub-side Assembly

The hub-side assembly consists of the following components:

Bearing Assembly

The blade is connected to the hub via a slew ring bearing to allows axial rotation of the blade. The bearing allows the control system of the wind turbine to adjust the angle of attack of the blade to maximise aerodynamic efficiency.

In the scope of this design, the bearing consists of two races with the ball bearings in between made of bearing quality steel with the grade 100CrMnSi6-4. The races each have co-axial holes through which the bolts pass.

Ball bearings are spherical in shape, and have a tangential contact with the inner surfaces of the races as shown in Figure 3.3. As they are packed in place within the races, the simplified cylindrical design (Figure 3.4) was considered a close approximation of the support provided by the ball bearings; this design choice avoids the development of stress concentration at the tangential contact region between the ball bearings and the races in case of spherical bearings.

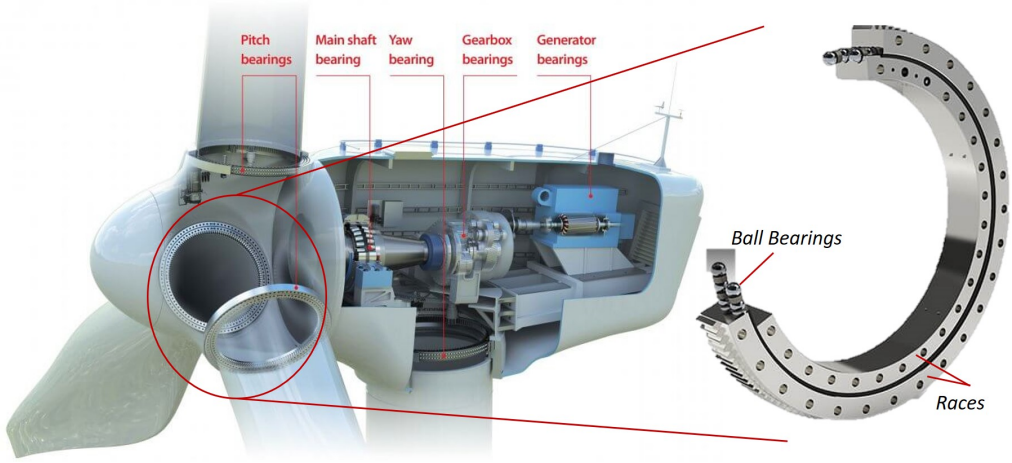

Figure 3.3: Hub (left) and the slew ring bearing (right) (not representative of the model) [38] [39]

Fixed Hub

The bearing assembly is connected via bolts to the nacelle. According to design requirements, the portion of the hub used for the model is made of Cast Iron. The position of the hub and its dimensions play a role in inducing bending stresses in the main bolt under consideration, and was used as a reference point to check for excess rotation, displacement, and strains in the blade assembly. Structurally, the hub connects the rotor blades to the nacelle, which houses the power components of the wind turbine like the generator and the gearbox. As the nacelle is connected to the tower in turn, the vibrations in the turbine tower in response to wind conditions are translated to the hub-rotor assembly, so the hub is not a fixed member in the frame of reference of the ground. For the scope of this design, it has been taken as a fixed support as the effect of tower vibrations are considered negligible with respect to the aerodynamic loads. Full-scale blade tests, including fatigue tests, analyse blade response with respect to a fixed support [40].

Spacer

The function of the spacer is to prevent damage to the bearings during the assembly of the wind turbine. The material assignment given to the spacer is the same as the other hub assembly components (except the fixed hub), i.e., structural steel.

Hub Bolt

The hub bolt connects the bearing assembly to the fixed hub. Pretension was applied to this bolt to ensure that enough clamping force is reached to avoid separation of the blade from the hub. The design of this bolt is a simple stud threaded at the ends.

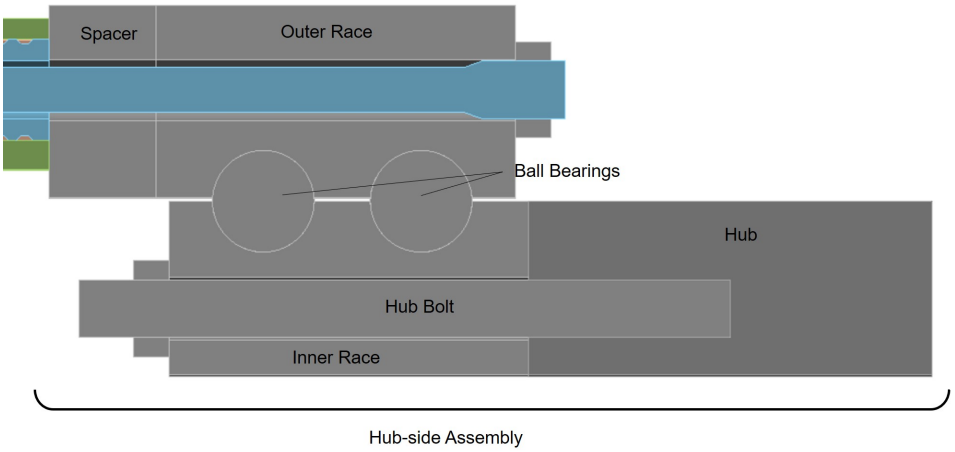

Figure 3.4: Geometric Model: Bearing Assembly, Hub, and Spacer

3.2.4. Blade-side Assembly

The design of the components on the blade-side of the root connection were based loosely on third-party design provided to Suzlon. During modelling, several design considerations were kept in mind:

1. The portion of the blade to be designed has to be at least 1.5m (1500 mm) to check for stresses being developed.
2. The topology of components should be such that it can be manufactured without the need for complex procedures.
3. There should be an attempt to increase the bonded area, especially between components of dissimilar materials.
4. Component topology should be such that they are similar to available shapes.
5. Laminate ply drops should be minimized as much as possible.
6. Severe changes in angles or general topology should be avoided in the laminate.
7. There should be an attempt to bridge the gap between stiffnesses of the different materials used.
8. During material selection, the weight, cost, and available manufacturing methods also have to be kept in mind.

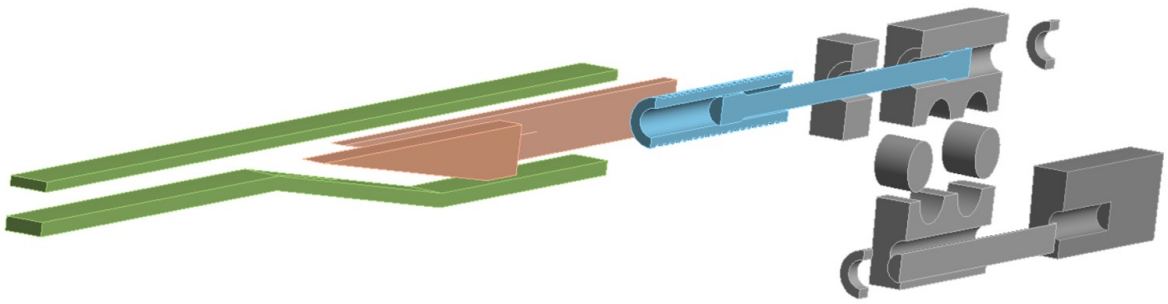

Figure 3.5: Design - Exploded View

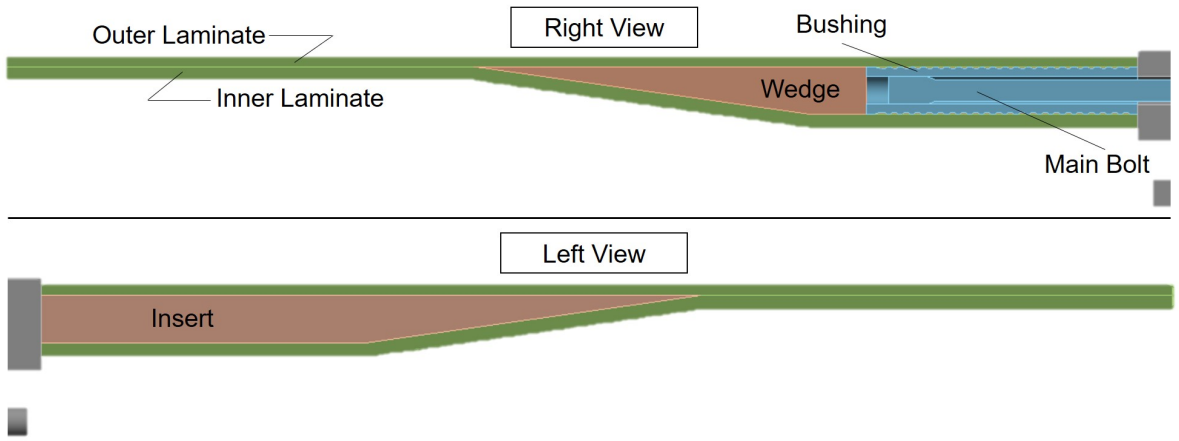

Figure 3.6: Design - Blade Side

Blade skin

Wind turbine blade skins are made of composite laminates, usually glass fiber-epoxy laminates. The blade root connection joins the composite blade structure to the hub. The major interface here is therefore between the bushing and the composite laminate. While the composite laminate material is a constant (multi-layered glass fibre-epoxy triax), the topology had to be designed such that ply-drops and sharp angles were kept to a minimum. The blade is thickest at the root ($L = 0$mm) to accommodate the bolt, and gradually tapers in the direction of the tip to the desired thickness. To enable a smooth meshing operation, the blade skin was divided into two separate section, one for the inner layer, and the other for the outer layer. The taper angle was kept at 8°, in accordance with ply drop-off design principles [41].

Although the blade is made of discrete layers of laminate, for the sake of simplicity in the model, the given composite material properties of 'triax' were been assigned to the bulk volume. Triax is the name given to a layup of alternating 0°, +45°, and -45° lamina. Each triax lamina has a thickness of about 1.225mm. For the outer laminate, 10 layers were taken for a thickness of about 13mm, and for the inner laminate, 15 layers were considered to reach a thickness of 18mm. The total laminate thickness is 31mm, or about 25 layers, where the outer and inner laminates meet. This material assignment is based in industry standards for numerical analysis [21].

Insert

The T-bolt connection featured a continuous and thick laminate at the root with drilled holes for barrel nuts and the bolts, which resulted in stress concentrations. With the bushing connection design, the blade root is interspersed with equally spaced bolts and bushings. While the drilling operation is eliminated, the design creates significant gaps between each consecutive bushing. The laminate can be wrapped around the bushings across the circumference, but this would create interruptions in the layup, potentially creating folds and resin-rich pockets in the laminate. Therefore, a design choice was made to include an insert to fill the gaps between each bushing such that there are no folds in the laminate layer. This can be seen in the Figure 3.5 and Figure 3.6. The initial material was chosen as resin, and was later replaced with a unidirectional laminate block to bridge the difference in stiffness.

Wedge

Compared to the composite laminate sections of the blade, the bushing has a relatively higher thickness. If the layup of the composite has to be placed over the bushing, it will face a drastic geometrical change, which makes the load path through the layup inefficient. The change in topology from the perspective of the laminate has been considered to be equivalent to a 'ply drop-off' in a laminate, wherein laminates are gradually tapered to a smaller thickness and lesser plies. Mukherjee and Varughese [41] suggest that the 'stagger distance' (distance between successive ply-drops) has to be at least eight times the thickness of the drop-off. The latter dimension here is 63mm (first design iteration), so the taper has to be in the range of 500mm at the very least. Therefore, a gradually tapering wedge (with an edge angle of 8° in the first iteration) has been incorporated to fill the gap between the bushing and the laminate. The wedge, together with the insert, takes up a considerable volume in the connection. Therefore, a trade-off was made between strength, stiffness, weight, and cost, as the latter two factors will be significant when the entire blade root is considered.

Main Bolt

The initial design choice of bolt (among standard bolt types available with fastener manufacturers) was to have an M36 double end stud with a reduced shank. The choice was made based on bolts being currently used by Suzlon; doing so would reduce the overall switching costs associated with sourcing a new bolt from the supplier. The reduced shank helps in weight reduction when the number of steel bolts is approximately a 100 in the root circumference.

Bushing

The bushing acts as an interface between the bolt and the laminate. Tapping threads directly into the composite laminate will lead to the risk of irregular stress patterns due to the anisotropic nature of composites. The bushing has an internal thread where one end of the bolt is connected through a threaded joint, and on the outer surface, it is bonded to the laminate and the insert through an epoxy adhesive.

The first design iteration of the bushing was a simple cylinder. The aim was to first understand the performance of the design and then modify the bushing geometry to an optimised one. As mentioned previously, the bushing had to be optimised for bonded contact area to the laminate, mode of stress transfer to the laminate, total weight, and cost of manufacturing. The topology of the bushing in the next design iteration was based on a patented design published by Kuipers in 2017 [10]. The patent's key claims are that the surface improves the transfer of shear stresses through mechanical joining, and increases the adhesively bonded area of the lap joint between the blade skin and bushing.

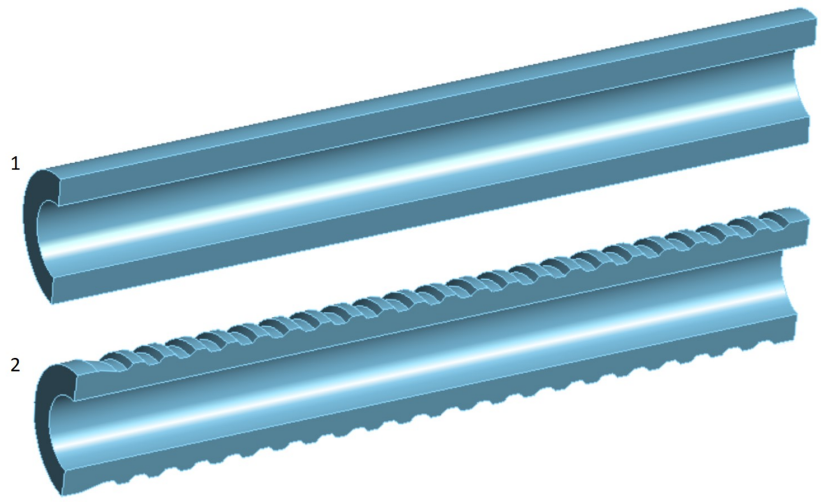

Figure 3.7: Initial design (top) and improved design (bottom)

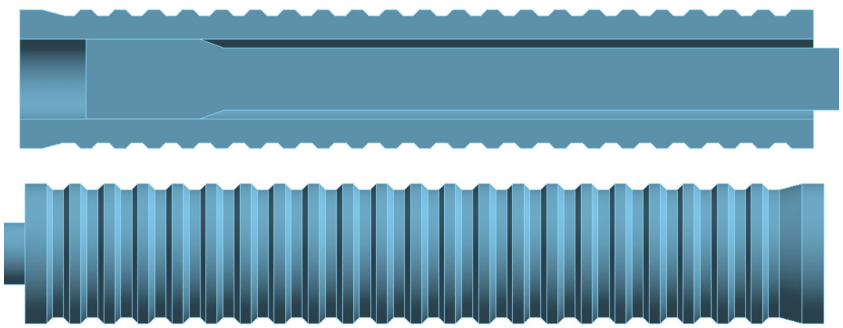

Figure 3.8: Sectional view (top) and external view of the improved bushing (bottom)

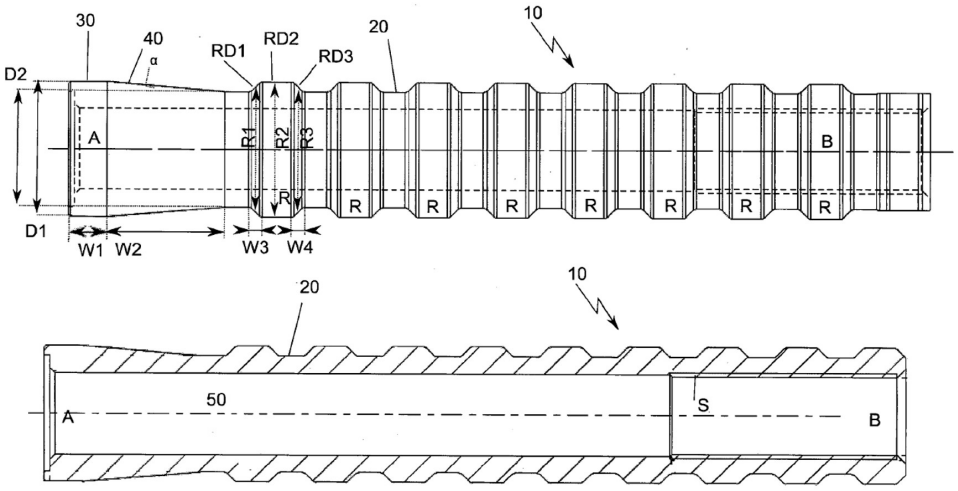

Figure 3.9: Bushing Design patented by Kuipers [10]

3.3. Meshing and Element Types

3.3.1. Choice of element type

General FE analysis can be modeled using either of the two main types of elements: shell elements, or solid elements. The choice of elements has to be made according to the application.

Shell elements are appropriate for models where one of the dimensions in a component is negligible (for example, thin structures like plates), and if stresses in the negligible dimension are also comparatively small. Shell elements can be considered for the global modelling of the blade, wherein the laminate thickness is very small compared to the overall length and diameter of the blade. An advantage of using shell elements is that computational times can be lowered to a significant degree while obtaining sufficiently accurate results. Within the realm of shell elements, there are two options: conventional shell elements, and continuum shell elements. Conventional shell elements have displacement and rotational degrees of freedom at the nodes, and their geometry is defined by the planar surface. Continuum shell elements result in a three dimensional model, but their behaviour is similar to that of conventional shell elements, as in the stress in the normal direction is declared zero.

The focus of this thesis is however the blade-root connection, which is assembled from multiple components of different materials and thicknesses. Almost all components of the model have a non-uniform cross-sectional area, that is, the area of their cross-section varies along the length of the body. The region of interest lies within 1.5m of the 63m blade. Within this area, the thickness dimension of all components is significant compared to their other dimensions and hence cannot be neglected.

The bending moments acting on the blade increase along the blade length towards the root and the stresses developed are the maximum at the root (at length L=0). Along with the applied pretension to the bolt, stress concentrations develop at locations where the geometry changes. The maximum stress was found to be at the root of the shank of the main bolt, and at the inner race of the bearing, both due to pretension.

Therefore, SOLID186 and SOLID187 type elements (ANSYS environment) were chosen for the modelling of the connection; these element types consist of either 10-noded tetrahedral brick elements or 20-noded hexahedral brick elements, both used to mesh three-dimensional volumes. Additionally, the SOLID elements can be used for both linear (elastoplastic or anisotropic) and non-linear (hyper-elastic) materials [42]. Although solid continuum elements are computationally heavy, the stresses developed in the bolt connection make the use of solid elements imperative.

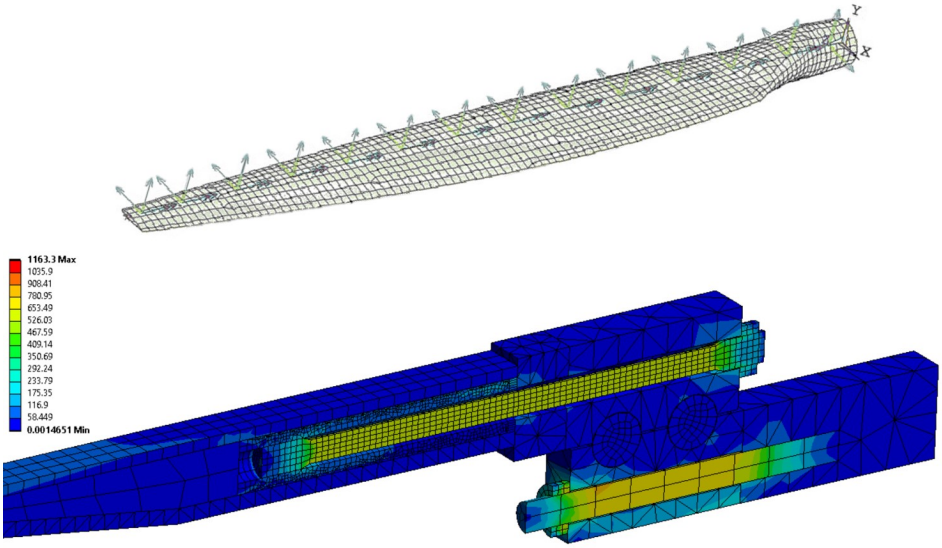

Figure 3.10: Shell model of the full blade (top) [43], where the length is much greater than the thickness of the blade, and the solid model used in the thesis (bottom), where all dimensions are significant and the model includes stress concentrations.

3.3.2. Mesh Generation

Meshing is the process of dividing a geometrical space into discrete elements, enabling the FE solver to compute the behaviour of each element and transform it over the macro-structure. The general meshing principle is to refine the mesh at areas of concern to achieve accurate results. Mesh refinement in the current study is however limited by the number of nodes and elements available (32k for Ansys Student). Moreover, a finer mesh, that is a mesh with smaller elements, is computationally time and memory consuming. Hence, here too, a trade-off was made so that the design model stayed within the mesh limits and provided an output with sufficiently accurate results.

For structural analysis, the meshing principle followed was to use hexahedral (cube or brick elements for a three-dimensional structure) over tetrahedral elements. Hexahedral elements are automatically used in case of a 'structured mesh' of the model. A structured mesh is one where a topological pattern can be identified throughout the geometry. It is also defined as 'a mesh where the inner nodes have the same number of elements around them'. To generate a structured mesh, the MultiZone method (in Ansys Workbench) was used to map components of interest into structured and unstructured zones. Within this method, the solver divides the geometry into sweepable (geometries with a constant area throughout) and irregular regions, and develops structured meshes in the former geometry.

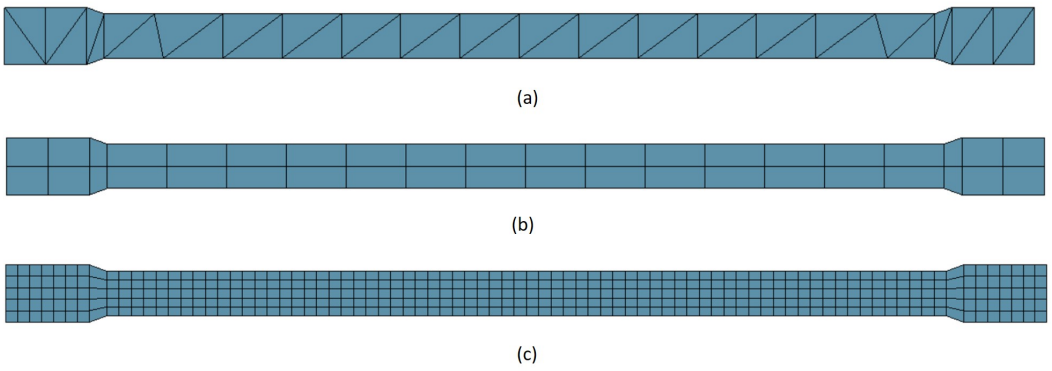

Figure 3.11: Evolution of the bolt through mesh structuring and refinement:(a) shows the bolt comprised of tetragonal elements, (b) shows the mesh redefined using hexagonal structured elements, and (c) shows the mesh refinement

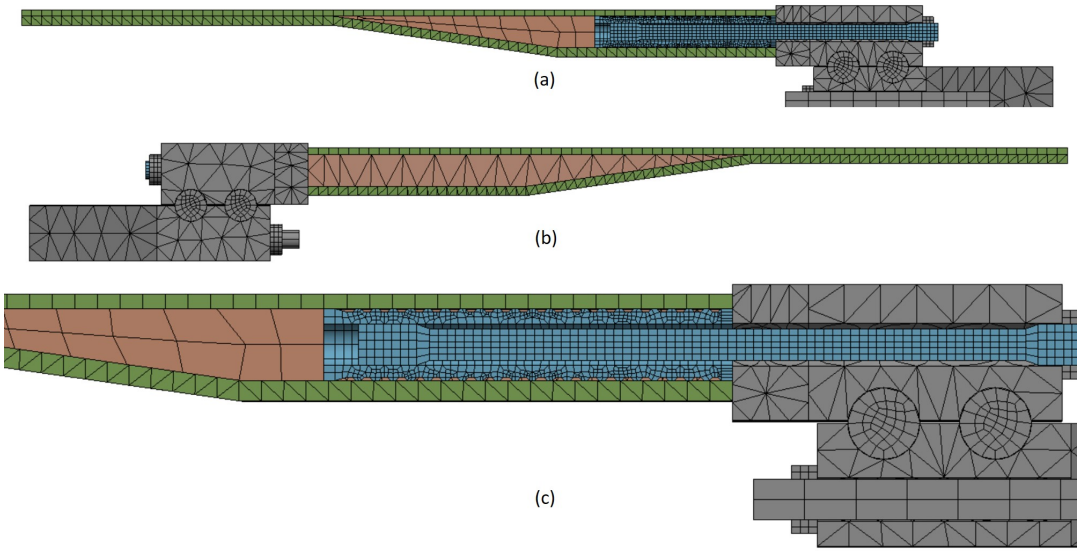

Figure 3.12: Mesh generated on the entire assembly (a) Right View (b) Left View (c) Mesh refinement at areas of stress concentration (i.e., on the bolt and the bushing)

3.4. Coordinate System

In accordance with the coordinate system illustrated in Figure 2.5, the Z-axis is aligned with the blade axis. For the laminate however, material assignment needs to considered according to the direction of the layup. Hence, a separate coordinate system has been generated according to the laminate geometry and the material has been assigned likewise. In case of the insert being assigned a unidirectional-composite material, the coordinate system for the insert will be the same as the laminate. The local coordinate system for the laminate is illustrated in Figure 3.13; the X axis is aligned with the blade axis as the tension-compression forces are along this axis, validating the choice of triax as a blade material due to its superior stiffness in the E_x path.

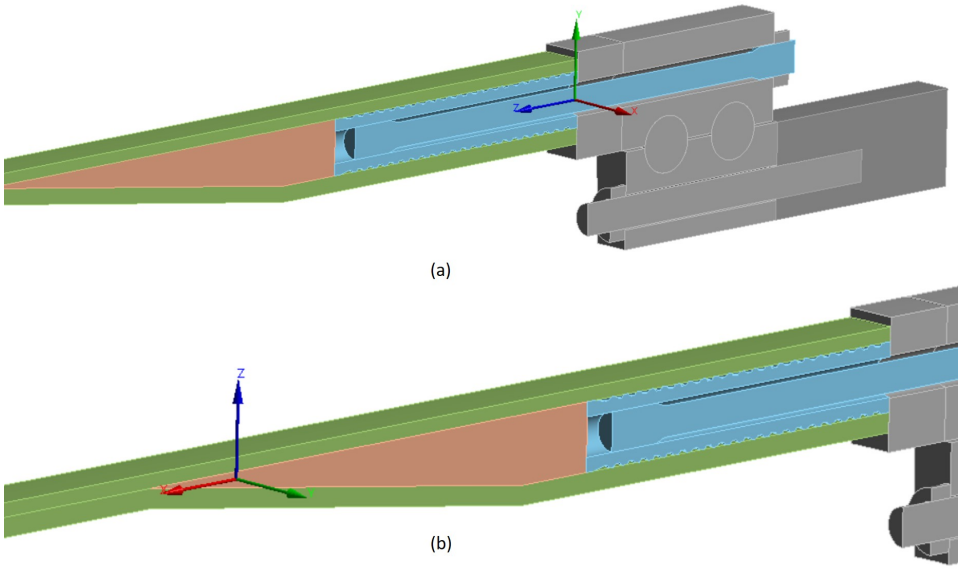

Figure 3.13: (a) Global coordinate system for the model (b) Local coordinate system for the laminate and the insert in case of UD material assignment

3.5. Contacts

Different components and multiple material assignments makes the use of appropriate contact formulations necessary. Three different types of contact interactions have been used in the model, which are listed below:

3.5.1. No Separation Contact

Bearings use grease or oil for lubrication between the races and the bearings to allow for sliding. Their main function in the wind turbine hub is to transmit radial and axial loads from the blades to the stationary hub. Hence, the contact should provide minimum friction to allow for movement between the races and the ball bearings, and at the same time, should not allow formation of a gap between them. To achieve this, the 'No Separation' contact formulation was applied between the ball bearings and the races. The coefficient of friction associated with this contact is $\mu = 0$.

3.5.2. Frictional Contact

As the name suggests, Frictional Contact formulation allows sliding between surfaces with a non-zero coefficient of friction. It allows for gap generation, that is the surfaces with this contact can be separated under sufficient force. With respect to the macro-structure of the blade, this separation is important to allow the wing tip deflection (on the order of several meters) without placing too much stress on the blade laminate). The bearing system is a separate component provided by a third-party manufacturer and is not bonded to the blade or the hub, and stays in place via the pretension on the bolt. According to industry standards [15] [14], the coefficient of friction has been set at $\mu = 0.18$ for all frictional pairs. The surface pairs that have frictional contact set up between them are illustrated as follows:

3.5.3. Bonded Contact

Bonded contact in this model has been used to replicate two types of bonds:

1. Threaded joint between the bolt \stud threads and the internal threads on the bushing \hub:
   Studies on the FE modelling of bolted joints consider the bolt and nut as a unified solid body [44]. In case of a deeper analysis on threaded joints, individual threads can be modelled, but the computational effort required exceeds the scope of this project. Hence, bonded contacts have been set up to simulate the threaded joints, assuming assembly torque ensures all threads are in contact to each other with no sliding.
2. Adhesive bonds using resin epoxy between the blade-side components (bushing/laminates/insert/wedge):
   Adhesive bonds show non-linear behaviour under shear stress, especially when the adhesive layer is thick. To simplify the design however, bonded contacts have been used to model the adhesively joined components, with the assumption that the adhesives have been fully cured during the assembly stage, and provide near-perfect bonds.

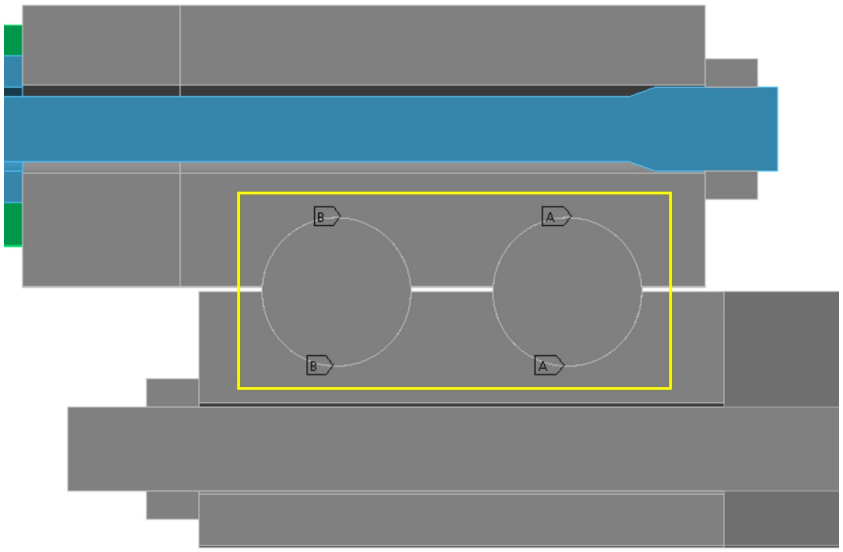

Figure 3.14: 'No Separation' contact regions between the races and the ball bearings (marked in the yellow frame)

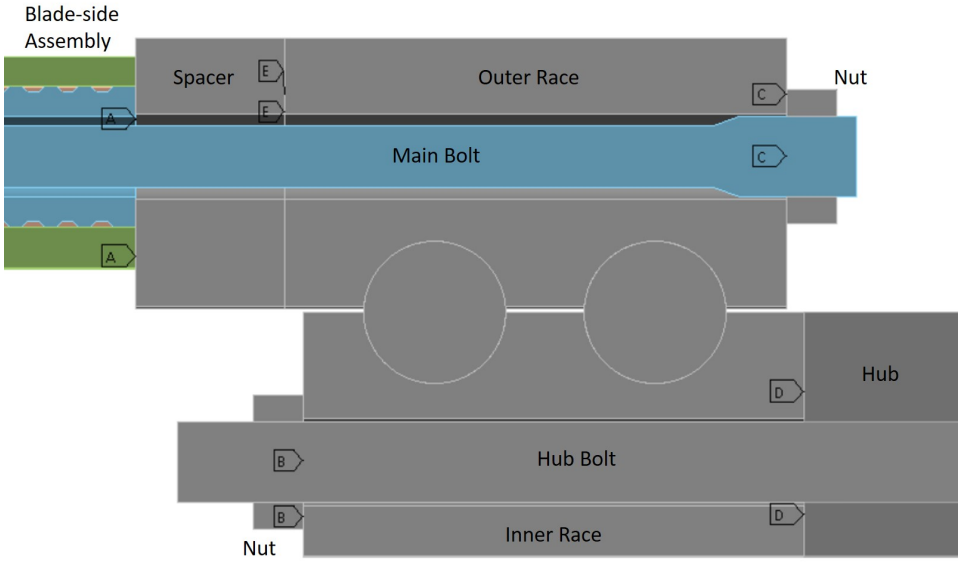

Figure 3.15: Frictional contacts are present between the bearing and the blade-side assemblies, between the hub section and the bearing assembly, and between each respective nut to the surfaces of the races (see labels A, B, C, D, and E)

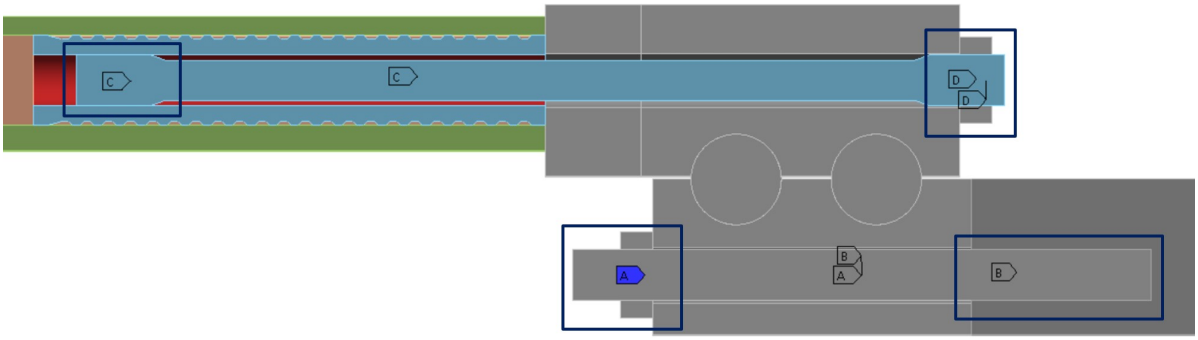

Figure 3.16: Bonded contact between threaded members, highlighted by the blue frames.

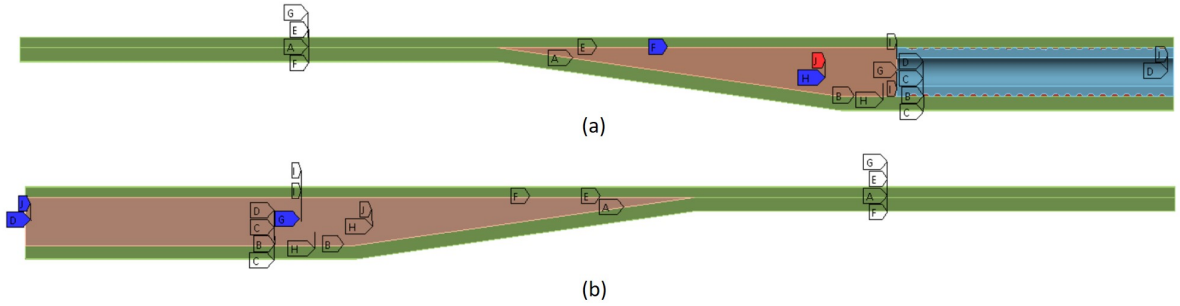

Figure 3.17: Bonded contact between adhesively-bonded members: Bushing, insert, wedge, and the laminate.

3.6. Boundary Conditions and Loads

3.6.1. Boundary Conditions

Boundary conditions are constraints set to the Finite Element model to simulate real-world conditions. The incorporation of a reduced model through symmetry considerations requires the use of symmetric boundary conditions. Within this design, in order to constrain the displacement and rotation normal to the planes of symmetry,

the boundary condition 'Frictional Support' available within the Ansys environment was applied on the faces as shown in Figure 3.18. This boundary condition allows movement/displacement in the same plane, and restricts displacement and rotation normal to the plane.

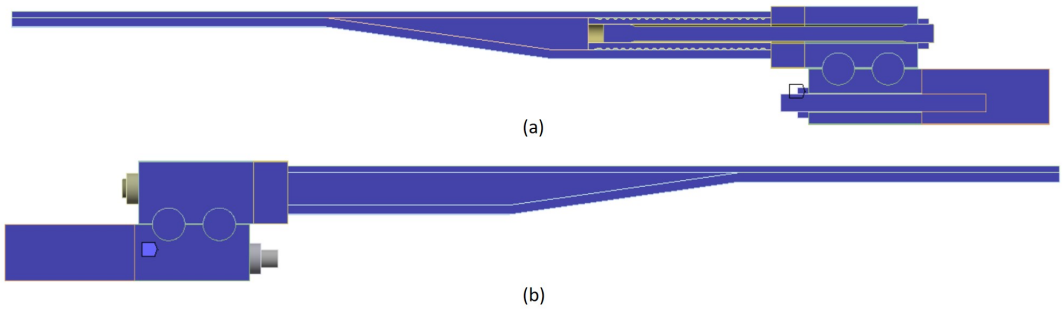

Figure 3.18: Frictional support (on the faces shaded in blue) to replicate the effect of applying symmetry reduction (a) Right View (b) Left View

A fixed boundary condition (restricting all motion and rotation is applied to the fixed hub as the displacement and stress in the blade needs to be analysed with respect to the hub. As mentioned previously, vibrations transmitted by the tower to the hub are considered negligible.

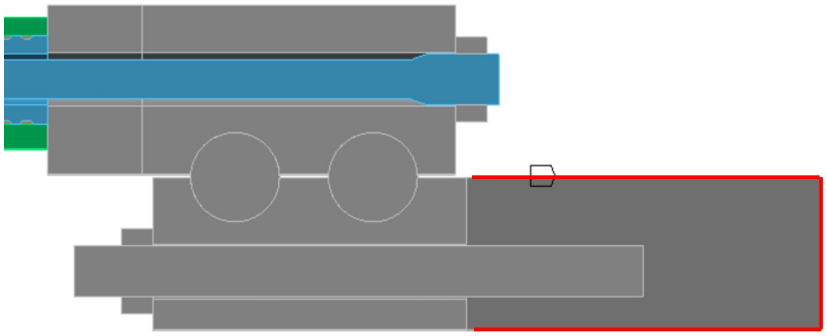

Figure 3.19: Fixed boundary condition applied on three faces of the hub component (marked with red lines)

3.6.2. Definition of Loads

External Moment

The bending moment cycles sustained by the root result in tension-compression cycles at the root extremes as shown in Figure 3.20. For the first iteration of 96 bolts, or the $(1/192)^{th}$ root section, or a $\theta = 1.875°$ angular section is considered. At this section, the bending moment can be assumed to be acting in pure tension or compression according to the position of the section on the blade. The formula for calculating the normal load being induced due to the moment at the root circumference is as follows:

$$P_n = \frac{2 \cdot M}{R_{BCD} \cdot N_b} \cdot sin(\theta_n) \tag{3.1}$$

where

$$\theta_n = 90 \pm \frac{360°}{N_{bolts}} \tag{3.2}$$

where P_n is the developed load, M is the applied moment, R_{BCD} is the radius of the root (BCD), N_b is the number of bolts, and θ_n is the angle of the section being analysed. The applied moments are used to calculate the normal loads developed on the thin angular section of the root. While this is an intelligent estimate on the normal loads developed at the root circumference, it is expected that the range of applied moments cover for these assumptions.

Within the model, the load has been applied on the end of the laminate as shown in Figure 3.21. This was confirmed with simpler model of a cylinder that was tested by first applying direct moment, then verifying the sectional load on a symmetric sub-model.

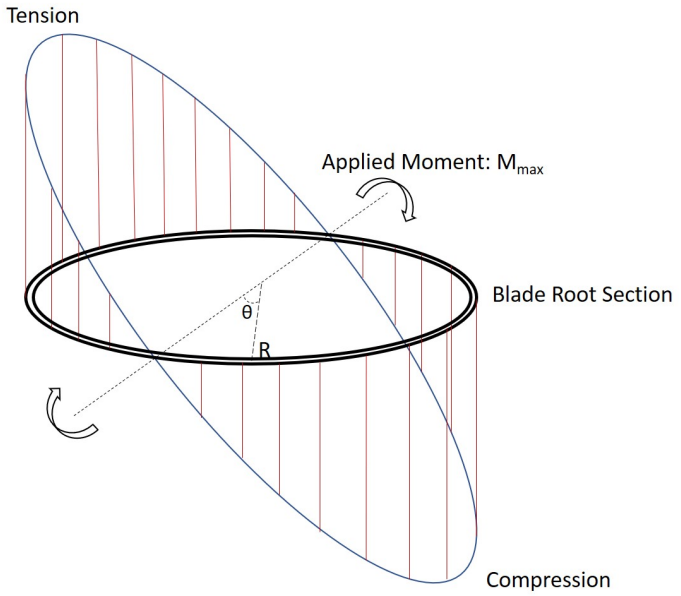

Figure 3.20: Stresses induced at the blade root circumference due to the applied moment

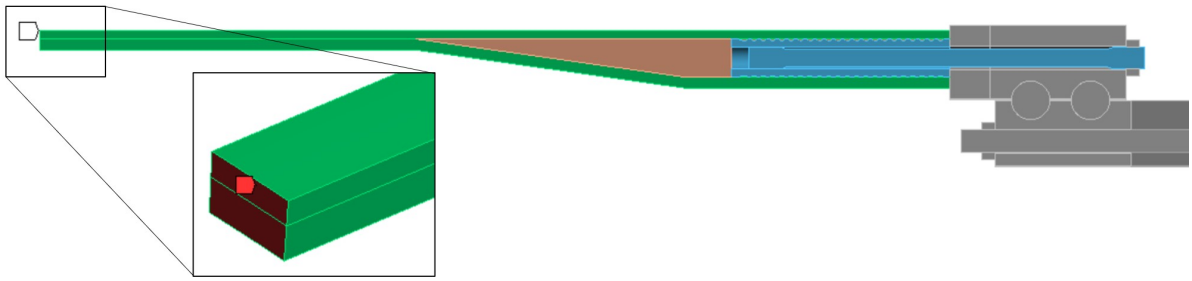

Figure 3.21: Surface on which load has been applied

As mentioned in Section 2.4.3, the maximum bending moment sustained at the root for a Suzlon-make blade of 63m is $12692.7kNm$. To allow for application of the root design to other blade variants, the maximum root bending moment for the 65m blade is also taken into account, which is $12997kNm$. These values have been provided by Suzlon through their results from proprietary software. Industry standards require the use of partial safety factors which have already been incorporated in these values.

However, the design has several assumptions in terms of dimensions, symmetry sub-modelling, and contacts. To accommodate for these assumptions, a range of applied moments were considered, from $16000kNm$ to $-16000kNm$, with increments of $2000kNm$, such that it encompasses assumptions taken in the previous stages of the design. The calculated values according to Equation 3.1 are given in Figure 3.22.

External Moment (kNm)	External Force (N)
-16000	-111111.1111
-14000	-97222.22222
-12000	-83333.33333
-10000	-69444.44444
-8000	-55555.55556
-6000	-41666.66667
-4000	-27777.77778
-2000	-13888.88889
0	0
2000	13888.88889
4000	27777.77778
6000	41666.66667
8000	55555.55556
10000	69444.44444
12000	83333.33333
14000	97222.22222
16000	111111.1111

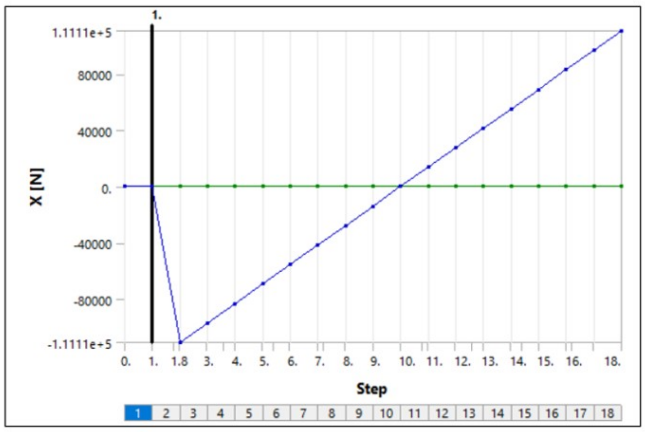

Figure 3.22: Tabular data of the applied normal force derived from Equation 3.1 (right) and the graph plotting the application of load with respect to the analysis step

Assembly Pretension

Pretension, or preload, is an important factor in the fatigue life of bolted joints. Application of the appropriate amount of pretension ensures that the external load applied is not borne solely by the bolt but is distributed to the clamped parts as well.

Wind turbine bolt fastening can be done through either using electric torque wrenches, or hydraulic bolt tensioners. These are illustrated in Figure 3.23. The industrial application of these methods is done to ensure that repeatable and precise values are reached while assembling the blade to the hub, as compared to manual tightening methods. However, scatter in the value of pretension achieved is common and due to a number of factors like machine error in the tensioning tools, dimensional changes in the bolted assembly due to temperature, settling or embedding of parts due to creep during operation, or eccentricity introduced due to roughness or errors in manufacturing. Hence, the common practice for analysis of bolted joints for real-life applications is to evaluate the response of the bolted connection under a range of values. To account for scatter and to reduce computational or testing time, bolt analysis is done at two value, minimum pretension and maximum pretension. Minimum pretension ensures that an adequate amount of clamping force is reached such that the clamped parts do not open. Maximum pretension accounts for the scatter in the preload value. The calculation of these values has been done through the steps detailed in Section 2.2.

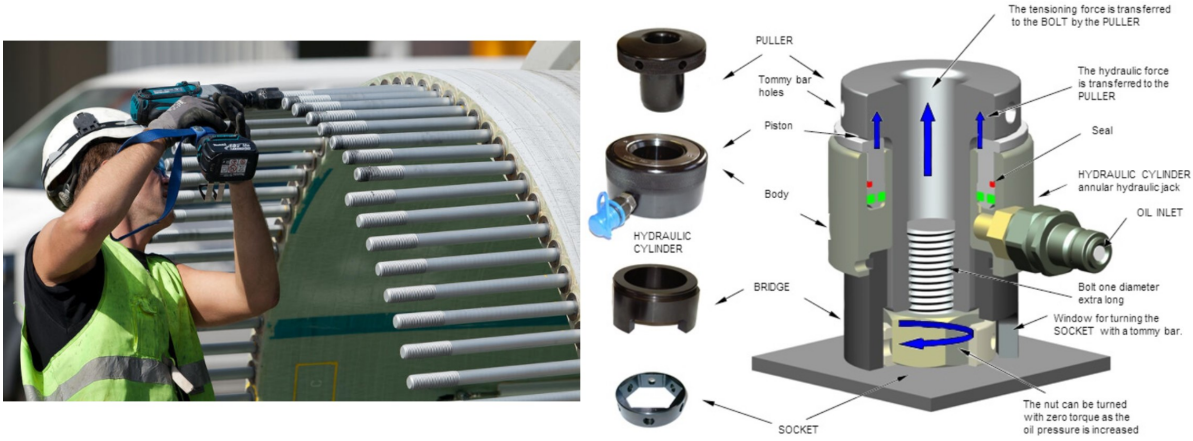

Figure 3.23: Application of preload through electric torque wrench on a wind turbine blade root [45] (left) and hydraulic tensioning, where the bolt thread or shank is stretched so that the nut requires zero torque [46] (right)

Minimum Pretension

According to Equation 2.4, minimum pretension is evaluated as follows:

$$F_{Mmin} = F_{Kerf} + (1 - \phi^*_{en})F_A + F_Z + \Delta F_{Vth} \tag{3.3}$$

The first term of the equation is calculated using the following equation:

$$F_{Kerf} = F_{KA} = F_{A_{max}} \cdot \frac{A_D \cdot (a \cdot u - s_{sym} \cdot u)}{I_{BT} + s_{sym} \cdot u \cdot A_D} + M_{B_{max}} \cdot \frac{A_D \cdot u}{I_{BT} + s_{sym} \cdot u \cdot A_D} \tag{3.4}$$

$F_{A_{max}}$ is the maximum axial load applied externally on the bolted joint. It is a function of the maximum bending moment observed at the root and was evaluated using Equation 3.1. A_D is the area to be clamped, which includes the faces of the bushing, the insert, and the laminate. (*Note: With reference to Figure 3.24, the gap between the bushing and the insert is to be filled with epoxy adhesive; for the scope of this study, it is assumed to be a perfectly bonded area with linear behaviour. The area A_D includes this gap as well*). a is the normal distance between the imaginary bolt axis, and the line of the application of external load. s_{sym} is the distance from the bolt axis to the imaginary symmetrical axis of the clamped part, and in this case, $s_{sym} = 0$. u is the distance of the opening edge from the bolt axis (Figure 3.25). I_{BT} is the moment of inertia of the clamped interface area A_D. For a singular bolt under analysis (symmetric sub-model), the effective external bending moment is converted to a purely axial load; hence, $M_{B_{max}} = 0$.

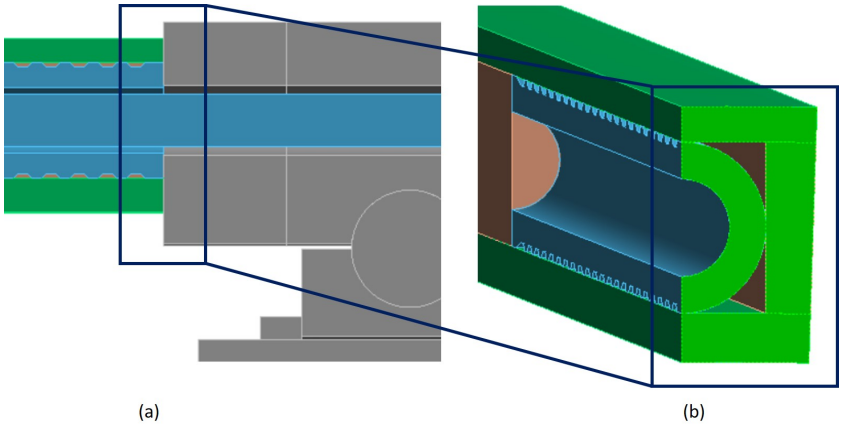

Figure 3.24: The highlighted surfaces on the right shows the clamped area A_D.

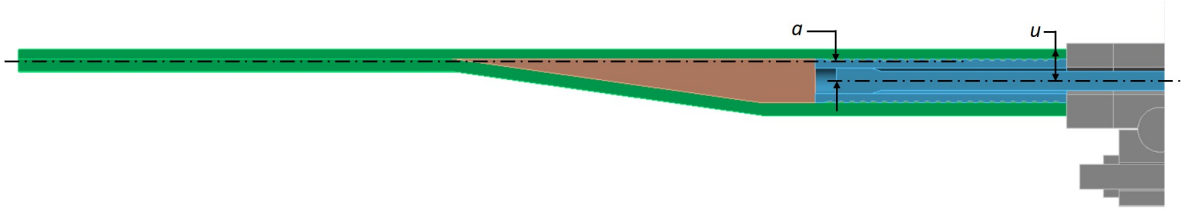

Figure 3.25: Coefficients a and u with respect to the joint geometry

The second term includes the load factor in case of eccentric loading and clamping ϕ^*_{en}. According to VDI [14], this factor has to be considered when the axis of application of load is significantly displaced from the bolt axis. This factor was not considered for the calculation of preload because of two reasons:

1. The eccentricity in load application in the joint under consideration is a, whose value for the first iteration was of the order of 30mm. In comparison, the point of load application is 1500mm from the transverse central axis of the bolt. Due to the eccentricity being just 2% of the critical dimension (Figure 3.25), opening of the clamped parts due to the additional bending moment was considered very small.
2. Even though the present analysis was conducted on a single bolt, when the entire blade root is considered, it is classified as a concentric plate. In this case, the moment (flapwise or edgewise) axis is coincident with the blade root axis, and the load application is no longer eccentric. Furthermore, bolt pretension in adjacent bolts affects and acts to increase the clamping load of the bolt under consideration.

Therefore, the second term is neglected during the calculation as the effect of eccentricity is negligible. F_Z and ΔF_{Vth} are additional loads to be factored in case of creep and changes in temperature. In this case too, they

have been considered negligible in the scope of the blade root. The minimum pretension required for a singular bolt was computed to be $277kN$; this value of applied preload is required to prevent sufficient clamping load to prevent separation of the blade from the hub.

Maximum Pretension

VDI [14] provides the values for tightening factor that are to be determined by the tightening method used during assembly and the size of the bolt. Given that the bolt to be used is M36, and the tightening method used will be torque controlled methods using either motorized torque wrenches or hydraulic tools, the tightening factor was chosen to be $\alpha = 1.4$. For this value of α, the setting method (or the preload verification method) to be used is pressure measurement, or through experimental verification of torque through bolt elongation.

According to the value of α, the maximum pretension comes out to be approximately $F_{Mmax} = 388kN$. For necked-down (reduced shank) metric bolts of size M36, coarse pitch (P = 4), and steel grade 10.9, the range of suggested assembly preload is in the range of $482kN$ to $370kN$. However, the upper limit of the bolt stress is limited by the ultimate strength in the bolt during assembly and operation. The range of maximum pretension values was analysed for bolt design criteria outline by VDI [14] using a MATLAB script.

1. Ultimate strength during assembly:
   Tensile stress in the shank during assembly:

$$\sigma_t = \frac{F_{Mmax}}{A_{shank}} \tag{3.5}$$

   where F_{Mmax} is the maximum pretension value on the bolt, and A_{shank} is the area of the bolt shank. Torsional stress developed in the shank is given by the following empirical relation:

$$\tau = F_{Mmax} \cdot \frac{1.155 \cdot \mu_g \cdot \frac{D_2}{2} + \frac{P}{2\pi}}{\frac{\pi}{16} D_{shank}^3} \tag{3.6}$$

   where μ_g is the coefficient of friction between the bolt and bushing threads, D_2 is the pitch diameter of the bolt, P is the pitch of the bolt thread, and D_{shank} is the diameter of the bolt shank. The effective stress is evaluated using the Huber-Hencky equation [24]:

$$\sigma_{HH} = \sqrt{\sigma_t^2 + 3 \cdot \tau^2} \tag{3.7}$$

   For the value of pretension to be acceptable, the ratio of σ_{yield} (yield stress of the bolt material: 940MPa) with σ_{HH} has to be greater than the material partial safety factor $\gamma_M = 1.1$ [15].
2. Ultimate strength during operation:
   It is assumed that during operation of the assembled joint, the torsional stress reduces by 50%. Hence:

$$\sigma_{HH-oper} = \sqrt{\sigma_t^2 + 3 \cdot (0.5 \cdot \tau^2)} \tag{3.8}$$

   The stress developed in the bolted joint due to external moment developed in the blade is found as follows (when there is no pretension being applied):

$$\sigma_{shank} = \frac{M_B}{BCD \cdot A_{shank} \cdot \frac{N_b}{4}} \tag{3.9}$$

   This is based on Equation 3.1, where BCD is the bolt circle diameter of the root, and N_b is the number of bolts in the root. The effective stress developed in the shank due to the external force on the joint is:

$$\sigma_{oper} = \sigma_{shank} \cdot \phi \tag{3.10}$$

   where ϕ_{stress} is the bolt stress ratio (ratio of stress developed in the bolt with respect to external force; this was found through the FE results). Further, the stress reserve factor SRF is found as follows:

$$SRF = \frac{\sigma_{yield} - \sigma_{HH-oper}}{\sigma_{oper}} \tag{3.11}$$

   For the bolt pretension value to be acceptable, $SRF > 1$.

As is the case with a design process, trial-and-error and engineering judgement was used to arrive at the value of minimum and maximum pretension. Pretension is an input parameter to the FE analysis, but the stress ratio required for calculation of the bolt pretension can only be found from the FE results. Therefore, a number of iterations were required before an acceptable value of bolt pretension could be finalised. A conservative approach taken and a value of $446kN$ for the maximum pretension was used for the analysis (for 96 bolts in the root). With the tightening factor $\alpha = 1.4$, the minimum value of pretension applied on the main bolt was $318.57kN$, well above the least possible value of $277kN$.

For the hub bolt, the value of pretension should be such that the bearing (and in turn, the blade) should have minimal to none rotation from the fixed hub. With several iterations, to ensure minimal rotation of the bearing assembly due to the external load,

Within the Ansys environment, bolt pretension can be applied directly to the bolt. The solver divides the face/body using the PSMESH command, creates a normal plane between the split faces/bodies, and automatically applies a pretension or 'pull' load, developing a tension state in the bolt [47]. The pretension is applied in the first step, and then set to 'lock' such that the bolts remain under tension throughout the further steps of applied external moment.

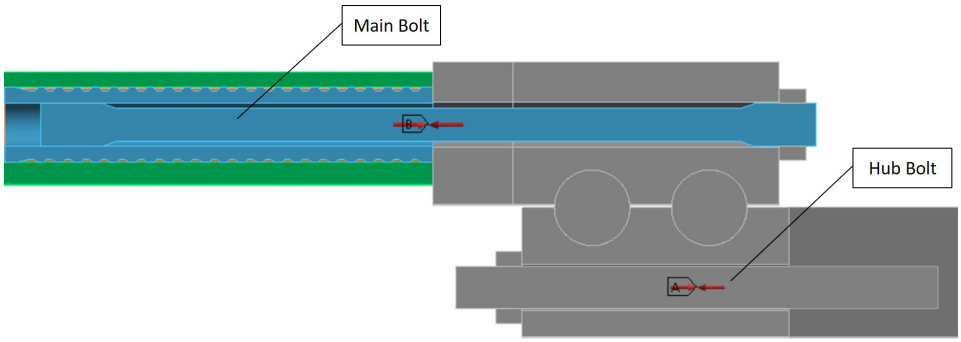

Figure 3.26: Pretension applied on the bolt shank for the main bolt and the hub bolt.

This page intentionally left blank.

4

Model Analysis and Validation

The key outputs that are required for validating the model are the bolt stress profile (the trend of developed stress with respect to the varying axial load being applied), and the load ratio of the bolt. The load ratio will be further used to check for accumulation of fatigue damage in the bolt. Before load ratios can be extracted from the data, the model behaviour has to be checked for a few key design criteria, which are explained in the following sections.

4.1. Preliminary design verification

Wing tip displacement

A significant number of wind turbine failures are attributed to the wing tip hitting the tower. Cox and Echtermeyer [48] calculated the maximum wing tip deflection for a 70m turbine blade to be at 8.46m (rotating condition, 30% clearance from the tower) and 11.48m (parked condition, 5% clearance from the tower). From these values, the maximum deflection in the Y direction for the 1.5m section of the blade being assessed (assuming a straight line deflection) is 180mm and 246mm respectively. Within the model, the maximum displacement in the Y direction was found to be at the tip of the filler wedge, indicating a gradient in stiffness due to the presence of three different materials at the point (composite laminate, UD material from the insert, and PVC foam used in the wedge). This displacement was in the order of 3mm (for minimum pretension), well within the maximum tip deflection suggested. The order of displacement also accounts for the laminate strains further towards the blade tip.

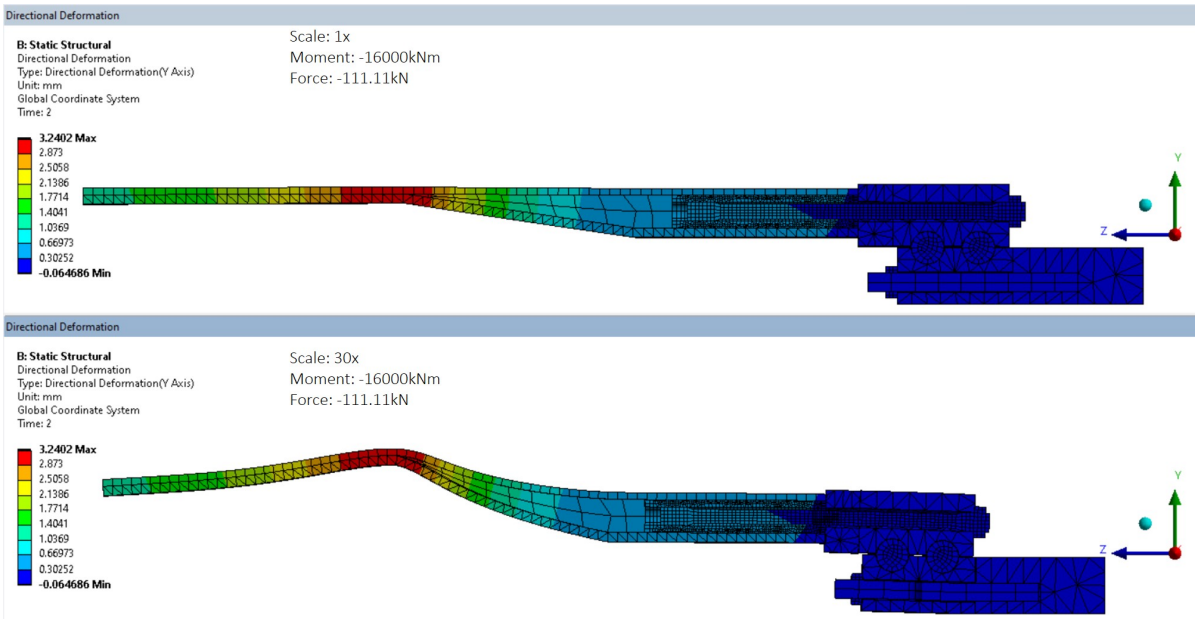

Figure 4.1: Deformations in the Y-axis at true scale (above) and 30x enlarged scale (below), at maximum compressive load

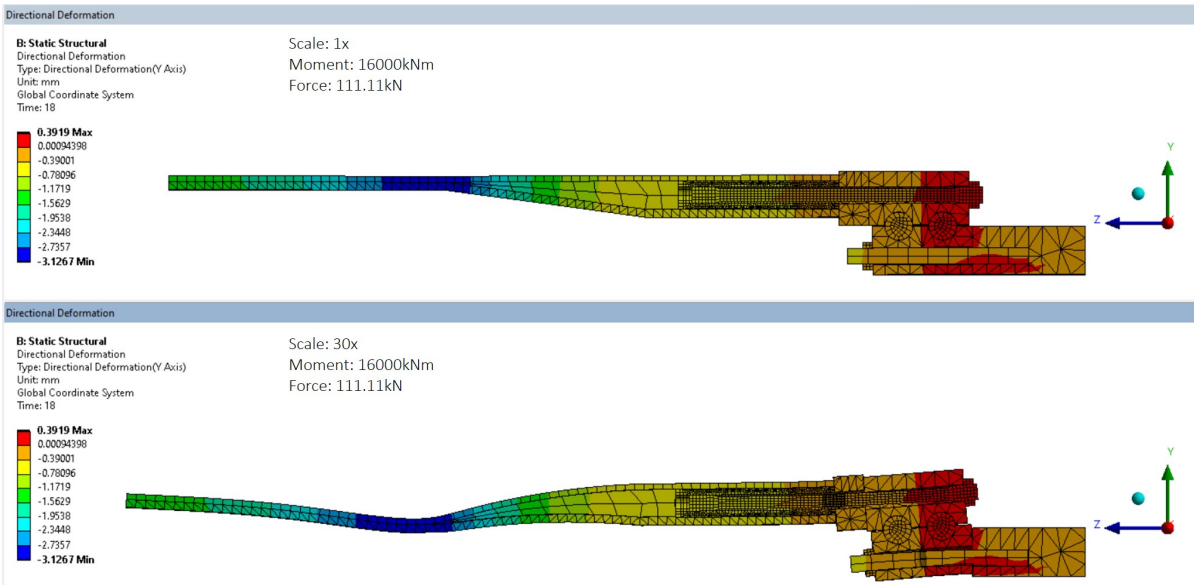

Figure 4.2: Deformations in the Y-axis at true scale (above) and 30x enlarged scale (below) at maximum tensile load

Strain Limits

Laminate strains are to be well within failure strain limits. The strains were checked in the direction of the ply layup, i.e., in the Z-axis according to the solver environment. The maximum acceptable value of tensile strain in the triax layup is 0.0244 in the principal direction, and compressive failure strain is -0.015. For the material used for the wedge (PVC), the tensile failure strain limit is 0.04.

Figure 4.3 shows the maximum strain developed in the direction of the load, for maximum compressive axial force (Z axis, along the blade). In the blade skin, the maximum strain developed in the laminate is -0.005, one-third of the failure strain value. For maximum tensile axial force (Figure 4.4), the maximum strain developed in the laminate is approximately 0.005, one-fifth of the failure strain value. Within the wedge, the PVC foam developed a strain of 0.006 at maximum tensile load, also well within its failure strain value. Maximum failure strains were also verified for the insert made of UD material and were found to be within acceptable limits.

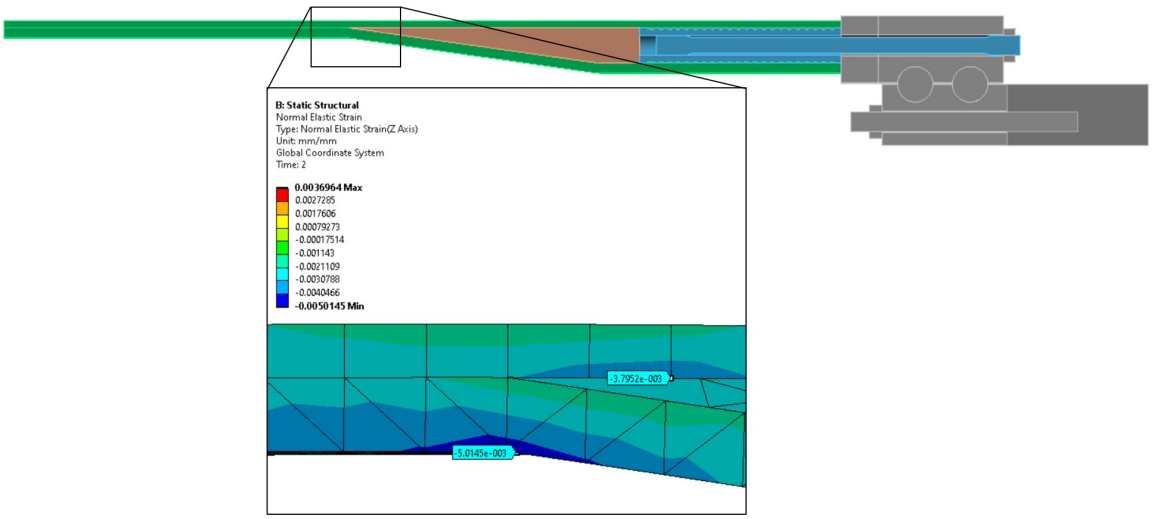

Figure 4.3: Strains in the laminate and wedge

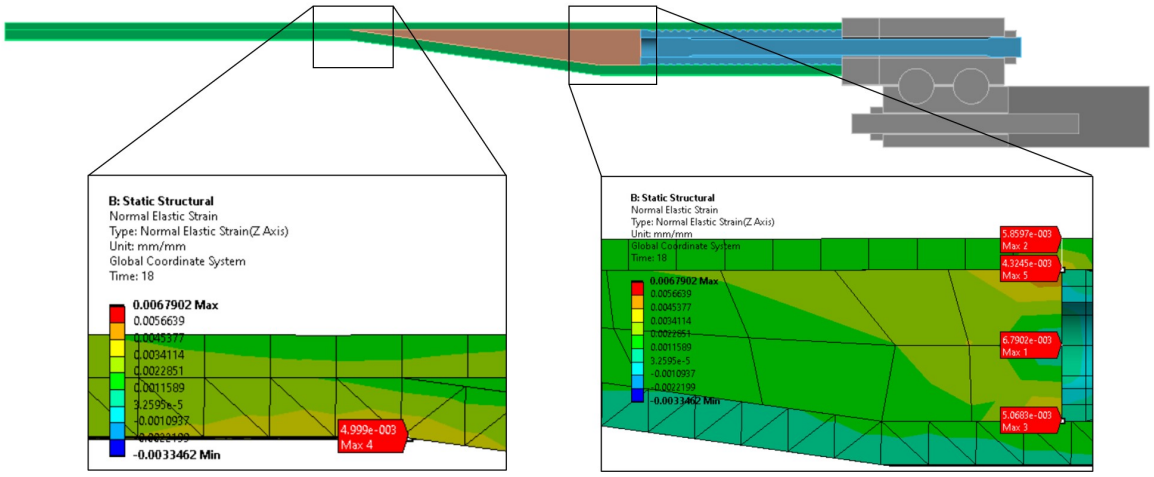

Figure 4.4: Strains in the laminate and wedge

Rotation of the blade-bearing assembly

Rotation of the blade-bearing assembly with respect to the fixed hub should be minimal. This has been validated by checking the displacement in the normal-Z direction (as $\theta = sin(\theta)$ for small angles), seen in Figure 4.5:

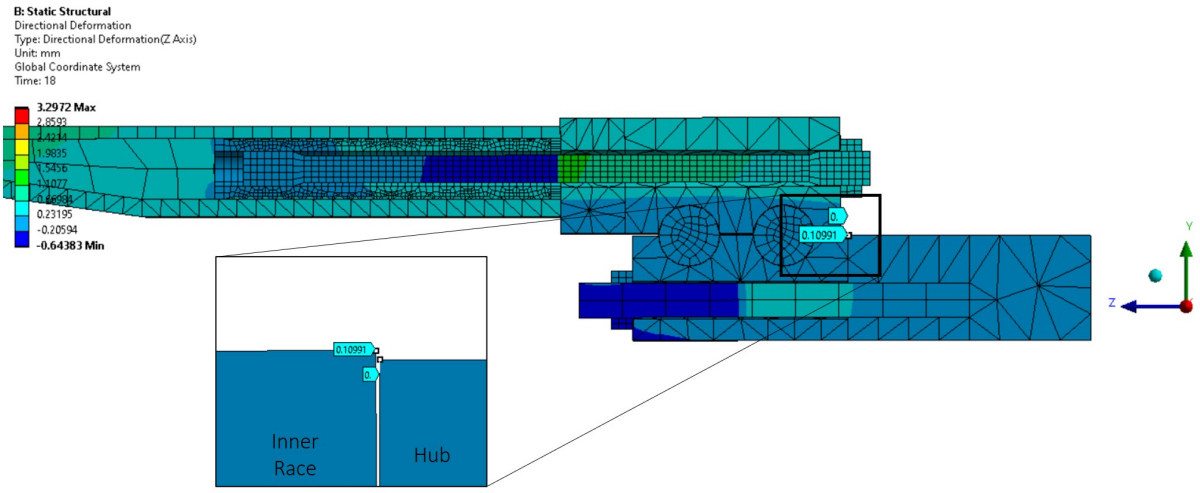

Figure 4.5: Maximum value of displacement in the Z-direction is 0.09mm, or 90μ m

Note: The above numerical values are the results of the first iteration of the blade-root connection design that was verified with existing data. The exact quantities are indicative of the general performance of the root and changed with respect to each iteration when comparative analysis was done.

4.2. Bolt Stress Profile

The stress profile of the bolt for the present analysis is a plot of the stresses developed in the bolt with respect to the applied external load derived from the bending moment at the blade. The Structures Department of Suzlon was provided with a prototype of the bushing design from a third-party consultant whose results included the stress profile of the bolt. The normalized values of the stress were used to verify the stresses being developed in the bolt.

To obtain the stress profile, stresses (along the blade axis, i.e., Z-axis) were extracted at key points in the bolt as shown in Figure 4.6. Nodes are selected 25mm from each shank end on the bolt, two towards the blade side, and two towards the hub side. For each side, one node selection is placed on the side of the bolt facing the outer layer of the blade skin, and the other facing the inner layer. Stresses at these four nodes on the extremes are assumed to provide an estimate for the entire bolt. The choice for these focus areas are based on design practices at Suzlon

[21]. The distance is kept $25mm$ to ensure the stress concentrations at the point where the diameter changes to the shank diameter does not influence the stress results. Given the reduced diameter of the shank, stresses are higher in this region, and is hence seen as a critical region for analysis.

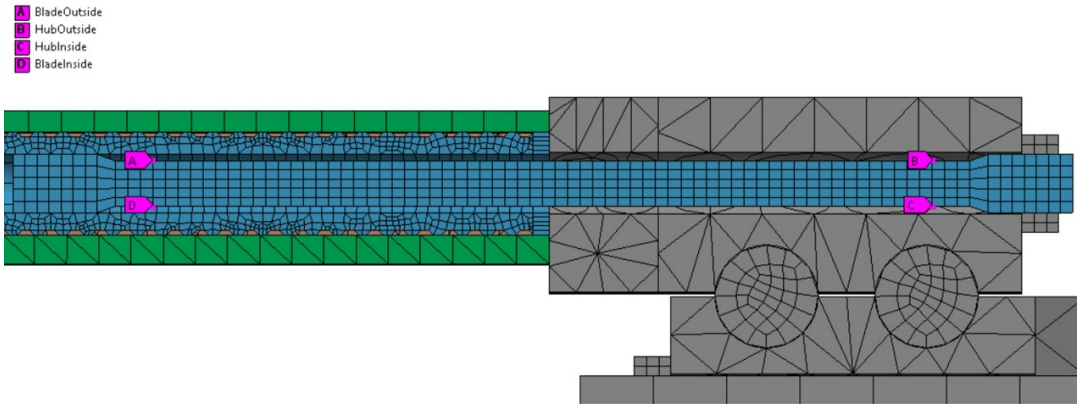

Figure 4.6: Stresses are extracted from the nodes named A (BladeOutside), B (HubOutside), C (HubInside), and D (BladeInside).

Stresses developed in the bolt

FE results of stresses developed in the bolt elements for different configurations is shown as follows:

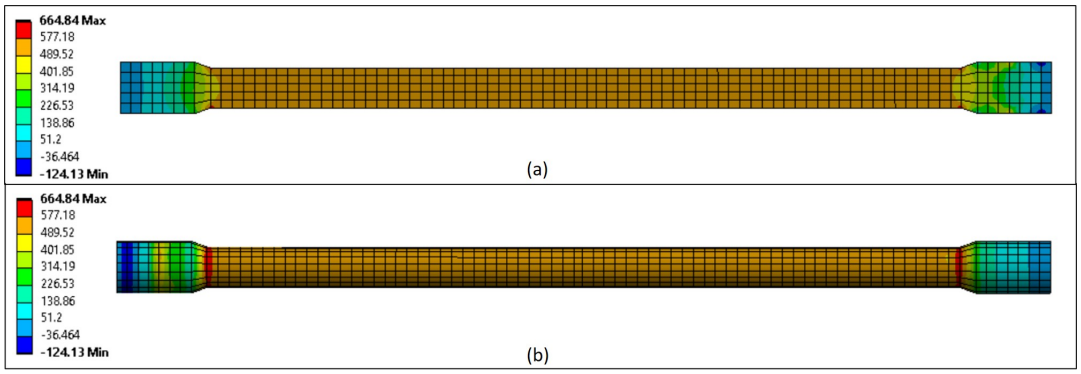

Figure 4.7: Stress developed in the bolt when pretension ($F_{vmin} = 318.57kN$) has been applied and there is not external load. (a) shows the sectioned view, and (b) shows the un-sectioned view of the bolt. Tensile stresses were developed in the bolt shank due to pretension, and compressive stresses at the ends where the bonded connection simulates the threaded joint. Stress concentrations can be seen at the area where the diameter decreases (*All values in MPa*).

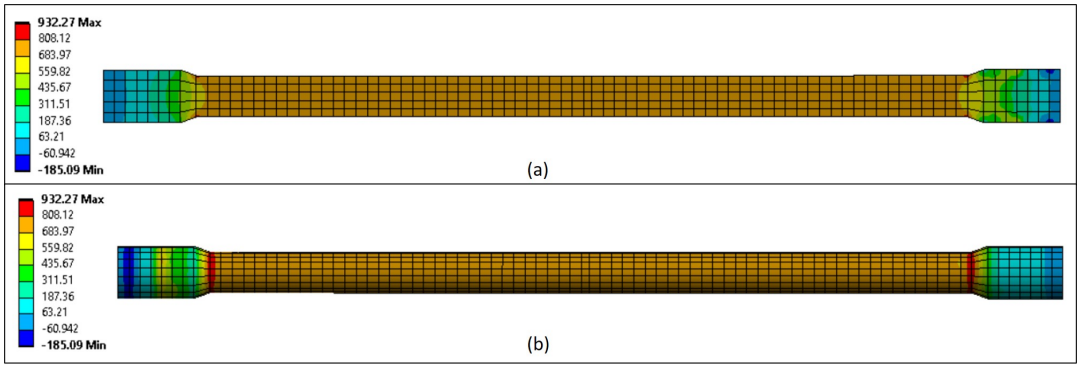

Figure 4.8: Stress developed in the bolt when pretension ($F_{Mmax} = 446kN$) has been applied and there is not external load.(a) shows the sectioned view, and (b) shows the un-sectioned view of the bolt. The increase in stress due to pretension can be seen in the legend (*All values in MPa*).

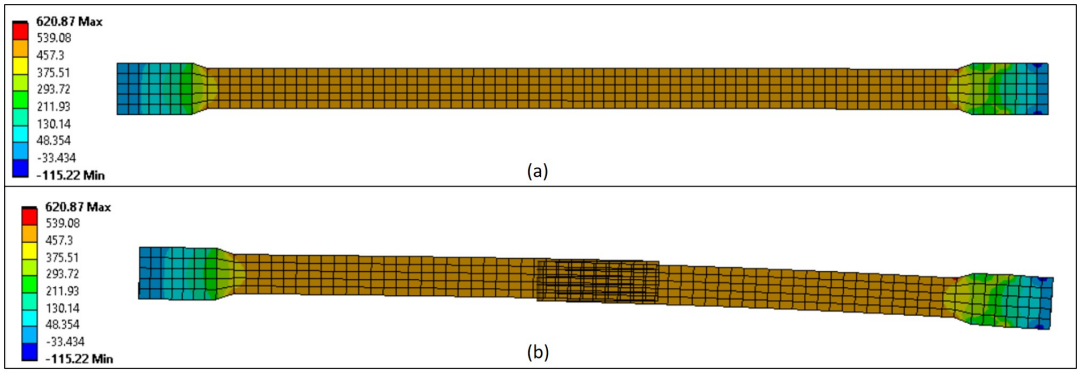

Figure 4.9: Stress developed in the bolt at F_{vmin} and at maximum compressive load corresponding to a bending moment of $-16000kNm$.(a) shows the bolt at 1x scale, and (b) shows the bolt at 50x scale. The compressive load relieves some of the stress in the preloaded bolt, which is evident from the decrease in stress compared to Figure 4.7(*All values in MPa*).

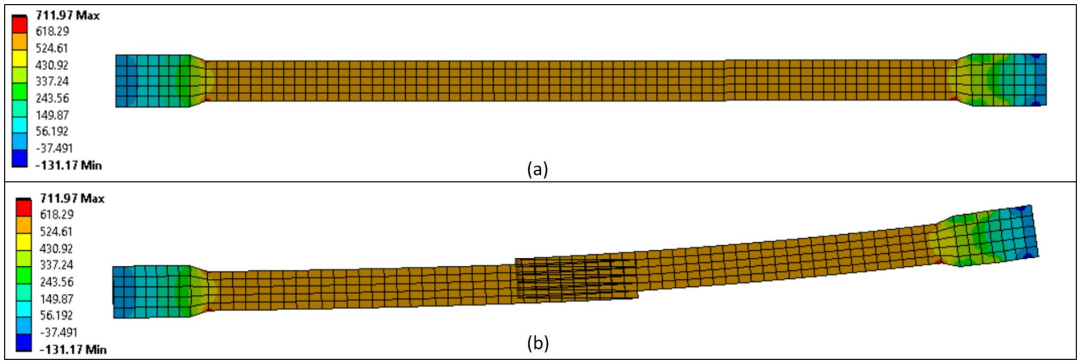

Figure 4.10: Stress developed in the bolt at F_{Mmin} and at maximum tensile load corresponding to a bending moment of $16000kNm$.(a) shows the bolt at 1x scale, and (b) shows the bolt at 50x scale. The external tensile load increases the effective stress in the bolt shank (*All values in MPa*).

Validation of the Bolt Stress Profile

The stress profiles were validated for the blade root with 96 bolts (this configuration has been taken to be the base iteration). The number of bolts was chosen to be 96 as the design prototype available with Suzlon analysed the connection with the same number of bolts. Stress profiles have been compared for $F_{Mmin} = 318.57kN$ in Figure 4.11.

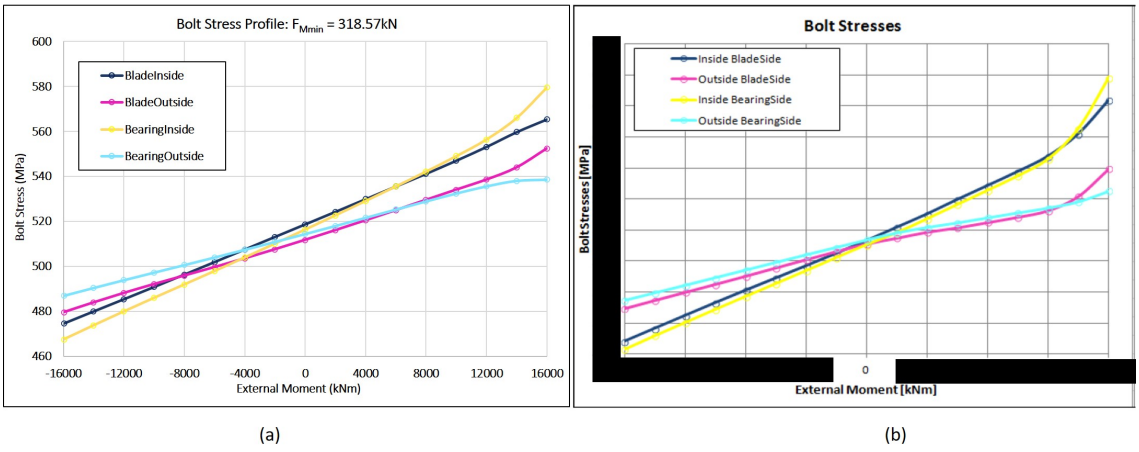

Figure 4.11: (a) shows the normalised stress profile that was the result of FE analysis on the connection (at minimum pretension) (b) shows the results from the design prototype available with Suzlon [21] with respect to the external moment (*Exact values have been redacted due to confidentiality clauses*)

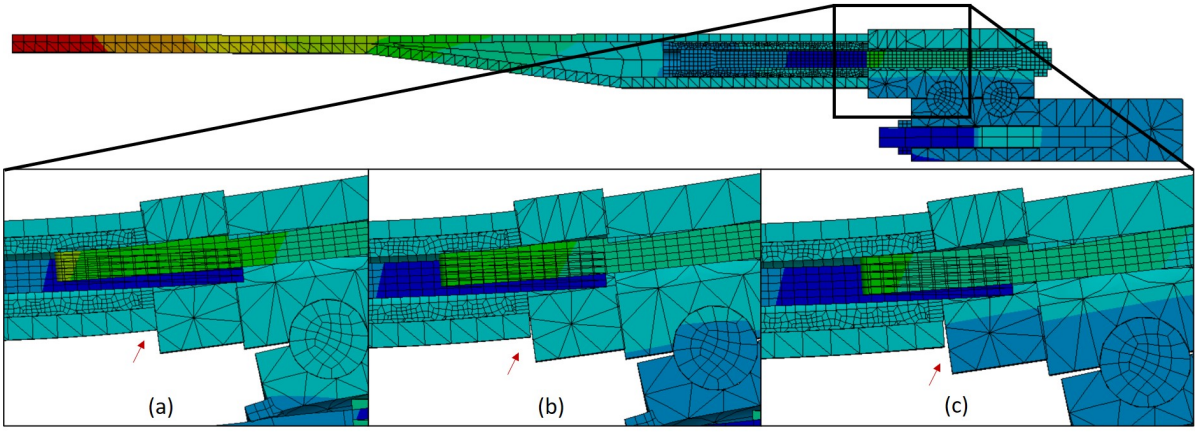

Figure 4.12: Displacement in the direction of tensile force at (a) 12000kNm (b) 14000kNm (c) 16000kNm (63x scale, $F_{vmin} = 318.57kN$)

Figure 4.11 compares the results of the present study (left) with the available stress profile provided by Suzlon. The following observations were made.

1. The inside profile of the bolt (the side facing the inner surface of the turbine blade) shows a particular trend (dark blue and yellow curves in Figure 4.11) that can be differentiated from the outside profile of the bolt (pink and light blue curves in Figure 4.11) in both results.
2. At maximum positive bending moment (maximum tensile load), there is a deviation in trends for both results. This can be explained by the observations seen in Figure 4.12. The inner surface of the blade (at the red arrow) stays in contact with the spacer/bearing assembly at $12000kNm$, and starts separating at $14000kNm$, with a significant displacement at $16000kNm$. The separation can be compared with the stress plot in Figure 4.11. The results are shown at a magnified scale for clarity; separation is not indicative of the scale used as the same was verified at other scales.
3. For the provided results ((b) in Figure 4.11), at zero external load, the stresses converge for all four extremes of the bolt. For the results of the present study, there is a deviation in stresses developed when there is no external load; this can be explained as an effect of preceding application of loads which might have an effect on subsequent stress results. Another source of this error might be the position of the bolt with respect to the blade for both models.

Stress profile comparison for $F_{Mmax} = 446kN$ has been given in Figure 4.13.

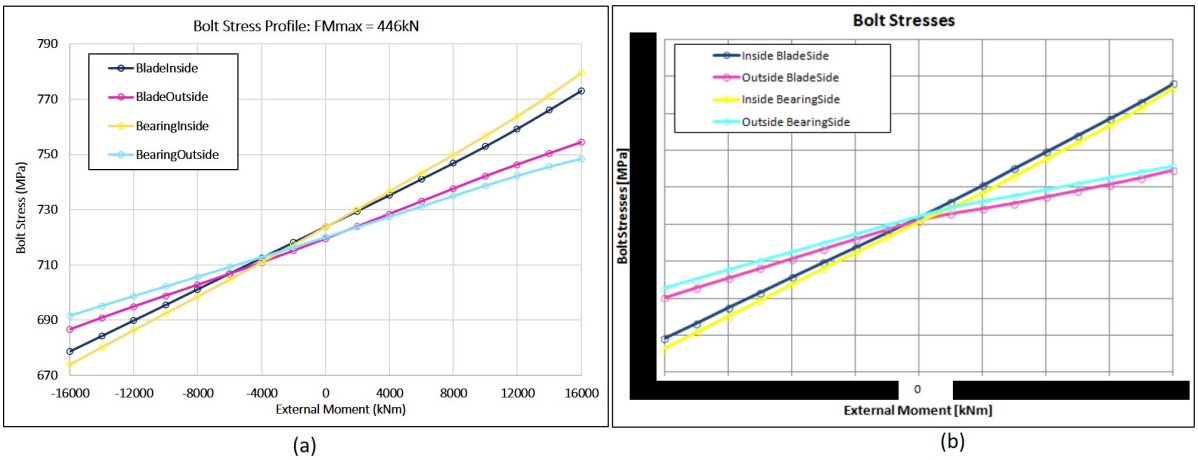

Figure 4.13: (a) shows the normalised stress profile that was the result of FE analysis on the connection (at maximum pretension) (b) shows the results from the design prototype available with Suzlon [21] with respect to the external moment (*Exact values have been redacted due to confidentiality clauses*)

It was observed in both cases (minimum and maximum pretension) that the stress profile matches the profiles

provided by Suzlon. The prototype design from which the stress profiles were taken from have been verified by Nijssen [9] to have qualified pull-out and fatigue tests.

Stress Ratio and SRF

Stress ratio (in context of the blade-root analysis) is defined as the proportion of stress that is developed at the bolt (or the component/node in question) with respect to the external force applied on the connection. The value of stress ratio were calculated using Equation 4.1.

$$\phi_{stress} = \frac{\sigma^b_{PT,EL} - \sigma^b_{PT}}{\sigma_{ext}} \tag{4.1}$$

where ϕ_{stress} is the stress ratio, $\sigma^b_{PT,EL}$ is the stress at bolt with both external force and pretension, σ^b_{PT} is the stress at bolt with only pretension, and σ_{ext} is the applied external stress.

Stress ratio is used to check for overstress in the bolt under operational stress. Based on the stress ratio, the Stress Reserve Factor (SRF) was evaluated. Stress Reserve Factor is an indication of the proportion by which external applied stress can be increased in a component. For an acceptable design condition, SRF has to be greater than 1; the value for SRF was evaluated from the steps defined in Section 3.6.2 using the following equation:

$$SRF = \frac{\sigma_{yield} - \sigma_{HH-oper}}{\sigma_{shank} \cdot \phi} \tag{4.2}$$

The following values of bolt stress ratio and corresponding values SRF were obtained

Minimum Pretension	Maximum Pretension
Stress Ratio	
0.175	0.155
SRF	
2.8757	3.2468

Figure 4.14: Stress Ratios and SRF

The values given in Figure 4.14 are for the base iteration with 96 bolts.

4.3. Fatigue Analysis

Loads sustained by the wind turbine blade due to the effective gravitational and aerodynamic loads have a variable amplitude in time-history data. While life can be predicted for a constant amplitude cycle using the S-N curve, for a variable-amplitude load history, fatigue life of the structure is a function of the damage accumulated. Palmgren-Miner's rule is used in this case for evaluation of damage, using data from the tabulated load spectra.

Load spectra can be tabulated in three ways: Range Spectrum, Range and Mean Spectrum, and Markov Matrices. The first two methods provide 1-dimensional and 2-dimensional information, i.e., as range of stress and corresponding number of cycles, and as both range and mean corresponding to number of cycles. Markov matrices provide sequence data; as linear damage accumulation is assumed [26], the effect of sequence of loading was not considered here. Data was provided in the form of Range-Mean-Cycle matrix for the edgewise bending moment sustained at the root (M_z). The matrix was a result of the Rainflow counting done by Suzlon's proprietary software.

The process followed for finding the fatigue life of the blade root connection is given in Figure 4.15. From the bending moment range and the bending moment mean, maximum and minimum bending moments were calculated using the following formula:

$$\begin{aligned} M_{max} &= \left[M_m + \frac{M_R}{2} \right] \\ M_{min} &= \left[M_m - \frac{M_R}{2} \right] \end{aligned} \tag{4.3}$$

where M_m is the mean bending moment, and M_R is the range of the bending moment.

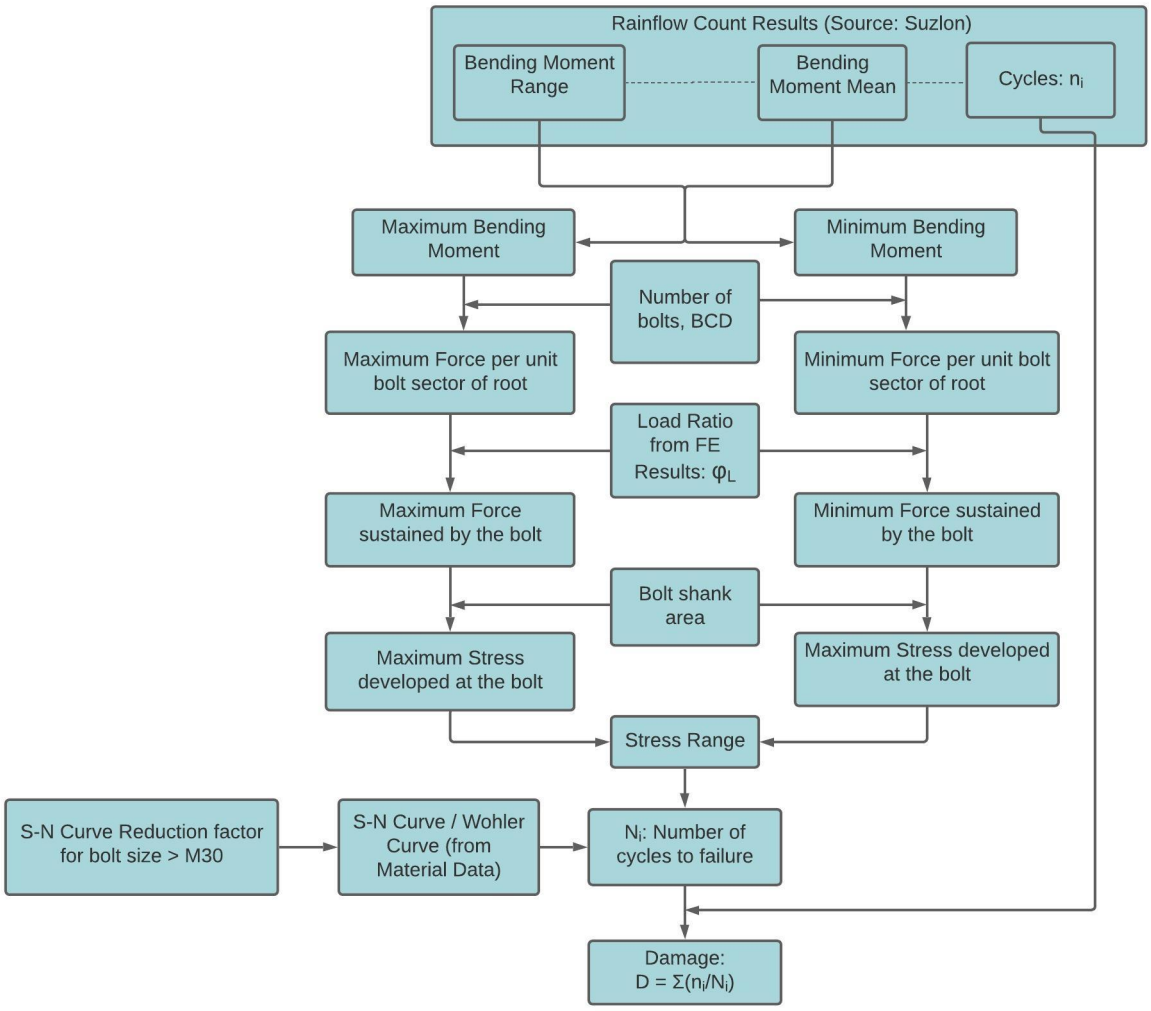

Figure 4.15: Steps used to evaluate fatigue damage

For each value of applied bending moment (maximum and minimum values, the equivalent force sustained by each unit bolt connection at the root was found. Referring to Figure 3.20, for each case, force is evaluated for the bolt at the extreme ends, i.e., where maximum tensile and compressive forces are developed along the root circumference. To find the effective axial force being applied on each individual bolt, load ratio found from FE analysis has to be multiplied to the force being applied to the bolted joint assembly. Load ratio is defined as the proportion of load being sustained by the bolt (or the component/node in question) with respect to the external force applied on the connection.

The value of load ratio was calculated using the following equation:

$$\phi_{load} = \frac{F^b_{PT,EL} - F^b_{PT}}{F_{ext}} \tag{4.4}$$

where ϕ_{load} is the load ratio, $F^b_{PT,EL}$ is the axial load at bolt with both external force and pretension, F^b_{PT} is the axial load at bolt with only pretension, and F_{ext} is the external force applied.

The relevance of using load ratios for bolted connections such as these are that they provide a singular value that reflects the effect of application of pretension in decreasing the stress on the bolt. Observations of application of external force on the bolted connection were made during numerical analysis, and it was found that for a given stress range, characterized by a maximum (σ_{max}) and minimum stress σ_{min}, the application of pretension on the bolt decreases the value of the stress range. It has verified that fatigue life is largely a function of the stress range σ_R (or stress amplitude, where $\sigma_R = 2 \cdot \sigma_a$), and not of the mean stress [19]. Hence, S-N curves are plotted with respect to σ_R or σ_a, and not maximum stress or mean stress. This trend is indicative of the fact that fatigue is a

result of cyclic loads. The trend of decreasing stress range on the bolt when pretension is applied demonstrates that the percentage increase in the value of maximum stress (σ_{max}) is less than the percentage increase in the value of minimum stress σ_{min}.

However, for a bolted connection that is subject to a variable amplitude load history with the number of cycles in the range of 10^9, it is time-consuming to evaluate the effect of pretension on the stress range of each cycle. The effect of pretension is a function of the stiffness of the bolt, the amount of pretension applied, the yield strength of the material, and the external normal or shear stress on the bolt. Hence, load ratios have been used here to replicate the effect of applying pretension on the life of the bolt during numerical analysis. Load ratios were found by static analysis of the structure using Equation 4.4, which were then used to estimate the fatigue life of the structure. The limitation of this method is that it is not an accurate representation of the effect of applying pretension on the life of the bolted joint. Experimental validation of fatigue life can provide an estimate on whether this method results in a conservative or non-conservative evaluation for the life of the material.

The consequent stress developed across the bolt shank was found by Equation 3.1:

$$\begin{aligned} \sigma_{max} &= \frac{M_{max} \cdot 4}{N_{bolts} \cdot BCD} \cdot \frac{\phi_{load}}{A_{shank}} + \sigma_{pretension} \\ \sigma_{min} &= \frac{M_{min} \cdot 4}{N_{bolts} \cdot BCD} \cdot \frac{\phi_{load}}{A_{shank}} + \sigma_{pretension} \end{aligned} \tag{4.5}$$

The stress range is given by:

$$\sigma_R = \sigma_{max} - \sigma_{min} \tag{4.6}$$

It is seen the though the value of stress due to pretension does not impact the stress range, the load ratio accounts for the effect.

The S-N curve for the bolt material has been plotted according to Germanischer Lloyd [15] and Eurocode (EN-1993-1-9) [49] regulations. For bolts larger than M30, a reduction factor has to be applied to the S-N curve to accommodate for the size effect. The statistical nature of fatigue performance indicates that larger the surface area, higher the probability of crack initiation sites. This is relevant to bolts as threads are areas of high stress concentration. The reduction factor has been calculated to be 0.9554 using the following empirical relation, where $d = 36$ when an M36 bolt is used:

$$k_S = \left(\frac{30}{d}\right)^{0.25} \tag{4.7}$$

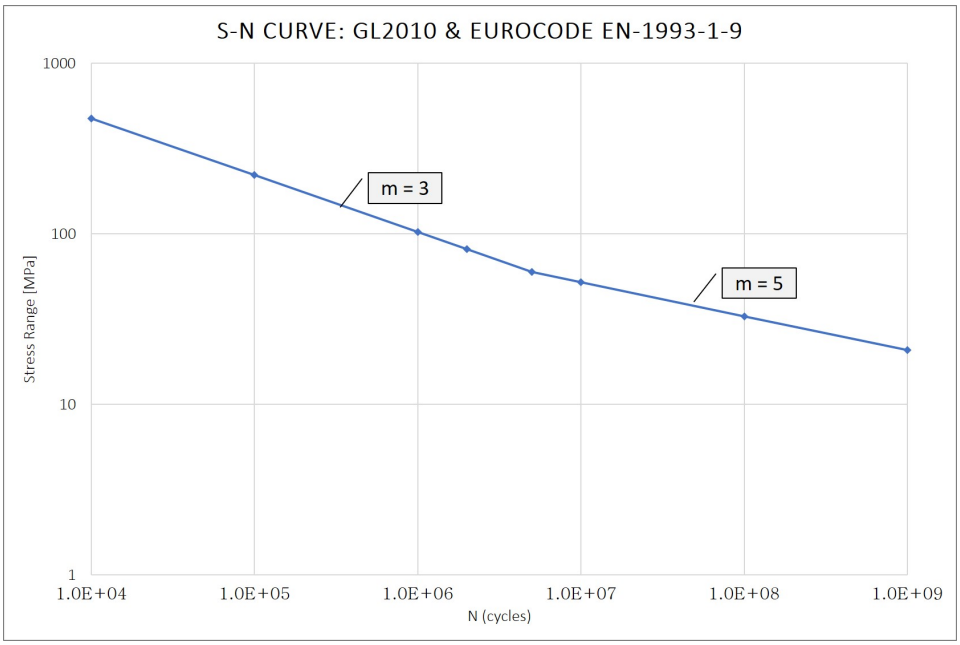

Figure 4.16: S-N Curve for bolt according to GL and Eurocode standards [15] [49]

The final S-N curve that was used for the analysis is shown in Figure 4.16. The Palmgren-Miner rule has been formulated as follows:

$$\Sigma \frac{n_i}{N_i} = \mathcal{D} \tag{4.8}$$

n_i is the number of cycles at the stress range or amplitude i, and is taken from the load history data. N_i is the number of cycles to failure at stress range or amplitude i, which was evaluated from the S-N curve in Figure 4.16. The Basquin relation is given by:

$$S_a^m \cdot N = K \tag{4.9}$$

where S_a is the stress amplitude (directly proportional to stress range), m is the slope of the S-N curve on a log-log scale, N is the number of cycles sustained at that particular stress range or amplitude, and K is a constant [19]. It was found that for $m = 3$, $K = 1.07127E + 12$, and for $m = 5$, $K = 3.83579E + 15$.

The value of N_i was found from the Basquin relation for each value of the stress range. The damage was calculated from Equation 4.8. The calculated value of damage was taken as a design constraint, i.e., $\mathcal{D} < 1$ was taken as a requirement for a valid design. However, due to the limitations of the method being used, the absolute value of $\mathcal{D}$ has been considered for evaluating the life of the joint, but only as a comparative specification factor when the effect of various parameters on the bolted joint is considered.

The calculated stress range was visualised along with the S-N curve to understand the load-history; this has been shown in Figure 4.17. A total of 797 data points, each corresponding a stress range with the number of cycles of operation, were plotted to result in the graph.

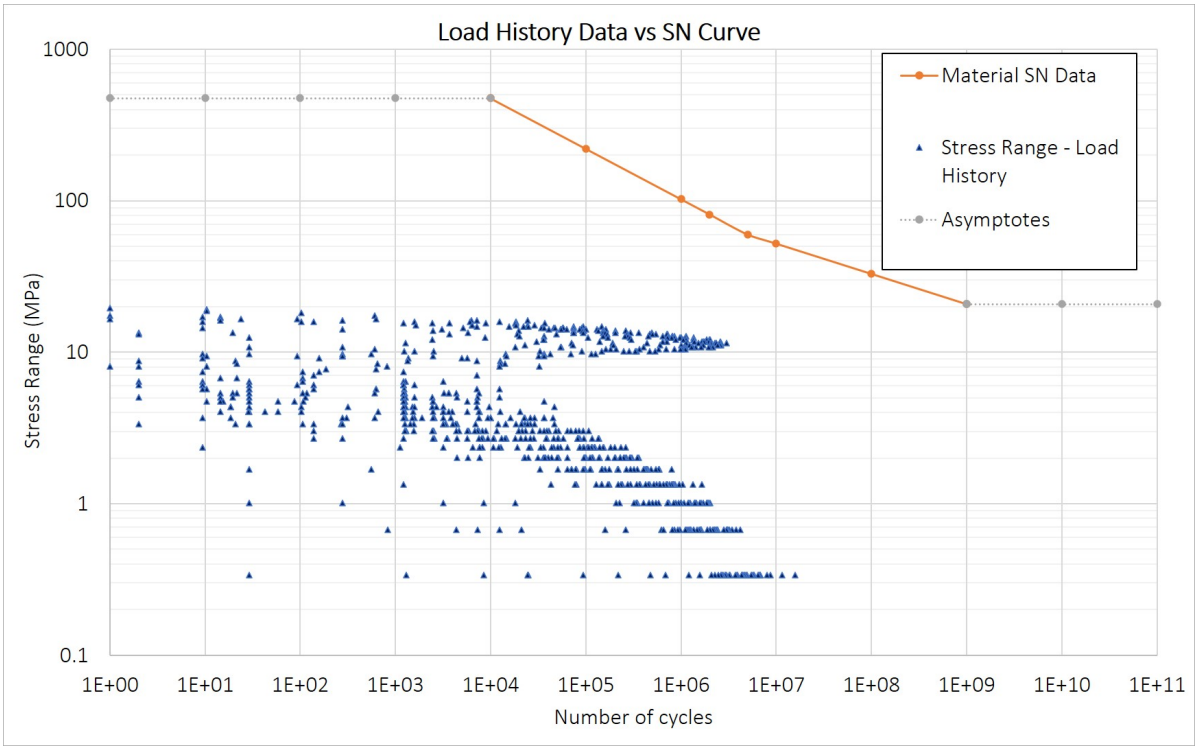

Figure 4.17: Load history for a load ratio of $\phi_{load} = 0.117$

One of the features of the S-N curve is the 'fatigue limit'. It the lower asymptote on the log-log scale of the curve, and it indicates a level of stress range or amplitude below which failure due to fatigue life cannot be discerned. In other words, if the stress amplitude of the fatigue cycle on a structure is below the fatigue limit, it will theoretically have an infinite life with respect to fatigue. The fatigue limit has been indicated by the horizontal dotted grey line (starting at 10^9 cycles) in Figure 4.17; the value of stress range at the fatigue limit is $20.3819MPa$. As it can be seen, the majority of the data points lie below the fatigue limit, and as is, would not have an effect on the fatigue life individually. When damage is evaluated, if the stress range is below the fatigue limit, then the value of N_i would tend to infinity, i.e., the particular stress cycle will not contribute to the decrease in fatigue life according to the linear damage accumulation rule.

However, the blade root is subject to the cumulative effect of these cycles. As a sum, these cycles will have a significant contribution to the fatigue life of the root. This highlights the limitation of using the Miner's rule for evaluating damage; stress ranges below the fatigue limit seemingly have a zero contribution to the fatigue damage, which is an impractical assumption.

To overcome this limitation and to come up with a conservative estimate of the accumulated damage, the value of N_i was given a finite value for stress ranges below the fatigue limit. For stress ranges below the fatigue limit, the number of cycles to failure was kept at 10^9; this is expected to result in a conservative figure of accumulated damage, but as life of the structure is not being evaluated, it has been considered sufficient for this study.

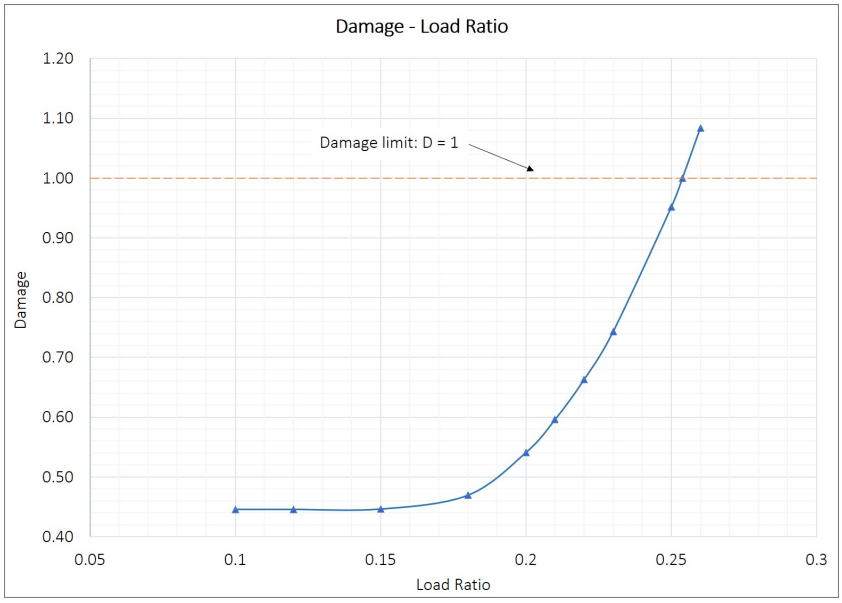

Figure 4.18: Value of damage $\mathcal{D}$ with respect to load ratio ϕ_{load}, for the base blade root configuration of 96 bolts

The plot in Figure 4.18 shows an almost constant value of damage for load ratios up to $\phi_{load} = 0.15$, and an exponential increase in $\mathcal{D}$ beyond that. This trend is indicative of the distribution of the load cycles seen in Figure 4.17. Load histories that are characterised by a greater number of high-amplitude cycles will be characterised by a steeper damage curve that reaches the damage limit faster.

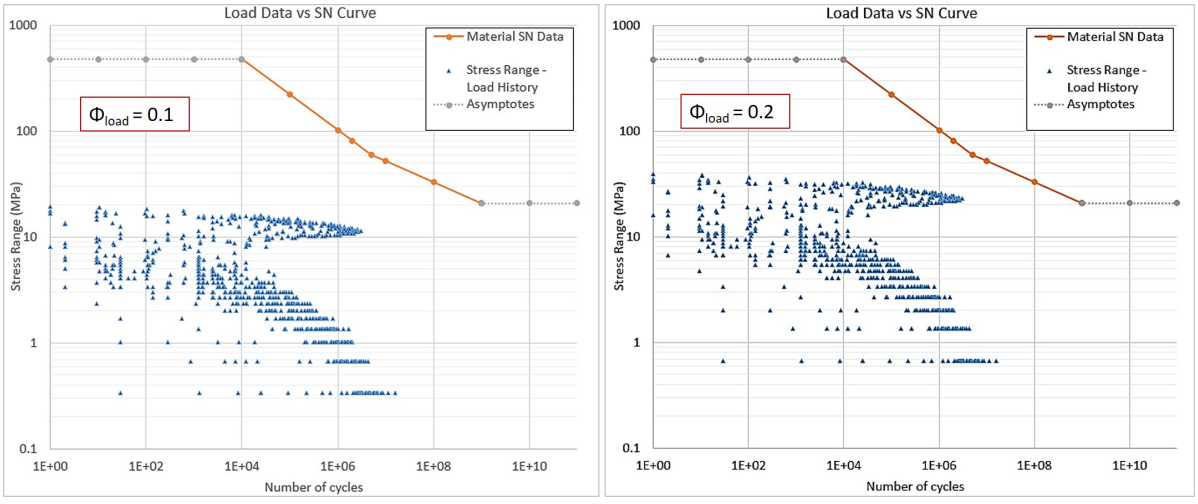

Figure 4.19: Effect of load history on the numerical value of damage

Figure 4.19 shows the effect of load ratio and the load history on the effective damage. For low values of ϕ_{load}, most of the cycles are below the fatigue limit. The load history is characterised by a peak in stress ranges

populated by a high number of cycles in the order of 10^6; this peak contributes to the accumulated damage for a higher load ratio.

Safety Reserve Factor for Fatigue

Safety Reserve Factor is an industry-defined factor that is used to indicate the tolerance for material and load parameters. It is used as a reference for designers to understand the degree by which external loads or material stiffness can be increased. In practice, the value of SRF should be greater than 1. It is calculated using the following method:

$$SRF = \frac{\phi_{load,at\mathcal{D}=1}}{\phi_{load}} \cdot \frac{1}{\gamma_M} \tag{4.10}$$

where $\phi_{load,at\mathcal{D}=1}$ is the value of load ratio when damage reaches its constraint limit. γ_M is the safety factor recommended for the fatigue design of components with 'periodic monitoring and maintenance with poor accessibility' where the 'component failure may result in design failure' (but not complete failure due to redundancy or damage tolerant design). According to GL [15], $\gamma_M = 1.15$.

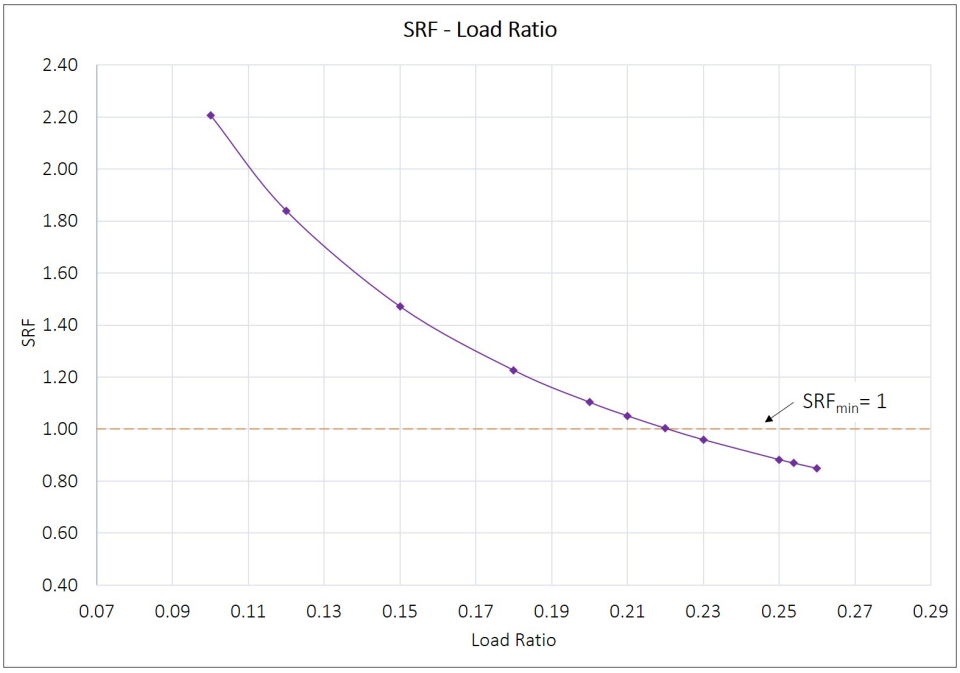

Figure 4.20: Trend of SRF with respect to Load Ratio (96-bolt configuration)

Due to the addition of the safety factor in evaluating SRF, the design limit for load ratio ϕ_{load} is lower than the design limit evaluated using damage $\mathcal{D}$.

5

Comparative Analysis

The blade root connection can be implemented as part of the wind turbine structure only when it has been certified through various experimental tests. Wind turbine blades require certification through fatigue tests, wherein the wind turbines are subject to flapwise and edgewise loads to millions of load cycles. The time and cost investment involved in the tests make it imperative that the effect of different configurations of the test setup should be known.

To understand the effect of changing various parameters in the bushing design, a number of comparative analyses were carried out. Each design iteration was validated for its stress profile, bolt overstress in assembly, the safety reserve factor in operation, and the accumulated damage. The quantitative measures on which each iteration was compared were normalized change in load ratio, change in accumulated damage, change in weight of the root, and the difference in overall cost.

The weight of the blade-root is a key parameter in the design of a wind turbine blade. The trend for weight in wind turbines follows a pattern similar to other aerodynamic structures such as aircraft: changes in weight have a snowball effect on the overall design. Heavier structures require more damage tolerant designs, which leads to addition of more components, resulting in even heavier structures. The same principle was followed in this section; the objective was to compare the effect of varying different parameters to study the effect on weight and subsequent cost of the root connection, with the design constraint being the damage $\mathcal{D}$ and the Safety Reserve Factor for fatigue. To identify which parameters could be varied, the base iteration was studied to determine which of the components contributed to the blade root in terms of weight and cost. The results are given in Figure 5.1.

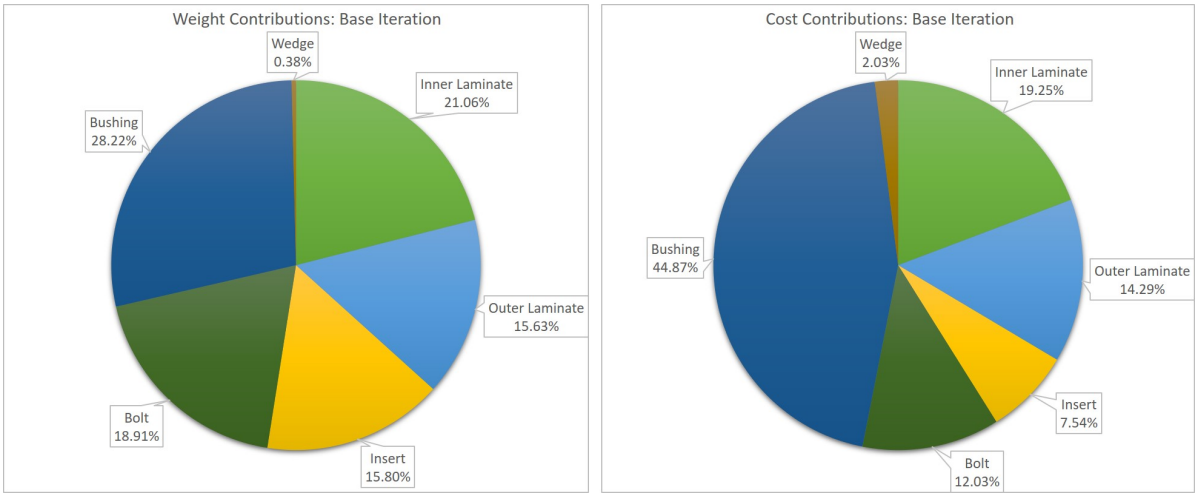

Figure 5.1: Contributions of the blade-root components to the total weight and cost

It was seen that the bolt-bushing assembly together are the heaviest components within the root; this can be attributed to the base material being steel. The cost of the bushing is comparatively higher as it factors in an estimate of manufacturing the topology of the surface. Therefore, the variable parameters were chosen such

that the contributions by the bushing and the bolt can be reduced in favour of lighter components; the following sections reflect these choices.

5.1. Parameter: Number of bolts

The initial design was chosen to have 96 bolts from an initial bushing design estimate. The T-bolt root connections used by Suzlon for the SE-make $63m$ blade has 104 bolts along the BCD. A favourable trend for the blade root performance is to increase the number of bolts at the root. This can result in either or both of the following:

- Fatigue damage accumulated per bolt is less due to redistribution of bending moment over an increase number of bolts. This can result in increasing the life of the blade root.
- Increasing the number of bolts by a minimal amount, with the same applied pretension, may increase the root capacity to sustain higher levels of bending moment. This allows the use of the same configuration of blade root for longer blades, saving time and costs in redesigning and addition of excess material.

As previously mentioned, the design iteration of 96 bolts at the BCD was considered as the base design with respect to which other design iterations were compared. For the two scenarios mentioned above, separate analysis cases were defined as follows:

5.1.1. Effect of modifying the number of bolts for a constant external moment

Two design iteration directions were considered in this particular case: decreasing the number of bolts to compare the benefit of a lighter blade root with the relative change in performance, and increasing the number of bolts to compare the improvement in performance with the change in blade root weight. The parameter that was kept constant was the total external moment. To achieve this, the clamping force, or the force reaction of the blade at the hub, was kept the same as the base iteration (96 bolts).

Decreasing the number of bolts

The direct effect of using a lesser number of bolts in the blade root is the decrease in weight and cost. As the bolt and bushing are dependent quantities, the percentage change in both weight and cost will be significant (see Figure 5.1). Keeping this in mind, two configurations were designed, one with 90 bolts, and the other with 85 bolts, as a sequential decrease in bolt number.

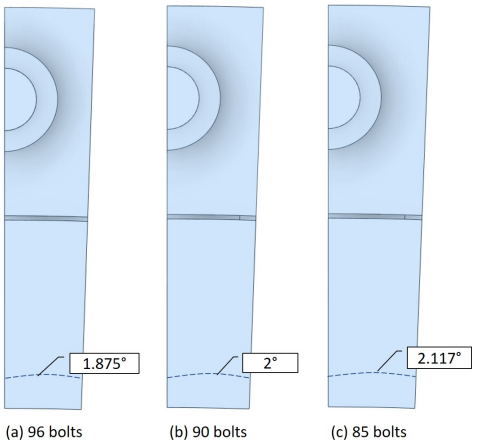

Figure 5.2: Rear view of the connection. Angular section per bolt increases as the bolts decrease.

As the external moment is distributed over the blade root circumference, lesser number of bolts would each carry an increased proportion of the effective axial force to achieve the same clamping force. Additionally, to avoid the separation of the blade from the root and to obtain the same amount of clamping force as the base iteration, a blade root with lesser number of bolts is required to have a higher applied pretension in each bolt. The value of F_{Mmax} was evaluated to be $446kN$ according to bolt grade specifications set by VDI [14], and conditions for bolt stress during assembly and operation. Within the FE environment, the bolt pretension was increased proportionally with respect to the decrease in bolt number to achieve the same clamping force. Initial validation tests on the bolt showed that the stress per bolt exceeded safety factor limits specified by VDI. This can

be explained by an overall increased stress per bolt over the blade root due to both pretension and external applied force (due to bending moment) as the bolt number is decreased. Therefore, further comparison was not carried out.

Increasing the number of bolts

The methodology followed in the previous exercise was followed for the configurations with an increased bolt number. Three additional configurations were chosen with an aim to understand the trend of the values: 100 bolts, 104 bolts, and 110 bolts (104 was chosen as SE has T-bolt configurations with 104 bolts present). Validation tests were conducted and no bolt overstress was found.

It was observed that as bolts were increased in the blade root, the load ratios increased (Figure 5.3). The hypothesis while designing this configuration was that there would be a decrease in bolt load ratios, as the unit bolt would bear a smaller fraction of the total bending moment. While this is not evident from the trend of load ratios, the hypothesis was proved correct when total damage was calculated. It was found that as the number of bolts increased, the tolerance for load ratios was higher, i.e., $\mathcal{D} = 1$ was obtained at higher values of load ratio (Figure 5.4). It can be suggested that a higher number of bolts within the blade root (for a bushing connection) may translate to a better fatigue performance. The trend for damage also indicates that increasing the number of bolts within the blade root will allow the blade to sustain higher or abnormal load cases while being within allowable fatigue damage limits.

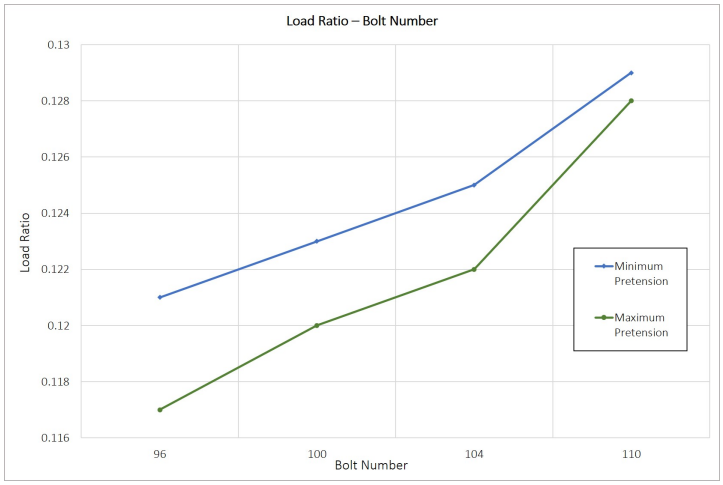

Figure 5.3: Change in Load ratio in the bolt with respect to number of bolts

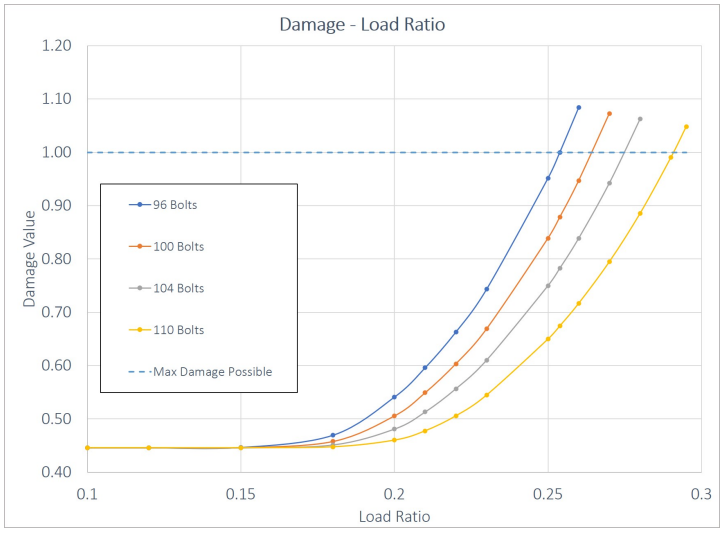

Figure 5.4: Trend of damage values with respect to number of bolts

Weight and cost for each configuration was evaluated and compared (Figure 5.5). As noted previously, the bushing and the bolt are major contributors to both the weight and cost, and this reflects in the significant increase in value for both. Given the observation that a higher number of bolts improves fatigue response of the root, a trade-off has to be made between performance and cost when the number of bolts is considered. Configurations with more bolts can be limited to turbines installed in locations prone to wind turbulence or abnormal aerodynamic loading.

It is to be noted that the values for cost are approximate and have been plotted to understand the trend. Relative estimates have been considered (rate of triax material as compared to UD material, for instance). As this is a commercial endeavour, rates of material will change according to source of supply and manufacturing methods used. The cost of assembly in testing will also differ from the cost of assembly in final production due to economies of scale.

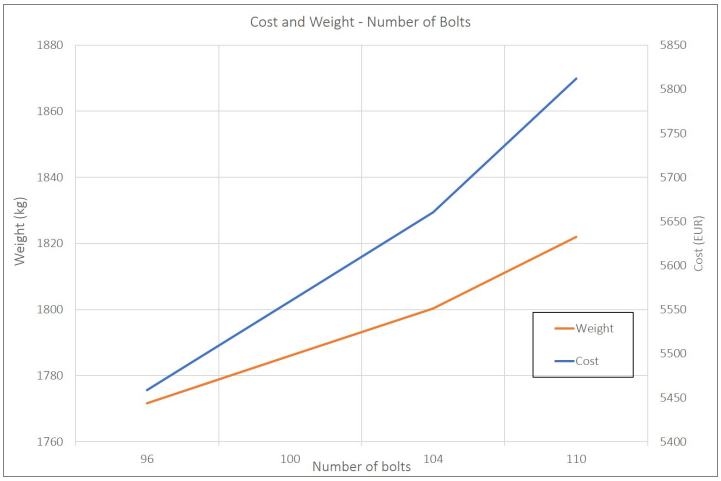

Figure 5.5: Trend of weight and cost of the full blade root with respect to number of bolts

5.1.2. Effect of number of bolts on external bending moment capacity

In the previous configurations, the effective preload on each bolt was decreased to achieve a uniform clamping force across all iterations where the bolt number was increased. An alternative hypothesis was tested to identify if an increased number of bolts, with the same amount of preload force on the bolt, would result in higher bending moment capacity of the blade root. The effective clamping force between the blade and the root would increase in this configuration.

The load step for external bending moment was kept at $2000kNm$ for other iterations; in this particular case, the load step was increased to $2500kNm$, raising the effective bending moment range to $-20000kNm$ to $20000kNm$. The maximum bending moment measured at the root through blade analysis for the current blade length was approximately $13000kNm$. Testing the blade root connection at higher loads is a basic method to find if longer blades for the same blade root configuration are theoretically possible. To perform an equitable comparison, the effect of a higher bending moment was tested on the base configuration, as well as the configuration with an increased number of bolts. The parameter that was kept constant for all configurations was the minimum and maximum values of pretension ($F_{Mmin} = 318kN$ and $F_{Mmax} = 446kN$ respectively). It was seen in Figure 5.7 that a higher bending moment at the root does increase the load and stress ratios, but increasing the bolt number at the root by just 4 bolts (96 to 100 bolts) has an effect of decreasing the effective stress and load borne by each unit bolt. Although these load ratios contribute to a minute change in accumulated damage, the trend of change in these ratios is relevant when choosing the number of bolts. The applied pretension value is the same for all iterations; the same bolt grade can be used for multiple scenarios.

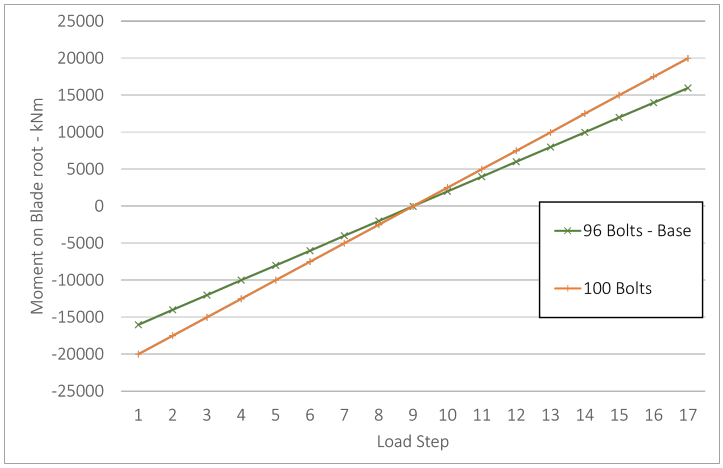

Figure 5.6: Increased external moment developed at blade root

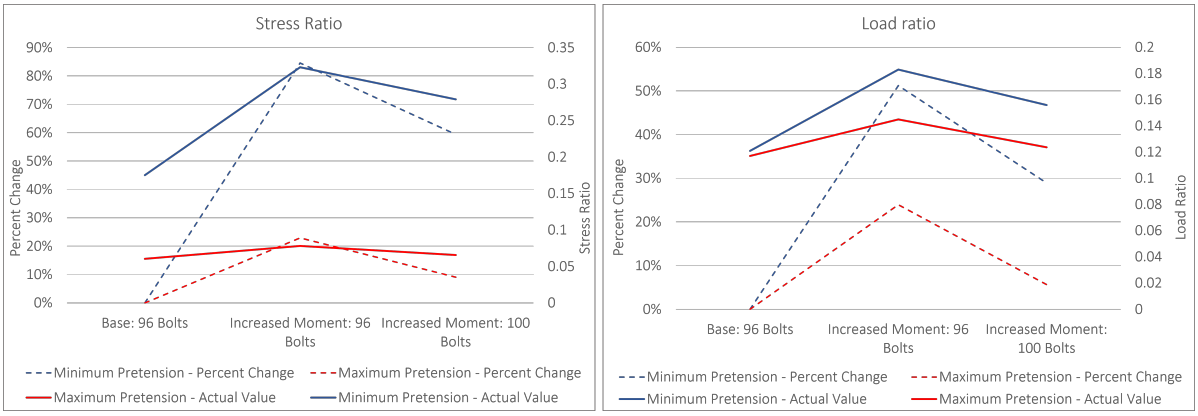

Figure 5.7: Effect of increased load on stress and load ratio

5.2. Parameter: Material of insert

A design principle that has been seen in literature and in published patents is the effort to bridge the gradient in stiffness of different components in the blade root. A higher stiffness gradient results in unpredictable deformations at interfaces and can lead to abnormal load cases that are undesirable at the blade root. For the base iteration, there is a difference in stiffness of the laminate (triax) and the bolt-bushing assembly (high-grade steel) by a factor of 7. Each bushing is separated by an insert made of UD material, chosen to bridge the stiffness between the bushings.

For the base configuration, a unidirectional composite block made of E-glass/resin epoxy mix (used by Suzlon) was assigned to the insert material. Stiffer composites used commercially were considered, like S-glass and Carbon-fiber composites. Additionally, two epoxy systems were compared for feasibility. Shell Chemical's Epon HPT 1072 was chosen as the resin system for all fibres for its stiffness and compatibility to the fibres [50].

Results of the comparison between glass fibres are shown in Figure 5.8; relative change in load ratio, weight, and cost are plotted. It can be seen that although the S-glass-epoxy UD material has superior stiffness properties and a slightly lower weight, the high cost is a disincentive. Increasing the stiffness lowers the load ratio, i.e., lowers the proportion of stress borne by each bolt. The change in load ratio is too small for a significant change in fatigue damage.

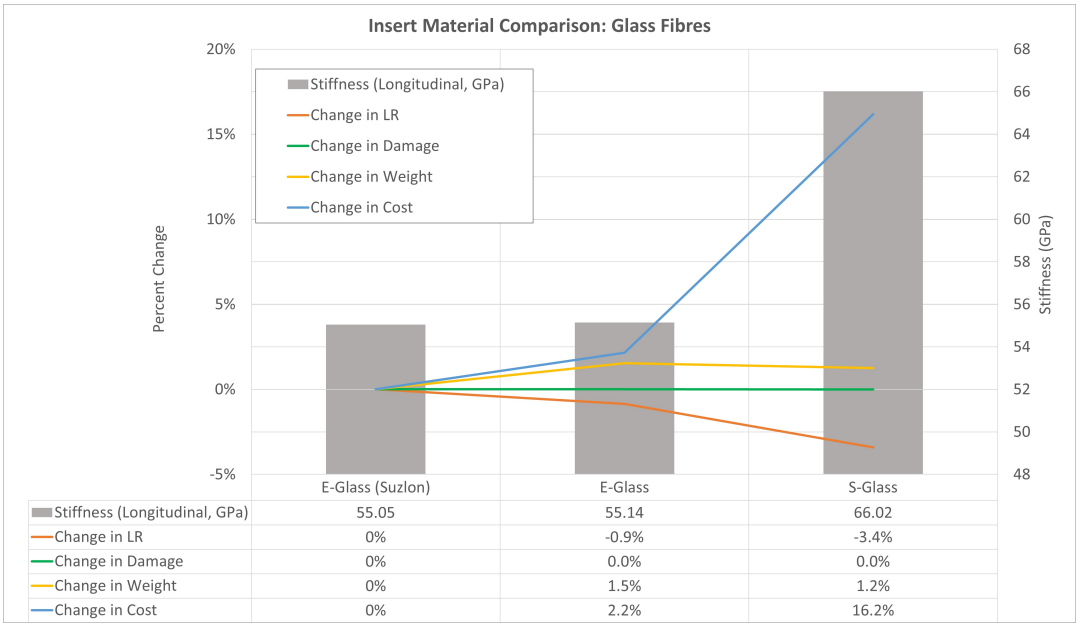

Figure 5.8: Performance of glass fibres

Similarly, the effect of using carbon fibre-epoxy UD material in the insert was analysed, and the results can be seen in Figure 5.9. The values for cost of the material are indicative of general availability in the commercial space; S-Glass is around 3 times more expensive than E-Glass fibre, and carbon fibres are generally anywhere between 10 to 20 times the cost of glass fibres [50].

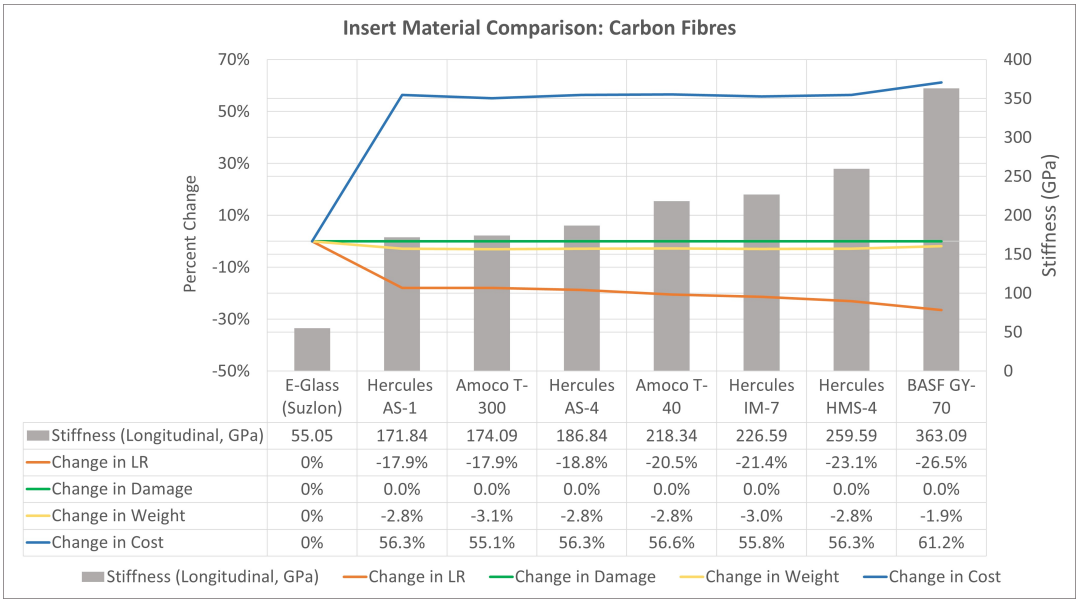

Figure 5.9: Performance of carbon fibres

5.3. Parameter: Bolt Length

Bolts are provided by fastener manufacturers in standard lengths, or can be custom-ordered for a significant number of bolts. Bolt length was chosen as a parameter as decreasing the bolt length would translate to a substantial savings in weight and cost. Both the bolt and the bushing lengths were decreased in steps of $26mm$ ($\approx 4\%$ of initial bolt length). From Figure 5.10, it was observed that there was a evident decrease in weight and cost. Due to the change in dimensions, it was seen that the load ratio also showed an increase. With decreasing bolt length, the effective geometric stiffness of the bolt also decreases, and this can be suggested as the reason for an increased

proportion of load being borne by the bolt. As the overall load ratios are well below the critical limit where the damage value exponentially increases, there was negligible change in damage. However, when the bolt length was decreased to $574mm$ (next step after $600mm$), there was a 259% jump in the load ratio, and the damage value was well above the allowable limit ($\mathcal{D} \approx 8$). This result has not been shown in the plot due to its extreme values.

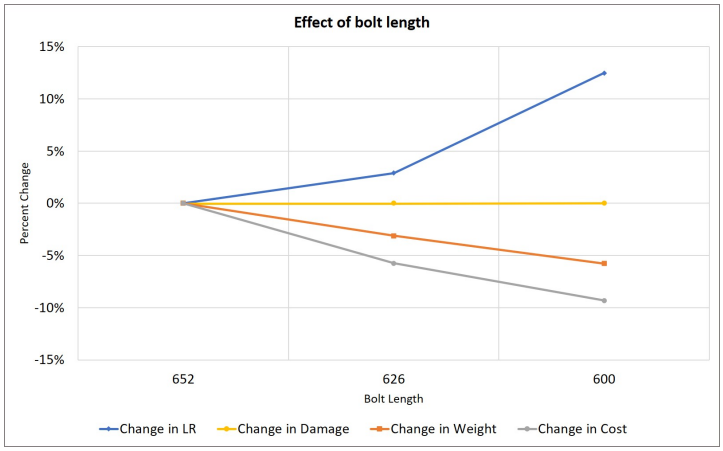

Figure 5.10

5.4. Parameter: Size of bushing

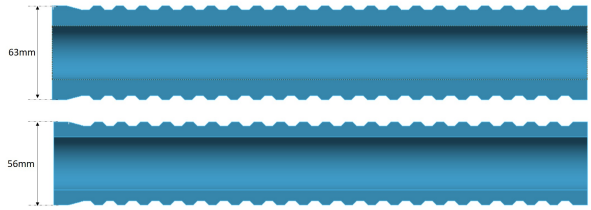

Figure 5.11: Base configuration (top), and configuration with reduced diameter (bottom)

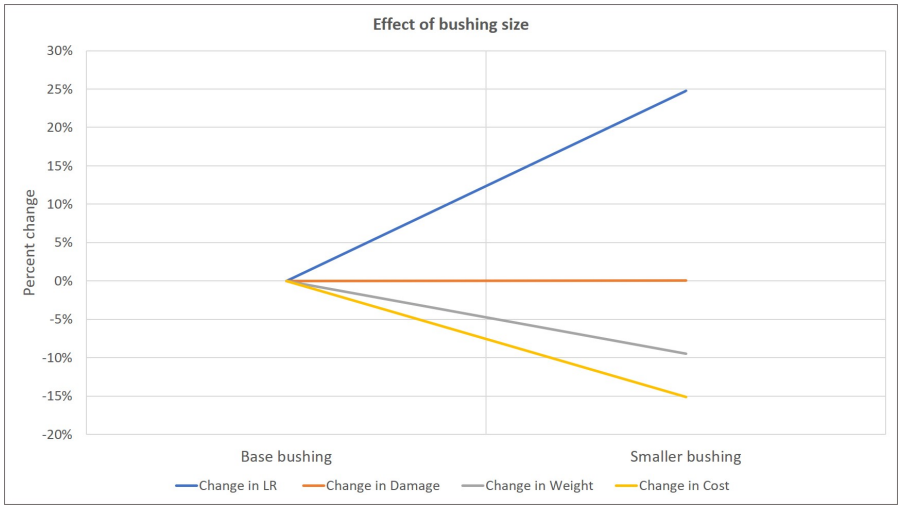

Figure 5.12: Effect of bushing size on load ratio, weight, and cost

Another geometrical parameter that was identified was the bushing. The topology of the bushing was kept the same to ensure that the manufacturing costs associated with turning of ridges remain same for both configurations.

The overall diameter of the bushing was reduced by $7mm$ (Figure 5.11). The observations made were the same as decreasing the lengths of bolt and bushing; there is a significant increase in load ratio (within the exponential region of load-ratio versus damage, keeping the change in damage $\mathcal{D}$ negligible).

5.5. Parameter: Wedge geometry

It was observed that the wedge was the lightest component, owing to the low density of foam (Figure 5.1). A design configuration that was hypothesised was that increasing the volume of the wedge would make the overall root lighter. The base configuration featured the wedge alternated by the insert with the UD material. Instead of a individual wedges, a foam ring that would act as a spacer to reduce ply drop and would decrease the overall weight was tested (see Figure 5.13).

It was observed that unlike the effect of changing in bushing and bolt geometry, the effect of increasing the wedge volume resulted in a mediocre increase in load ratio, and an almost equivalent change in total weight and cost (see Figure 5.14). As the cost of PVC foam is significant, this configuration can be considered for an economic design.

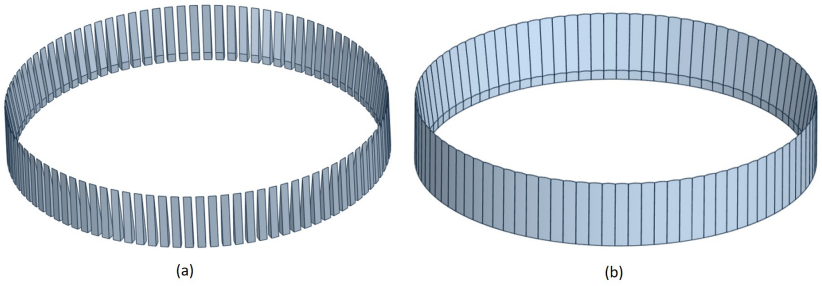

Figure 5.13: (a) Geometry of wedge in base configuration; (b) Modified geometry featuring a ring wedge, seen for the full root

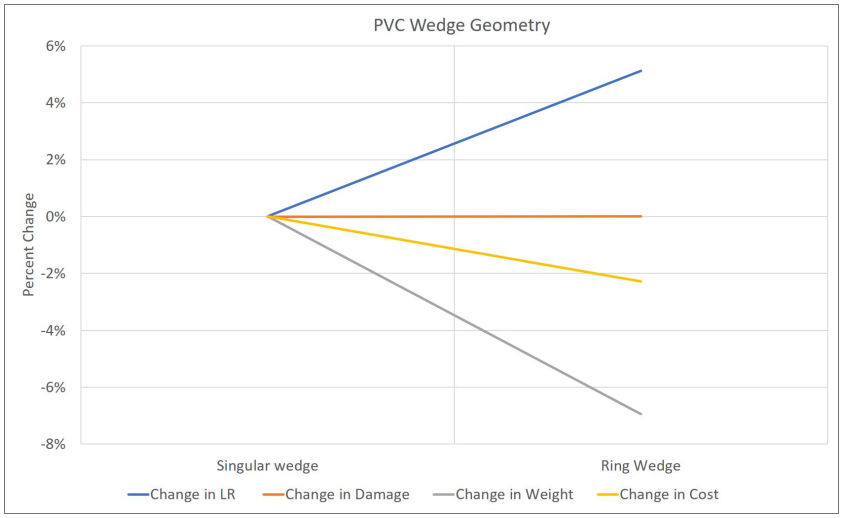

Figure 5.14: Effect of increasing wedge volume on load ratio, weight, and cost

6

Results

In this chapter, the design study conducted in this thesis is summarized and important conclusions are deducted. The feasibility of the bushing connection is critically reflected upon as a viable blade-root structure that can replace the existing T-bolt connection.

6.1. Comparison with the T-bolt connection

6.1.1. Stresses and stress ratios

The principal difference between the bushing connection and the T-bolt connection is the region of stress concentration. It has been shown in several studies, both numerical and experimental, the pin-induced (due to barrel nut) bearing pressure leads to delaminations in the blade-skin region surrounding the drilled hole. Off-axis reinforcements are required to counter the increased probability of failure within the laminate, leading to a reduced stiffness in the axial direction of the blade [6]. The stress concentrations developed in the laminate region can be observed in the FE analysis of the blade root with T-bolt connection. Most literature on the field focus on laminate failure within the root as delamination was the most commonly observed phenomena for a T-bolt connection.

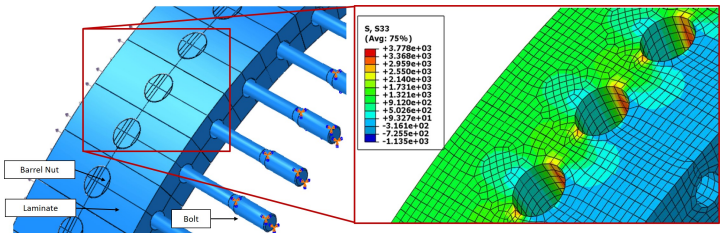

Figure 6.1: Stress concentrations developed at the root laminate around the barrel nut hole [37]

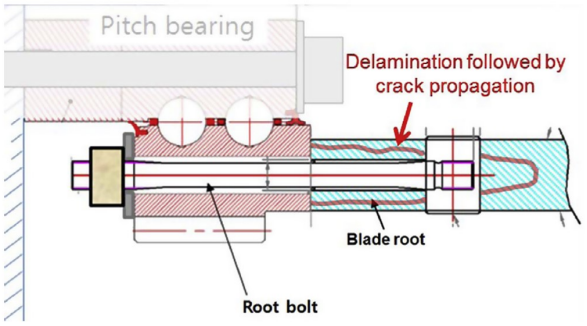

Figure 6.2: Failure mode of T-bolt [51]

For the bushing connection design, it was found that the lack of bearing pressure and abrupt changes in geometry, along with the high stiffness of the bolt-bushing assembly, resulted in higher stresses being developed

at the bolt connecting the blade to the hub bearing. This can be seen in Figure 6.3; the laminate develops less than a tenth of the stress developed at the bolt shank. The fatigue behaviour of metal structures is well documented through experimental studies and can be predicted through numerical theories. In composite laminates however, fatigue behaviour can be unpredictable and validation can only be performed through full-scale experimental tests. Therefore, it is favourable to have critical stresses on metal components instead of laminates. For longer blade lengths, the bushing connection can hence prove more reliable.

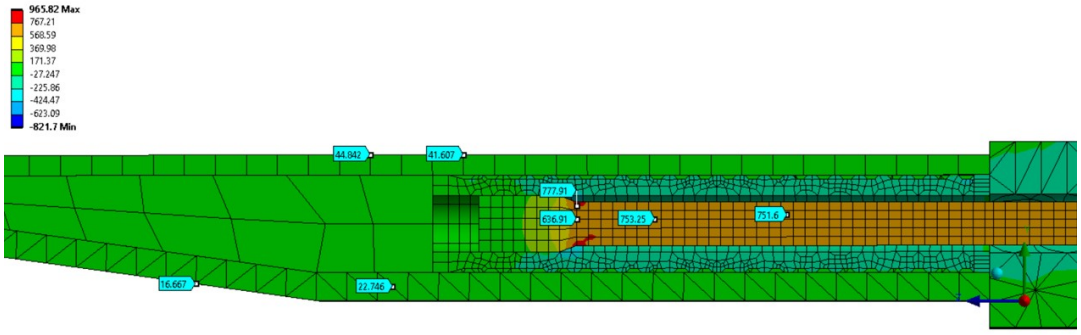

Figure 6.3: Stresses formed at the connection (for $F_{Mmax} = 446kN$; all values in MPa)

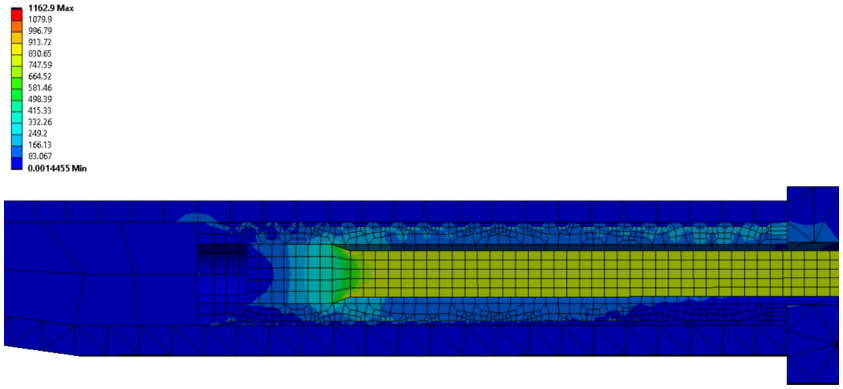

Figure 6.4: Equivalent (Von-Mises) stress formed at the blade root (for $F_{Mmax} = 446kN$; all values in MPa)

Stress ratios developed at the bolt were compared for both the connections.

- **T-bolt connection**: The values for the stress ratio of the T-bolt connection have been derived for the half-root model, with a total of 96 bolts over the whole blade root. The applied external moment at which $\phi_{stress-compression}$ and $\phi_{stress-tension}$ has been evaluated are $-12500kNm$ and $12500kNm$ respectively. The bolt pretension applied is approximately $400kN$.
- **Bushing connection**: The stress ratio $\phi_{stress-tension}$ has been evaluated at maximum bending moment $16000kNm$. Maximum stress ratio for compression $\phi_{stress-compression}$ was reached at $-2000kNm$. The value of pretension applied is $F_{Mmax} = 446kN$, and the configuration has 96 bolts at the blade root.

	Bushing Connection	T-bolt connection
$\phi_{tension}$	0.155	0.147
$\phi_{compression}$	0.142	0.150

Table 6.1: Stress ratios: Bushing connection and T-bolt connection

It was observed that the order of stress ratios for the bushing connection is very similar to that obtained with the T-bolt. The stress ratio in tension in the bushing connection is slightly higher than that of the T-bolt connection. Although this translates to a slightly weaker fatigue performance for the bolt in a bushing connection,

development of stresses in the laminate are avoided. As bolted connections have the inherent advantage of being a non-permanent joining method, bolts in the bushing connection can be replaced during periodic maintenance and life of the structure can be maintained. In the T-bolt connection, the presence of delaminations at the root indicates the end of life of the structure, or involves prohibitively high costs of repair.

6.1.2. Weight, cost and manufacturing

Manufacturing considerations

The popularity of the T-bolt connection among wind turbine manufacturers has been because of the relative ease of manufacturing of the blade root. Laminate drilling and barrel nut assembly can be automated and inspection can be carried out through conventional methods.

The main difference in the T-bolt and the bushing connection manufacturing methods will be the stage of laminate curing. Drilling is done post-curing of the laminate in the T-bolt connection. For the bushing design proposed in this study, the metal bushings, inserts, and the wedge can be assembled during the layup stage. The bonding can be carried out through a resin epoxy system and will be required to bond the the bushing to the peripheral components.

In the proposed design, the bushing topology is such that the outer cylindrical surface can be converted to a series of ridges through conventional turning methods. Configurations with the smooth bushing and the ridged bushing were analysed and the resultant stress and load ratios were comparable. The ridges have been proposed to increase the bonding area and improve shear stress characteristics through mechanical locking. Another feature of the design is that the bushing is hollow, with internal threads. The hollow design was chosen to allow for a simpler manufacturing, and to allow ease of inspection of the internal surface. During assembly of the blade-root, the hollow structure may lead to leaking of adhesive into the internal threads. This can be avoided by the addition of a separate end-cap for the bushing. Once the economic and manufacturing limitations have been considered, the modified geometry should be analysed for performance.

Weight and cost

The weight of bushing connection and the T-bolt connection has been compared in Table 6.2.

	Bushing connection: 96 bolts
Blade Assembly	**Weight for the blade root (kg)**
Triax (E-Glass)	*487.440*
Resin Epoxy	*162.480*
Insert	*279.859*
Bushing	*499.949*
Wedge	*6.784*
	1436.512

	T-bolt connection: 96 bolts
Blade Assembly	**Weight for the blade root (kg)**
Triax Laminate	*910.400*
Barrel nut	*203.620*
Drilling - Barrel nut	*-63.700*
Drilling - Bolt	*-48.500*
Sealing	*45.000*
	1046.820

Table 6.2: Weight comparison between the two connection types (Bolt weights have not been added)

It can be seen that the weight of the bushing assembly is approximately 38% more than the weight of the T-bolt connection. This is explained by the fact that each bolt is associated with a metal bushing in the new design, which is much larger than the barrel nut associated with the bolt for the T-bolt design. Barrel nuts have a simpler construction, while the bushing has a topology designed to increase the bonded area. It is expected that the additional time and methodologies required for the bushing manufacturing and assembly will lead to a significantly expensive blade-root connection. As the main advantage of the bushing connection is that it is expected to show a better fatigue performance than the T-bolt connection, especially for abnormal load cases, it is recommended that the bushing connection be used for turbines that are installed in locations that see wind turbulence and gusts. Owing to its desirable damage tolerant values, the bushing connection can be used on conjunction with longer blades in the future.

6.2. Performance of the bushing connection

6.2.1. Fatigue performance

As fatigue is the critical parameter for wind turbines, the bushing connection was analysed for fatigue damage. Initial FE results for stress showed that a significant proportion of stress was developed at the bolt shank. While a higher quantity of stress was seen at the region of the bolt where the diameter changes, the values of stress were

not considered for analysis, as the stress concentration was expected to result in unpredictable results. Load ratio was used as a singular factor for evaluating damage within the bolt.

The damage rule formulation was defined such that it provided a conservative estimate of accumulated damage $\mathcal{D}$. Load ratios remained in the order of $\phi_{load} = 0.1$ to 0.2, for which the damage values were $\mathcal{D} = 0.445888$ and 0.54096 respectively. The corresponding safety factor, or SRF (stress reserve factor), was $SRF = 2.2074$ and 1.1037. As $\mathcal{D} < 1$ and $SRF > 1$, the damage evaluated as considered acceptable for the connection. This case is when all values of stress range below the fatigue limit are considered to fail at the 10^9 cycles (the cycles to failure for stress range at fatigue limit).

6.2.2. Comparative analysis: Discussion of results

Chapter 5 discusses the procedures followed for the comparative analysis. The significant results and their implications are discussed in this section.

Effect of bolt number

The number of bolts considered for analysis was kept at 96 for the base configuration, same as the number of bolts used in the T-bolt connection designed for the root with $BCD = 3m$. The number of bolts used in a T-bolt connection is limited by the minimum distance between each drilled hole; barrel nut holes can only be drilled at the location where the stress gradient of the adjacent hole is minimal. Stress concentrations arising from notches decreases radially along the notch boundary and is dependent on the notch size and the base material [19]. Therefore, T-bolt designs define a minimum bolt and barrel nut separation distance.

With the bushing connection, the drilling process is eliminated, and in theory, the total number of bolts may be increased above 96 (limited by cost of the assembly). The assembly process will involve parallel layup of the bushing and the inserts with the blade-skin laminate. Post-curing, the laminate will not be disturbed, bringing down the probability of delaminations. From the findings in Section 5.1, the following observations were made:

- Decreasing the bolt number from the base configuration of 96 resulted in bolt overstress. Applied pretension depends on the effective stress developed per bolt; increasing the overall stress in the bolt might lead to non-compliance of the stress profile with the standards followed. Although this case leads to savings in both weight and cost, decrease of bolt number has to be followed by verification of stress developed in bolt through analytical and experimental methods
- Two cases were studied for the case where the bolt number in the root was increased:
  - Constant clamping force: In this case, the bolt number was increased while keeping the clamping force constant; this was designed so that the bending moment borne at the root would be the same (that is, for the same blade length). It was seen that it resulted in a higher tolerance of damage values, making a high bolt number variant a viable candidate for turbines that are installed in locations prone to gusts or turbulence. However, the associated weight and cost also increases. It has to be noted that only the material cost increases; manufacturing and assembly costs will see a negligible change in this case.
  - Constant preload/pretension: A potential of having higher number of bolts is the possibility of longer blades. Longer blades are subject to higher bending moments at the root. When the bending moment range was increased by 25%, it was found that the change in ϕ_{stress} ϕ_{load} is significantly less with only 4 additional bolts, as compared to using the same bolts. Another observation from Figure 5.7 was that at higher pretension levels, the change in stress and load was lower in value when compared to lower pretension levels (note the flatter curves). Higher values of preload make the bolted joint act stiffer with respect to external load; this is also an indication of the effect of pretensioning bolts on the operational and fatigue performance of bolted joints.

The selection of number of bolts for the root is hence a trade-off between the requirement for fatigue performance and the overall cost of materials. The increase in cost may not be proportional to the weight in all cases as the cost of procurement may decrease with the number of parts ordered or manufactured. Hence, this has to be an economic decision.

Insert Material

A design principle that was followed in previous designs was to keep a minimal stiffness gradient between components in the blade root. Due to the presence of both metal and composite materials, both of which are required, stiffness gradient cannot be completely eliminated. Differences in stiffness affect the the adhesively bonded area

between the components and might give rise to delaminations in the composite materials. Between the insert and the wedge, the stiffness of the insert is more key due to the shear forces between it and the bushing. Furthermore, the insert acts as an intermediary between adjacent bushings, bearing the same bending moment at the blade root. Hence, the stiffness in the principal direction of the UD material chosen should ideally be close to the stiffness of the high-grade steel ($E = 210GPa$).

Two material classes were considered, glass fibre,and carbon fibre. Glass fibre composite is the material of choice for the blade-skin composite due to its satisfactory properties, high stiffness to weight ratio, and lower costs compared to carbon fibre composite. Carbon fibre was considered due to the relatively lower volume of composite required for the insert. S-glass fibres have a higher stiffness in the principal direction, as seen in Figure 5.8. While the increase in load ratio in the model with the replaced material was not proportional to the associated increase in stiffness of the S-glass fibres, it was seen that a general increase in stiffness does translate to a lower fraction of load being developed at the bolt. This can be explained by the fact that load is dissipated among the different components according to the relative stiffnesses.

A similar trend was seen when carbon fibres were used. A clear relation between the stiffness of the insert and the load ratio developed at the bolt was observed. Theoretically, the ideal material choice for the insert should be the Amoco T-40/Epon HPT 1072 carbon-epoxy system (or similar), owing to the least difference in stiffness. Carbon fibres are also accompanied by a slight decrease in the overall weight. As the decrease in load ratio is relatively low, there is a negligible change in the damage value. However, the material choice is inhibited by the cost of material. Carbon fibres are 10 to 20 times more expensive than glass fibres; this pushes up the overall cost of the root by more than 50%. Experimental fatigue testing for glass fibre inserts can be conducted and examined for delaminations near the bonded regions. With acceptable fatigue performance, the choice of glass fibre would be the most feasible choice for the insert.

Length of bolt (and bushing), and Bushing size

Bolt lengths, within the wind turbine industry, can be customised to manufacturer requirements. The design can be hence optimised for reducing weight and associated cost. When the bolt length was decreased in steps of $26mm$ (accompanied with an equal decrease in), a significant decrease in load ratios, accompanied by a slightly lower decrease in weight. As hypothesised, shorter bolts bear proportionally higher loads. However, bolt length has to be selected carefully as the load ratio increases drastically for a length below a certain limit. As this configuration shows a mediocre improvement in cost, a longer bolt can be considered for ensuring load ratio within the bolt does not go beyond damage value requirements.

Another parameter that was evaluated was the bushing diameter. The base configuration featured a bushing wall thickness with a maximum value of $27mm$, which was reduced to $20mm$. The trend was similar to decreasing the bolt length. These observations show that although procedures to enable weight and cost reduction increase the effective load carried by the bolt, the final fatigue damage values are well within the acceptable range (provided the volumetric decrease in bolt and bushing is of a tolerable value).

Volume of wedge

The wedge is used as a spacer to decrease the ply drop within the laminate. The position of the wedge (parallel to the load path, sandwiched between the blade-skin laminate) suggests that the component does not contribute significantly to the structural performance of the blade-root. Hence, the preferred material property should be weight, and not stiffness. PVC foam was chosen for this purpose; the total contribution of the wedge in the base configuration is just 0.38% of the total weight. It is to be noted that the associated cost is approximately 2% of the root cost, indicating a costlier material.

To take advantage of the weight of the foam, an alternative design was considered. The volume of the wedge was increased (taking up a fraction of the insert volume), such that it formed a continuous ring around the blade root. The analysis of this configuration showed a mediocre increase in the load ratio, with a proportional decrease in weight. Though the total volume of the insert also decreased, it was seen the this did not lead to a drastic decrease in performance. This indicates the structural requirement of a stiffer component increases towards the root edge of the blade.

The advantage of having a continuous ring of the PVC wedge will be evident during the assembly stage; this configuration decreases the assembly steps of placing the wedges by a number equivalent to the number of bolt-bushing assemblies ($n - 1$ wedges for n bolts in the base configuration, with assembly step theoretically reduced to 2 for each half of the blade root). This can be directly linked to a reduction in total manufacturing time.

This page intentionally left blank.

7

Conclusions and Recommendations

Through the results presented in this study, it was found that a blade-root connection with bushings can serve as an adequate, and in some cases, a better alternative to the T-bolt connection. The principal advantage of switching to a bushing connection for Suzlon Energy would be the overall improved performance of the root through visibly lesser probability of delaminations of the blade-skin. Due to the stresses being concentrated at the bolt, the cost and ease of inspection and repair in case of abnormal loading conditions is significantly lower for the bushing connection.

Results obtained through this study show that the improved performance of the connection method can be exploited in longer blades, which is a dominant research sub-field within the wind turbine industry. Longer blades translate to a higher annual yield of the wind turbine, which may offset the initial cost of assembly and manufacturing. Furthermore, the components within the connection are flexible in terms of optimisation for cost and weight. Several permutations of the assembly can be tested to reach an economically feasible solution. The economic evaluation of the design shows that the cost of assembly and manufacturing associated with the bushing connection might be a deterrent. It is expected that the bushing connection will require newer machines and methods, and might need longer assembly times. Therefore, it is recommended that the bushing connection can be used as a feasible connection method for current and future blade designs.

7.1. Conclusions

Following the demand for higher power output, present wind turbine structural research is investigating the feasibility of longer blades. As bending moments increase towards the blade root, one of the areas of focus in blade design is the design of a suitable root connection. Glass fibre-epoxy composite being the material of choice, it is susceptible to various failure modes like delaminations, interface failure, and buckling. T-bolt connections transfer load through mechanical locking, namely through bearing stress developed at the laminate. While majority of the blade failures occur at the aerodynamic surface of the blade, the root is also prone to delaminations due to the presence of multi-material components, stiffness gradients, and the possibility of blade separation from the hub that might lead to exposure to moisture. To enable blade developments, Suzlon theorised a blade root connection that would ideally enable load transfer through shear forces and results in stress concentration at the root bolt and the mating bushing.

Within the sphere of bushing design, several variations of the bushing topology are possible. However, effort was made to increase the bonded area and at the same time to keep the design simple enough to manufacture without the need of complex turning profiles. The design chosen as the base configuration in this study is based on a published patent [10] and can be turned through simple CNC manufacturing. The fatigue validation process conducted in this study show promising results for this root joint in terms of fatigue performance, with an acceptable range of damage values. The value of accumulated damage $\mathcal{D}$ is inversely proportional to the life of the structure, in terms of load cycles that the connection is subject to. The acceptable range of $\mathcal{D}$ is between 0 and 1; this corresponds to a theoretically infinite cycles at $\mathcal{D} = 0$, and failure on one stress cycle at $\mathcal{D} = 1$. While the theoretical life would also depend on multiple factors, and would proportionally be unpredictable with the irregularity in loading amplitude, the value of $\mathcal{D}$ is indicative of the approximate failure of the root. The strongest claim for use of a bushing connection to replace the T-bolt connection is the stress profile at the root. Adequate stiffness provided by the bolt and bushing ensure minimal stresses at the laminate. Although the weight of the

bushing design is significantly higher than that of the T-bolt design ($\approx 38\%$ higher), blade root delaminations can be reduced by a high degree with the use of a bushing design.

The flexibility of the components also makes the bushing design a feasible design choice. Several adjustments can be made within the root design to achieve the desired combination of performance, weight, material cost, and manufacturability. Sub-components can be sourced from external suppliers with in-house assembly. It is hypothesized that the overall time required for assembly will be higher than that of the T-bolt connection; this is due to a significant bonded area which requires adequate curing time and temperature. On the other hand, the assembly of the root components and the adhesive bonding can be done concurrent to the laminate curing.

In conclusion, the bushing design is a promising alternative to the T-bolt connection. The results presented in this study are expected to support further developments and optimisations of the blade-root connection, and also act as a reference for experimental tests.

7.2. Recommendations for Future work

During the course of this project, several assumptions were considered at key steps. As the region of focus was the bolt shank, other components were modeled as close to the actual parts, but with simplifications intended to aid with computational limits. The adhesive bonding between the laminate, the bushing, the insert, and the wedge is one such example. Within the FE solver, it was assumed that the adhesive bond behaved linearly, and that it reached a perfect cured stage so as to transfer forces efficiently. However, in the actual blade root, these bonds may be subject to temperature and humidity gradients, and may show non-linear behaviour. For this reason, adhesive bonds are avoided within the aerospace industry due to lack or difficulty in certification as compared to bolted or welded joints. The influence of actual adhesive bond behaviour is hence unknown and should be validated with experiments.

Another simplification that was assumed was the blade-skin laminate. Instead of modelling discrete lamina bonded to form a laminate, the laminate was assigned properties that matched with a multi-layer triax material. The design decision was taken in view of negligible stresses being developed within the composite laminate. Further studies can be done wherein the laminate can be modelled as discrete shell elements and the effect on the fatigue can be studied.

As mentioned, the smallest sub-model was chosen for analysis in view of limitations on the number of nodes and elements. Although symmetrical boundary conditions simulated the section, the effective axial force on the unit-bolt connection was evaluated from the assumption of the blade root being a uniform thin-walled cylindrical beam, where each section is subject to an axial load. The actual full root model will be subject to bending moments arising from aerodynamic loads. The values of stress ratio available for the T-bolt show minimal difference with the stress ratios of the bushing connection. A full model study for the bushing connection can be conducted to verify the actual performance.

Furthermore, verification of the results presented in this chapter needs to be carried through extensive coupon testing. Certification of the joint can be finalized only after full-scale tests (including fatigue testing) due to the presence of adhesive bonds within the joint. The fatigue results obtained through this study are indicative and a result of conservative estimates. On-site wind conditions can be replicated via applied bending moments during a full-scale blade test and the fatigue life of the root can be verified.

References

[1] Wikipedia. *Renewable energy*. 2021. URL: https://en.wikipedia.org/wiki/Renewable_energy (visited on 03/12/2021).

[2] Wikipedia. *Wind Power*. 2021. URL: https://en.wikipedia.org/wiki/Wind_power (visited on 03/12/2021).

[3] Wikipedia. *Wind power by country*. 2021. URL: https://en.wikipedia.org/wiki/Wind_power_by_country (visited on 03/12/2021).

[4] Povl Brondsted Rogier Nijssen, ed. *Advances in wind turbine blade design and materials*. 1st ed. Woodhead Publishing, Oct. 2013. ISBN: 9780857097286.

[5] Eftihia Tzen. "Chapter 3 - Wind-Powered Desalination—Principles, Configurations, Design, and Implementation". In: *Renewable Energy Powered Desalination Handbook*. Ed. by Veera Gnaneswar Gude. Butterworth-Heinemann, 2018, pp. 91–139. ISBN: 978-0-12-815244-7. DOI: https://doi.org/10.1016/B978-0-12-815244-7.00003-9. URL: https://www.sciencedirect.com/science/article/pii/B9780128152447000039.

[6] Alex Ashworth Briggs, Z Zhang, and Hom Dhakal. "T-Bolt Bearing Strengths in Composite Blade Applications". In: June 2012.

[7] John E. Eckland and James V. Frerotte. "Wind turbine blade attachment methods". Apr. 1990. URL: https://patents.google.com/patent/US4915590A/en.

[8] Erich Hau. *Wind Turbines - Fundamentals, Technologies, Application, Economics*. 2nd ed. Translated by von Renouard, H. Springer-Verlag Berlin Heidelberg, 2006. ISBN: 978-3-540-29284-5.

[9] R.P.L Nijssen et al. *Connection methods in wind turbine rotor blades*. Tech. rep. WMC Knowledge Centre, Oct. 2018. URL: https://www.topsectorenergie.nl/sites/default/files/uploads/TT_WIIP1_1601_WMC_Public_Report.pdf.

[10] Edo Johannes Hendrikus Kuipers. "Bushing intended for connecting a blade root of a wind turbine blade directly or indirectly to a hub of a turbine". EP3111083NWB1. Jan. 2017. URL: https://data.epo.org/publication-server/rest/v1.0/publication-dates/20200318/patents/EP3111083NWB1/document.pdf.

[11] K. J. Jackson et al. "Innovative design approaches for large wind turbine blades". In: *Wind Energy* 8.2 (2005), pp. 141–171. DOI: https://doi.org/10.1002/we.128. eprint: https://onlinelibrary.wiley.com/doi/pdf/10.1002/we.128. URL: https://onlinelibrary.wiley.com/doi/abs/10.1002/we.128.

[12] Richard Schmidt, Christian Weimer, and Hubert Stadtfeld. "Blade connection for the rotor blades of a wind-energy turbine and a method for the production thereof". Oct. 2003. URL: https://patents.google.com/patent/WO2003082551A1/en?oq=WO03082551A1.

[13] Mark Hancock and Anton Bech. "Method of manufacturing a wind turbine blade shell member with a fastening member and a wind turbine blade with a fastening member". CA2593477C. July 2006. URL: https://patents.google.com/patent/CA2593477C/en?oq=CA2593477C.

[14] *Systematic calculation of highly stressed bolted joints - Joints with one cylindrical bolt*. Tech. rep. 2230 - Part 1. VDI - Verein Deutscher Ingenieure, Sept. 2015.

[15] *Guideline for the Certification of Wind Turbines*. IV - Part 1. Germanischer Lloyd, July 2010.

[16] W.A.P. Fisher, R.H. Cross, and G.M. Norris. "Pre□tensioning for Preventing Fatigue Failure in Bolts: Simple Theory and an Account of Experiments Carried Out at the R.A.E." In: *Aircraft Engineering and Aerospace Technology* 24.6 (1952), pp. 160–163. DOI: https://doi.org/10.1108/eb032166.

[17] Hanamant Kate and Sandeep Bhor. "Evaluation the Effect of Pretension on the Fatigue Life of Double Lap Bolted Joint - A Review". In: *International Journal of Science and Research (IJSR)* 4 (1 2013), pp. 56–57.

[18] A. R. Shahani and I. Shakeri. “Experimental Evaluation of the Effect of Preload on the Fatigue Life of Bolts”. In: *International Journal of Steel Structures* 15 (3 2015), pp. 693–701. DOI: https://doi.org/10.1007/s13296-015-9015-5.

[19] Jaap Schijve. *Fatigue of Structures and Materials*. 1st ed. Springer Netherlands, 2001. ISBN: 978-0-306-48396-7. DOI: 10.1007/0-306-48396-3.

[20] W. Elber. “The Significance of Fatigue Crack Closure: Damage tolerance in aircraft structures”. In: *ASTM STP 486* (1971), pp. 230–242. DOI: https://doi.org/10.1520/STP26680S.

[21] Peter Joosse, Valter L. Bellotto, and Carlos Ochoa. *Personal Communication (E-mail, Meetings)*. Suzlon Energy, 2020.

[22] *What is the Nut Factor and How Does it Affect Torque?* URL: http://www.smartbolts.com/insights/nut-factor-affect-torque/ (visited on 04/18/2021).

[23] Valter Luis Bellotto. *Blade Root Analysis*. SB63S1-R-01-00008. SE Blades Technology, Nov. 2018.

[24] M.T. Huber. “Specific work of strain as a measure of material effort”. In: *Archives of Mechanics* 56 (4 2004), pp. 173–190. URL: https://am.ippt.pan.pl/am/article/viewFile/v56p173/pdf.

[25] Richard J. Moulds. “Chapter 3 - Design and Stress Calculations for Bonded Joints”. In: *Adhesives and Sealants*. Ed. by Philippe Cognard. Vol. 2. Handbook of Adhesives and Sealants. Elsevier Science Ltd, 2006, pp. 197–231. DOI: https://doi.org/10.1016/S1874-5695(06)80014-X. URL: https://www.sciencedirect.com/science/article/pii/S187456950680014X.

[26] Herbert J Sutherland. “On the Fatigue Analysis of Wind Turbines”. In: (June 1999). DOI: 10.2172/9460. URL: https://www.osti.gov/biblio/9460.

[27] Valter Luis Bellotto. *Design Loads*. SB63S1-R-01-00003. SE Blades Technology, Nov. 2018.

[28] Seongpil Cho et al. “Numerical modeling of the hydraulic blade pitch actuator in a spar-type floating wind turbine considering fault conditions and their effects on global dynamic responses”. In: *Wind Energy* 23.2 (2020), pp. 370–390. DOI: https://doi.org/10.1002/we.2438. eprint: https://onlinelibrary.wiley.com/doi/pdf/10.1002/we.2438. URL: https://onlinelibrary.wiley.com/doi/abs/10.1002/we.2438.

[29] Robert Kroese. *Design Loads*. SB65S1-R-01-00003. SE Blades Technology, Mar. 2019.

[30] *Fatigue and Reliability Analysis with Time-Varying Stress Using the Cumulative Damage Model*. 2017. URL: weibull.com (visited on 03/18/2021).

[31] J. Berglind and Rafael Wisniewski. “Fatigue Estimation Methods Comparison for Wind Turbine Control”. In: (Nov. 2014).

[32] Yung-Li Lee and Tana Tjhung. “Chapter 3 - Rainflow Cycle Counting Techniques”. In: *Metal Fatigue Analysis Handbook*. Ed. by Yung-Li Lee, Mark E. Barkey, and Hong-Tae Kang. Boston: Butterworth-Heinemann, 2012, pp. 89–114. ISBN: 978-0-12-385204-5. DOI: https://doi.org/10.1016/B978-0-12-385204-5.00003-3. URL: https://www.sciencedirect.com/science/article/pii/B9780123852045000033.

[33] S.D. Downing and D.F. Socie. “Simple rainflow counting algorithms”. In: *International Journal of Fatigue* 4.1 (1982), pp. 31–40. ISSN: 0142-1123. DOI: https://doi.org/10.1016/0142-1123(82)90018-4. URL: https://www.sciencedirect.com/science/article/pii/0142112382900184.

[34] C. Amzallag et al. “Standardization of the rainflow counting method for fatigue analysis”. In: *International Journal of Fatigue* 16 (1994), pp. 287–293.

[35] Paul S. Veers. “Simplified fatigue damage and crack growth calculations for wind turbines”. In: *Eighth ASME Wind Energy Symposium* 7 (Jan. 1989).

[36] Flavien Boussuge et al. “Symmetry-based decomposition for meshing quasi-axisymmetric components”. In: *Procedia Engineering* 203 (2017). 26th International Meshing Roundtable, IMR26, 18-21 September 2017, Barcelona, Spain, pp. 375–387. ISSN: 1877-7058. DOI: https://doi.org/10.1016/j.proeng.2017.09.812. URL: https://www.sciencedirect.com/science/article/pii/S1877705817343758.

[37] Stijn Ketele. “Detailed modeling of connections in large composite wind turbine blades”. MA thesis. Universiteit Gent, 2013.

[38] *What different kinds of bearings are used in wind turbines?* 2017. URL: windpowerengineering.com (visited on 04/18/2021).

[39] *Extending wind turbine life with pitch bearing upgrades*. 2020. URL: windpowerengineering.com (visited on 04/18/2021).

[40] *"World's longest wind turbine blade is put to the test"*. LM Wind Power. 2016. URL: https://www.youtube.com/watch?v=5m-jwwM3qRs&ab_channel=LMWindPower.

[41] A Mukherjee and B Varughese. "Design guidelines for ply drop-off in laminated composite structures". In: *Composites Part B: Engineering* 32.2 (2001), pp. 153–164. ISSN: 1359-8368. DOI: https://doi.org/10.1016/S1359-8368(00)00038-X. URL: https://www.sciencedirect.com/science/article/pii/S135983680000038X.

[42] *Elements Reference*. Ansys, Inc., USA, 2007.

[43] Panu Pratumnopharat, Pak Leung, and Richard Court. "Extracting fatigue damage parts from the stress–time history of horizontal axis wind turbine blades". In: *Renewable Energy* 58 (Oct. 2013), pp. 115–126. DOI: 10.1016/j.renene.2013.03.009.

[44] Jeong Kim, Joo-Cheol Yoon, and Beom-Soo Kang. "Finite element analysis and modeling of structure with bolted joints". In: *Applied Mathematical Modelling* 31.5 (2007), pp. 895–911. ISSN: 0307-904X. DOI: https://doi.org/10.1016/j.apm.2006.03.020. URL: https://www.sciencedirect.com/science/article/pii/S0307904X0600062X.

[45] *Bolting and Fastening for Wind Turbines*. 2020. URL: https://blog.maxprocorp.com/bolting-and-fastening-for-wind-turbines (visited on 04/20/2021).

[46] *1500 Bar Hydraulic Bolt Tensioning Tools*. URL: http://www.parla-tech.com/1500-bar-hydraulic-bolt-tensioning-tools.php (visited on 04/20/2021).

[47] Doug Oatis. *Analysing Bolt Pretension in the ANSYS Workbench Platform*. Phoenix Analysis & Design Technologies, Inc., Arizona, U.S.A., 2007.

[48] Kevin Cox and Andreas Echtermeyer. "Structural Design and Analysis of a 10MW Wind Turbine Blade". In: *Energy Procedia* 24 (2012). Selected papers from Deep Sea Offshore Wind R&D Conference, Trondheim, Norway, 19-20 January 2012, pp. 194–201. ISSN: 1876-6102. DOI: https://doi.org/10.1016/j.egypro.2012.06.101. URL: https://www.sciencedirect.com/science/article/pii/S1876610212011411.

[49] *Eurocode 3: Design of steel structures - Part 1-9: Fatigue*. Tech. rep. EN 1993-1-9. European Committee for Standardization, May 2005.

[50] P.K. Mallick. *Fiber-Reinforced Composites: Materials, Manufacturing, and Design, Second Edition*. Dekker Mechanical Engineering. Taylor & Francis, 1993. ISBN: 9780824790318. URL: https://books.google.nl/books?id=z0MIzzOFMqkC.

[51] Hak Gu Lee, Min Gyu Kang, and Jisang Park. "Fatigue failure of a composite wind turbine blade at its root end". In: *Composite Structures* 133 (2015), pp. 878–885. ISSN: 0263-8223. DOI: https://doi.org/10.1016/j.compstruct.2015.08.010. URL: https://www.sciencedirect.com/science/article/pii/S026382231500687X.

This page intentionally left blank.

A

Material Data

Properties of various materials used throughout the design study are listed in the following tables. Table A.1 lists the material properties as provided by Suzlon for the study (these are based on materials being currently used for the wind turbines). The materials used for comparative analysis are listed in Table A.2. These values were taken from Fiber-Reinforced Composites by P.K. Mallick[50] and from publicly available sources.

	Triax (1800 gsm)	Structural Steel	Bearing Steel (100CrMnSi6-4)	Cast Iron	E-Glass/Epoxy UD (Suzlon System)	PVC Foam
Density (kg/m3)	*1469.4*	*7850*	*7800*	*7100*	*1480*	*60*
Ex	*28.95 GPa*	*200 GPa*	*210 GPa*	*169 GPa*	*40 GPa*	*57.5 MPa*
Ey	*15.6 GPa*	-	-	-	*14 GPa*	*57.5 MPa*
Ez	*9.85 GPa*	-	-	-	*14 GPa*	*42.5 MPa*
Gxy	*8.64 GPa*	*76.923 GPa*	*80 GPa*	*66.535 GPa*	*4 GPa*	*22 MPa*
Gyz	*5.69 GPa*	-	-	-	*4 GPa*	*20 MPa*
Gxz	*5.69 GPa*	-	-	-	*4 GPa*	*20 MPa*
nxy	*0.486*	*0.3*	*0.3*	*0.27*	*0.3*	*0.3*
nyz	*0.397*	-	-	-	*0.3*	*0.3*
nxz	*0.397*	-	-	-	*0.3*	*0.3*

Table A.1: Material Data: Base configuration

	Fibre	Resin	E_{11}	E_{22}	ν_{12}	ν_{21}	G_{12}	G_{21}	Density ρ
Glass Fibre Systems	E-Glass	Epon HPT 1072: Shell Chemical	*55.14*	*11.85*	*0.24*	*0.05*	*4.45*	*4.45*	*2195.00*
	S-Glass	Epon HPT 1072: Shell Chemical	*66.02*	*12.10*	*0.25*	*0.05*	*4.53*	*4.53*	*2157.50*
Carbon Fibre Systems	Hercules AS-1	Epon HPT 1072: Shell Chemical	*171.84*	*12.94*	*0.24*	*0.02*	*4.81*	*4.81*	*1640.00*
	Amoco T-300	Epon HPT 1072: Shell Chemical	*174.09*	*12.94*	*0.24*	*0.02*	*4.82*	*4.82*	*1610.00*
	Hercules AS-4	Epon HPT 1072: Shell Chemical	*186.84*	*12.98*	*0.24*	*0.02*	*4.83*	*4.83*	*1640.00*
	Amoco T-40	Epon HPT 1072: Shell Chemical	*218.34*	*13.06*	*0.24*	*0.01*	*4.85*	*4.85*	*1647.50*
	Hercules IM-7	Epon HPT 1072: Shell Chemical	*226.59*	*13.07*	*0.24*	*0.01*	*4.86*	*4.86*	*1625.00*
	Hercules HMS-4	Epon HPT 1072: Shell Chemical	*259.59*	*13.13*	*0.24*	*0.01*	*4.88*	*4.88*	*1640.00*
	BASF GY-70	Epon HPT 1072: Shell Chemical	*363.09*	*13.23*	*0.24*	*0.01*	*4.91*	*4.91*	*1760.00*

Table A.2: Material Data: Comparative Analysis

SN Curve Material Data - Structural Steel			
Cycles	**Range (MPa)**	**Slope**	**Constant K**
1E+04	*474.9343843*	*3.00*	*1.07127E+12*
1E+05	*220.4450135*	*3.00*	*1.07127E+12*
1E+06	*102.3215113*	*3.00*	*1.07127E+12*
2E+06	*81.21263734*	*3.00*	*1.07127E+12*
5E+06	*59.83798281*	*5.00*	*3.83579E+15*
1E+07	*52.09198964*	*5.00*	*3.83579E+15*
1E+08	*32.86782345*	*5.00*	*3.83579E+15*
1E+09	*20.7381946*	*5.00*	*3.83579E+15*

Table A.3: Material data used for generating SN Curve (Bolt steel) [15]

This page intentionally left blank.

B

FE Model - Iterations

The blade root design went through several iterations, following the flowchart shown in Figure 3.1. This can be seen in Figure B.1. As the results are unknown, the first design was a rough assembly to understand the position of components.

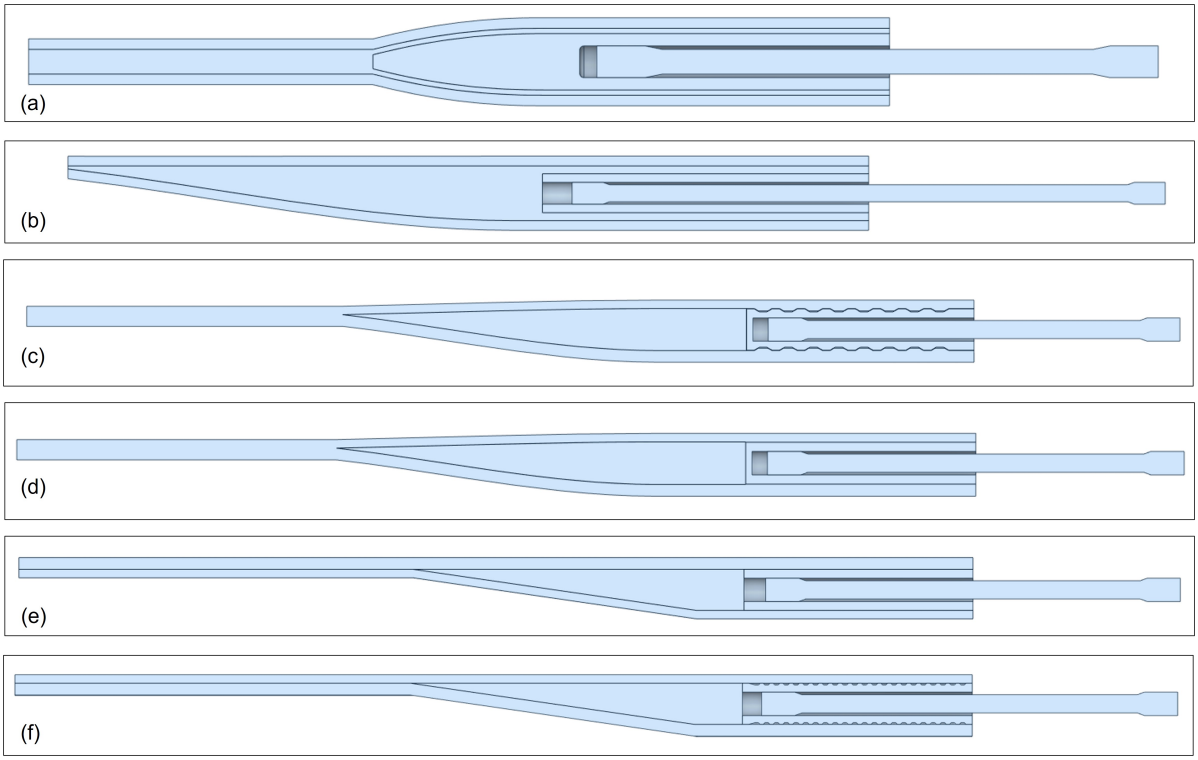

Figure B.1: Iterations of the blade root, given in sequential order

It can be seen from the first design that a bullet-shaped bushing was modelled to encase the bolt. In view of the final design chosen, this was an over-engineered model. Furthermore, the outer surface of the blade-skin (exposed to the environment) bulged out, which would be a poor design choice aerodynamically. Further analysis was not conducted with this design.

The second iteration was modelled such that there was a composite insert that formed the interface between the bushing and the laminate. The reasoning behind this design choice was to bridge the stiffness gradient in a gradual manner from the bushing to the laminate. However, the design was rejected due to manufacturing constraints. The composite insert would require either drilling, negating its advantages over the T-bolt joint, or would require complex layup methods to avoid crimping.

The third model (c) was designed such that the laminate followed the bushing contour. While this practice can be followed while manufacturing the root (wrapping fiber rovings through the bushing ridges), the model resulted in inconsistent stress profile due to irregular meshing. A simpler design was chosen for the next iteration such that the stress profile matched that of the provided plots.

Model (e) featured a flatter laminate to satisfy aerodynamic requirements, a simple cylindrical bushing which was hollow throughout, and a simple wedge and insert design. The final iteration was chosen as the base configuration; in this design, the bushing profile was modelled to increase the bonded area and provide mechanical locking to the adhesive, and to contribute to weight savings.

C

Model Dimensions

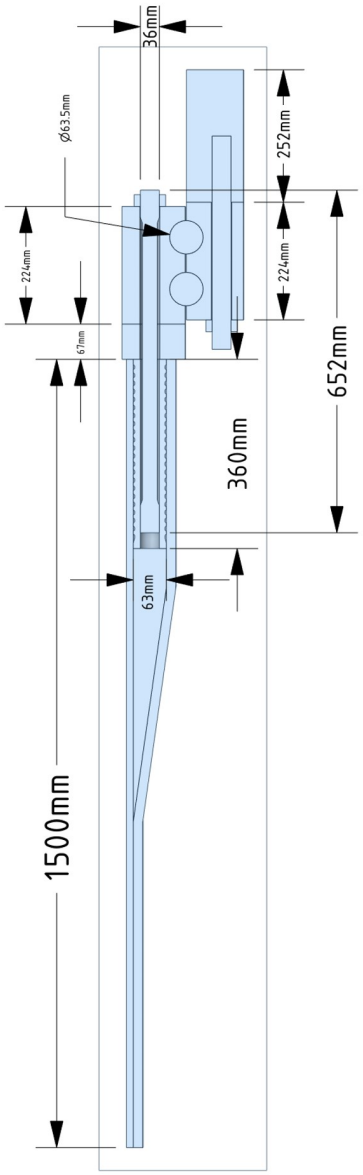

Figure C.1: Dimensions

This page intentionally left blank.

D

MATLAB Code: Validation of bolt stress

```
%constants
BCD = 3000; %m
Dshank = 28; %mm
Dpitch = 36; %mm
Ashank = (pi/4)*Dshank^2; %mm2
Apitch = (pi/4)*Dshank^2; %mm2
P = 4; %pitch
sigma_yield = 940; %MPa

%Design
Nb = 96; %no of bolts
Mmax = 16000; %max moment in kNm
PTmax_2 = 446; % Max pretension in kN
PTmax = PTmax_2/2;
alpha = 1.4; % tightening factor
PTmin_2 = PTmax_2/alpha;
PTmin = PTmin_2/2;
phi = 0.155;



%% Ult Strength during assembly
sigmaT = PTmax_2*1000/Ashank;
tau = PTmax_2*1000*((1.155*0.09*Dpitch/2) + P/(2*pi))/((pi/16)*Dshank^3);

sigma_HH = sqrt(sigmaT^2 + 3*(tau^2));

sigma_adm = sigma_yield/sigma_HH;

if sigma_adm > 1.1
    fprintf("No Overstress \n");
else
    fprintf("OVERSTRESS \n");
end
%
%% Ult Strength during operation

sigmaToper = PTmax_2*1000/Ashank;
tauoper = (PTmax_2 *1000* ((1.155*0.09*Dpitch/2) + P/(2*pi))/((pi/16)*Dshank^3))
    *0.5;

sigma_HHoper = sqrt(sigmaToper^2 + 3*(tauoper^2));

```

```
43
44 sigma_shank_no_pt = (Mmax*10e5)/(BCD*Ashank*Nb/4);
45 %F_shankoper_no_pt = sigma_shank_no_pt*Ashank;
46
47 sigma_oper = sigma_shank_no_pt*phi;
48 sigma_oper_total = sigma_oper + sigma_HHoper;
49
50 SRF = (sigma_yield - sigma_HHoper)/sigma_oper ;
51
52 if SRF > 1
53     fprintf("OK \n");
54 else
55     fprintf("NOT OK \n");
56 end
57
58 %% Min Pretension Calculation
59 FAmax = 111111.1111; %N
60 Ad = 3588; %mm
61 a = 29;%mm
62 u = 44.5; %mm
63 Ibt = 3714311.604; %mm
64
65 Fka = FAmax*Ad*a*u/(Ibt);
66 fprintf("\n Min pretension \n");
67 F_PT_min = Fka*2/1000
```

E

Bolt Stress Profile

E.1. Bolt stress profile - Minimum Pretension

Blade Side Values - Minimum Pretension									
External Moment kNm	External Force N	External Stress MPa	Axial Force (FEA) kN	Axial Stress (FEA) MPa	Blade Inside MPa	Blade Outside MPa	Stress Ratio - Blade Inside	Stress Ratio - Blade Outside	Load Ratio
-16000	*-111111.11*	*-360.90*	*147.22*	*478.1794*	*474.58*	*479.55*	*0.122*	*0.089*	*0.10602*
-14000	*-97222.22*	*-315.78*	*148.74*	*483.1165*	*480.02*	*483.95*	*0.123*	*0.088*	*0.105531*
-12000	*-83333.33*	*-270.67*	*150.22*	*487.9236*	*485.44*	*488.15*	*0.123*	*0.087*	*0.10536*
-10000	*-69444.44*	*-225.56*	*151.67*	*492.6333*	*490.89*	*492.09*	*0.123*	*0.087*	*0.105552*
-8000	*-55555.56*	*-180.45*	*153.11*	*497.3105*	*496.39*	*495.88*	*0.124*	*0.088*	*0.10602*
-6000	*-41666.67*	*-135.34*	*154.55*	*501.9877*	*501.96*	*499.64*	*0.124*	*0.089*	*0.1068*
-4000	*-27777.78*	*-90.22*	*156.01*	*506.7299*	*507.56*	*503.51*	*0.124*	*0.091*	*0.10764*
-2000	*-13888.89*	*-45.11*	*157.50*	*511.5695*	*513.14*	*507.56*	*0.123*	*0.093*	*0.108*
0	*0.00*	*0.00*	*159.00*	*516.4416*	*518.71*	*511.75*	-	-	-
2000	*13888.89*	*45.11*	*160.53*	*521.4111*	*524.28*	*516.06*	*0.123*	*0.096*	*0.11016*
4000	*27777.78*	*90.22*	*162.07*	*526.4131*	*529.91*	*520.45*	*0.124*	*0.096*	*0.11052*
6000	*41666.67*	*135.34*	*163.64*	*531.5125*	*535.56*	*524.94*	*0.125*	*0.097*	*0.11136*
8000	*55555.56*	*180.45*	*165.22*	*536.6445*	*541.18*	*529.53*	*0.125*	*0.099*	*0.11196*
10000	*69444.44*	*225.56*	*166.82*	*541.8414*	*547.01*	*534.07*	*0.125*	*0.099*	*0.112608*
12000	*83333.33*	*270.67*	*168.45*	*547.1357*	*553.12*	*538.55*	*0.127*	*0.099*	*0.1134*
14000	*97222.22*	*315.78*	*170.31*	*553.1771*	*559.7*	*543.97*	*0.130*	*0.102*	*0.116331*
16000	*111111.11*	*360.90*	*172.48*	*560.2254*	*565.35*	*552.39*	*0.129*	*0.113*	*0.12132*

Table E.1: Values of bolt stress, load ratios and stress ratios - Blade Side, for F_{Mmin}

Hub Side Values - Minimum Pretension									
External Moment kNm	External Force N	External Stress MPa	Axial Force (FEA) kN	Axial Stress (FEA) MPa	Blade Inside MPa	Blade Outside MPa	Stress Ratio - Blade Inside	Stress Ratio - Blade Outside	Load Ratio
-16000	*-111111.11*	*-360.90*	*147.22*	*478.1794*	*467.46*	*486.92*	*0.135*	*0.076*	*0.106*
-14000	*-97222.22*	*-315.78*	*148.74*	*483.1165*	*473.77*	*490.45*	*0.135*	*0.076*	*0.106*
-12000	*-83333.33*	*-270.67*	*150.22*	*487.9236*	*479.95*	*493.89*	*0.135*	*0.076*	*0.105*
-10000	*-69444.44*	*-225.56*	*151.67*	*492.6333*	*485.99*	*497.26*	*0.135*	*0.076*	*0.106*
-8000	*-55555.56*	*-180.45*	*153.11*	*497.3105*	*491.94*	*500.60*	*0.135*	*0.077*	*0.106*
-6000	*-41666.67*	*-135.34*	*154.55*	*501.9877*	*497.90*	*503.98*	*0.136*	*0.077*	*0.107*
-4000	*-27777.78*	*-90.22*	*156.01*	*506.7299*	*503.95*	*507.41*	*0.138*	*0.078*	*0.108*
-2000	*-13888.89*	*-45.11*	*157.50*	*511.5695*	*510.11*	*510.89*	*0.139*	*0.078*	*0.108*
0	*0.00*	*0.00*	*159.00*	*516.4416*	*516.36*	*514.41*			
2000	*13888.89*	*45.11*	*160.53*	*521.4111*	*522.68*	*517.97*	*0.140*	*0.079*	*0.110*
4000	*27777.78*	*90.22*	*162.07*	*526.4131*	*529.08*	*521.60*	*0.141*	*0.080*	*0.111*
6000	*41666.67*	*135.34*	*163.64*	*531.5125*	*535.55*	*525.27*	*0.142*	*0.080*	*0.111*
8000	*55555.56*	*180.45*	*165.22*	*536.6445*	*542.14*	*528.91*	*0.143*	*0.080*	*0.112*
10000	*69444.44*	*225.56*	*166.82*	*541.8414*	*549.01*	*532.41*	*0.145*	*0.080*	*0.113*
12000	*83333.33*	*270.67*	*168.45*	*547.1357*	*556.42*	*535.60*	*0.148*	*0.078*	*0.113*
14000	*97222.22*	*315.78*	*170.31*	*553.1771*	*566.00*	*538.04*	*0.157*	*0.075*	*0.116*
16000	*111111.11*	*360.90*	*172.48*	*560.2254*	*579.55*	*538.56*	*0.175*	*0.067*	*0.121*

Table E.2: Values of bolt stress, load ratios and stress ratios - Hub Side, for F_{Mmin}

E.2. Bolt stress profile - Maximum Pretension

Blade Side Values - Maximum Pretension									
External Moment kNm	External Force N	External Stress MPa	Axial Force (FEA) kN	Axial Stress (FEA) MPa	Blade Inside MPa	Blade Outside MPa	Stress Ratio - Blade Inside	Stress Ratio - Blade Outside	Load Ratio
-16000	*-111111.11*	*-360.90*	*210.64*	*684.17*	*678.58*	*686.55*	*0.125*	*0.091*	*0.109*
-14000	*-97222.22*	*-315.78*	*212.16*	*689.11*	*684.16*	*690.81*	*0.125*	*0.091*	*0.108*
-12000	*-83333.33*	*-270.67*	*213.66*	*693.98*	*689.79*	*694.88*	*0.126*	*0.091*	*0.108*
-10000	*-69444.44*	*-225.56*	*215.14*	*698.79*	*695.44*	*698.83*	*0.126*	*0.092*	*0.109*
-8000	*-55555.56*	*-180.45*	*216.62*	*703.59*	*701.11*	*702.75*	*0.126*	*0.093*	*0.109*
-6000	*-41666.67*	*-135.34*	*218.11*	*708.43*	*706.79*	*706.74*	*0.125*	*0.094*	*0.110*
-4000	*-27777.78*	*-90.22*	*219.63*	*713.37*	*712.46*	*710.87*	*0.125*	*0.095*	*0.111*
-2000	*-13888.89*	*-45.11*	*221.15*	*718.31*	*718.11*	*715.12*	*0.125*	*0.096*	*0.112*
0	*0.00*	*0.00*	*222.70*	*723.34*	*723.77*	*719.47*			
2000	*13888.89*	*45.11*	*224.27*	*728.44*	*729.48*	*723.91*	*0.127*	*0.098*	*0.113*
4000	*27777.78*	*90.22*	*225.85*	*733.57*	*735.23*	*728.41*	*0.127*	*0.099*	*0.113*
6000	*41666.67*	*135.34*	*227.45*	*738.77*	*741.01*	*732.99*	*0.127*	*0.100*	*0.114*
8000	*55555.56*	*180.45*	*229.06*	*744.00*	*746.83*	*737.59*	*0.128*	*0.100*	*0.114*
10000	*69444.44*	*225.56*	*230.69*	*749.29*	*752.87*	*742.1*	*0.129*	*0.100*	*0.115*
12000	*83333.33*	*270.67*	*232.33*	*754.62*	*759.28*	*746.33*	*0.131*	*0.099*	*0.116*
14000	*97222.22*	*315.78*	*234.00*	*760.05*	*766.08*	*750.39*	*0.134*	*0.098*	*0.116*
16000	*111111.11*	*360.90*	*235.70*	*765.57*	*773.06*	*754.39*	*0.137*	*0.097*	*0.117*

Table E.3: Values of bolt stress, load ratios and stress ratios - Blade Side, for F_{Mmax}

Hub Side Values - Maximum Pretension									
External Moment kNm	External Force N	External Stress MPa	Axial Force (FEA) kN	Axial Stress (FEA) MPa	Blade Inside MPa	Blade Outside MPa	Stress Ratio - Blade Inside	Stress Ratio - Blade Outside	Load Ratio
-16000	*-111111.11*	*-360.90*	*210.64*	*684.17*	*673.97*	*691.57*	*0.138*	*0.079*	*0.109*
-14000	*-97222.22*	*-315.78*	*212.16*	*689.11*	*680.23*	*695.16*	*0.138*	*0.079*	*0.108*
-12000	*-83333.33*	*-270.67*	*213.66*	*693.98*	*686.40*	*698.69*	*0.138*	*0.079*	*0.108*
-10000	*-69444.44*	*-225.56*	*215.14*	*698.79*	*692.50*	*702.19*	*0.138*	*0.079*	*0.109*
-8000	*-55555.56*	*-180.45*	*216.62*	*703.59*	*698.59*	*705.70*	*0.139*	*0.079*	*0.109*
-6000	*-41666.67*	*-135.34*	*218.11*	*708.43*	*704.74*	*709.23*	*0.140*	*0.080*	*0.110*
-4000	*-27777.78*	*-90.22*	*219.63*	*713.37*	*710.99*	*712.78*	*0.141*	*0.080*	*0.111*
-2000	*-13888.89*	*-45.11*	*221.15*	*718.31*	*717.31*	*716.38*	*0.142*	*0.080*	*0.112*
0	*0.00*	*0.00*	*222.70*	*723.34*	*723.70*	*720.01*			
2000	*13888.89*	*45.11*	*224.27*	*728.44*	*730.15*	*723.69*	*0.143*	*0.082*	*0.113*
4000	*27777.78*	*90.22*	*225.85*	*733.57*	*736.67*	*727.43*	*0.144*	*0.082*	*0.113*
6000	*41666.67*	*135.34*	*227.45*	*738.77*	*743.26*	*731.22*	*0.145*	*0.083*	*0.114*
8000	*55555.56*	*180.45*	*229.06*	*744.00*	*749.87*	*735.03*	*0.145*	*0.083*	*0.114*
10000	*69444.44*	*225.56*	*230.69*	*749.29*	*756.70*	*738.76*	*0.146*	*0.083*	*0.115*
12000	*83333.33*	*270.67*	*232.33*	*754.62*	*763.80*	*742.30*	*0.148*	*0.082*	*0.116*
14000	*97222.22*	*315.78*	*234.00*	*760.05*	*771.38*	*745.60*	*0.151*	*0.081*	*0.116*
16000	*111111.11*	*360.90*	*235.70*	*765.57*	*779.47*	*748.49*	*0.155*	*0.079*	*0.117*

Table E.4: Values of bolt stress, load ratios and stress ratios - Hub Side, for F_{Mmax}

E.3. Normal force and pretension: Varying bolt number

Number of bolts –>	96		100		104		110	
Pretension –>	Min	Max	Min	Max	Min	Max	Min	Max
kN –>	318.5714	446	313.5714	439	308.7143	432.2	302.2857	423.2
External Moment (kNm)	Normal Force (N)		Normal Force (N)		Normal Force (N)		Normal Force (N)	
-16000	-111111.1111		-106666.6667		-102564.1026		-96969.69697	
-14000	-97222.22222		-93333.33333		-89743.58974		-84848.48485	
-12000	-83333.33333		-80000		-76923.07692		-72727.27273	
-10000	-69444.44444		-66666.66667		-64102.5641		-60606.06061	
-8000	-55555.55556		-53333.33333		-51282.05128		-48484.84848	
-6000	-41666.66667		-40000		-38461.53846		-36363.63636	
-4000	-27777.77778		-26666.66667		-25641.02564		-24242.42424	
-2000	-13888.88889		-13333.33333		-12820.51282		-12121.21212	
0	0		0		0		0	
2000	13888.88889		13333.33333		12820.51282		12121.21212	
4000	27777.77778		26666.66667		25641.02564		24242.42424	
6000	41666.66667		40000		38461.53846		36363.63636	
8000	55555.55556		53333.33333		51282.05128		48484.84848	
10000	69444.44444		66666.66667		64102.5641		60606.06061	
12000	83333.33333		80000		76923.07692		72727.27273	
14000	97222.22222		93333.33333		89743.58974		84848.48485	
16000	111111.1111		106666.6667		102564.1026		96969.69697	

Table E.5: Normal force developed per unit bolt connection for the given external moment, and calculated pretension for a uniform clamping force